Immobilized Diimine Complexes of Palladium and Copper as Catalyst Precursors for Oxidation Reactions

by
Hendrik de Vries Kotzé

Thesis presented in partial fulfilment of the requirements for the degree Master of Science in Chemistry at the University of Stellenbosch

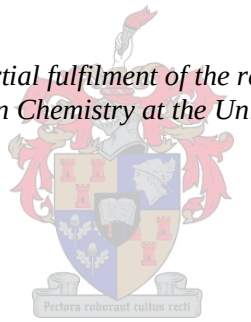

Supervisor: Prof. Selwyn Mapolie
Faculty of Science
Department of Chemistry and Polymer Science

March 2011

DECLARATION

By submitting this thesis/dissertation electronically, I declare that the entirety of the work contained therein is my own, original work, that I am the sole author thereof (save to the extent explicitly otherwise stated), that reproduction and publication thereof by Stellenbosch University will not infringe any third party rights and that I have not previously in its entirety or in part submitted it for obtaining any qualification.

March 2011

ABSTRACT

In this thesis the synthesis of a wide range of model and siloxane functionalized *N*-(n-propyl)-1-(2-pyridyl and quinolyl)-imine ligands (**L1**-**L6**) are described. Functionalized ligands (**L4**-**L6**) were obtained by the reaction of the pyridyl and quinolyl aldehydes with 3-aminopropyltriethoxysilane. Model ligands were characterized by FT-IR and ^{1}H NMR spectroscopy while ^{13}C{^{1}H} NMR spectroscopy was additionally used for functional ligand characterization. Functionalized complexes of both Pd(II) and Cu(I) were found to be more thermally stable than their model counterparts. Overall the model Pd(II) complexes showed a higher thermal stability than the model Cu(I) complexes.

Ligands (**L1**-**L6**) were reacted with either Pd(II) or Cu(I) metal precursors to produce both the model and functionalized Pd(II) (**C1**-**C6**) and Cu(I) (**C7**-**C12**) metal complexes. These metal complexes were all characterized by FT-IR spectroscopy, ^{1}H NMR and UV/Vis spectroscopy for the model Cu(I) complexes. Functionalized complexes were additionally characterized with ^{13}C{1H} NMR spectroscopy.

Siloxane functionalized complexes of Pd(II) and Cu(I) were immobilized on MCM-41 and SBA-15 silica materials to produce heterogenized immobilized catalysts. These immobilized catalysts were characterized by a wide range of solid state techniques including: BET nitrogen adsorption/desorption, scanning electron microscopy (SEM), thermal gravimetric analysis (TGA), ICP-AES, FT-IR spectroscopy, powder XRD and solid state ^{13}C{^{1}H} NMR spectroscopy. ICP-AES and BET surface analysis showed that better complex immobilization occurred for SBA-15 supported materials despite SBA-15

having a significantly lower surface area than MCM-41. This higher immobilization was ascribed to the larger pore sizes of SBA-15 (50 Å) vs. that of MCM-41 (26 Å).

Immobilized catalysts were tested for the oxidation of benzyl alcohol to benzaldehyde. Immobilization had a positive effect on the catalytic activity of the Pd(II) complexes with higher conversions being observed for immobilized Pd(II) catalysts when compared to their model analogues. Overall the MCM-41 immobilized Pd(II) catalysts showed a higher increase in activity than SBA-15 immobilized catalysts. For Ti-doped supports a generally higher activity was seen for the Ti-SBA-15 system. The Cu(I) systems however were not as effective in the oxidation reactions.

OPSOMMING

In hierdie tesis word die sintese van `n wye reeks model sowel as gefunksioneerde *N*-(n-propiel)-1-(2-piridiel en kinoliel)-imien ligande (**L1**-**L6**) beskryf. Gefunksioneerde ligande (**L4**-**L6**) is gevorm deur die reaksie van piridiel en kinoliel aldehied met 3-amniopropieltriëtoksiesilaan. Model ligande is gekaraktariseer deur FT-IR en ^{1}H KMR spektroskopie terwyl ^{13}C{^{1}H} KMR spektroskopie addisioneel gebruik is vir die karaktarisering van die gefunksioneerde ligande.

Ligande (**L1**-**L6**) is gereageer met Pd(II) of Cu(I) metaal voorgangers om beide model sowel as gefunksioneerde Pd(II) (**C1**-**C6**) en Cu(I) (**C7**-**C12**) metaal komplekse op te lewer. Hierdie metaal komplekse is almal gekaraktariseer deur FT-IR, ^{1}H KMR en UV/Vis spektroskopie vir die model Cu(I) komplekse. Gefunksionalseerde komplekse is addisioneel gekaraktariseer deur gebruik te maak van ^{13}C{^{1}H} KMR spektroskopie. Dit is gevind dat gefunksionaliseerde komplekse van beide Pd(II) sowel as Cu(I) termies meer stabiel was as hulle ooreenstemmende model komplekse. Oor die algemeen het die Pd(II) komplekse hoër termiese stabiliteit as die Cu(I) komplekse getoon.

Siloksaan gefunksioneerde komplekse van Pd(II) en Cu(I) is geimmobiliseer op MCM-41 en SBA-15 silika materiale om heterogene geimmobiliseerde katalisatore op te lewer. Hierdie geimmobiliseerde katalisatore is gekaraktariseer deur van `n wye reeks vaste toestand tegnieke gebruik te maak. Hierdie suit in: SEM, TGA, ICP-AES, FT-IR, poeier XRD en vaste toestand ^{13}C{^{1}H} KMR spektroskopie. ICP-AES en BET oppervlak analieses het getoon dat beter kompleks immobilisering vir die SBA-15 silika material plaas gevind het, ondanks die feit dat SBA-15 `n laer oppervlak area beskik. Hierdie

hoër graad van immobilisering is toegeskryf aan die groter poriegrootte van SBA-15 (50 Å) teenoor die van MCM-41 (26 Å).

Geimmobiliseerde katalisatore is getoets in die oksidasie van bensielalkohol na bensaldehied. Dit is gevind dat die immobilisering van die Pd(II) komplekse op die silika materiaal `n positiewe uitwerking op die aktiwiteit van die katalitiese van die komplekse gehad het. Die hoogste toename in aktiwiteit is gesien vir geimmobiliseerde Pd(II) katalisatore wanneer hulle met hul ooreenstemmende model komplekse vergelyk is. Oor die algemeen is gevind dat MCM-41 geimmobiliseerde Pd(II) katalisatore n hoër toename in aktiwiteit getoon het as die van SBA-15. Vir die Ti-gedokterde silika materiale het die Ti-SBA-15 sisteem oor die algemeen `n hoër aktiviteit getoon as die Ti-MCM-41 sisteem. Die Cu(I) sisteme was egter nie so effektief in oksidasie reaksies nie.

ACKNOWLEDGEMENTS

Firstly I would like to thank my supervisor Prof Selwyn Mapolie for his patience, guidance and support to successfully complete this project.

I would also like to thank my colleagues from the Organometallic Research Group at Stellenbosch University; Dr. Rehana Malgas-Enus, Jane Mugo, Andrew Swarts, Wallace Manning, Danie van Niekerk, Dr Gangadhar Bagihalli and Dr Douglas Onyancha for their friendship, extensive support and invaluable discussions.

I would like to thank the staff and technical assistants in the Department of Chemistry and Polymer Science of Stellenbosch University, especially the CAF group for assisting with various analytical techniques.

Financial support from the NRF is gratefully acknowledged.

Lastly I would like to thank my family and friends, especially Karen MacGregor, for their unwavering support and encouragement throughout.

CONFERENCE CONTRIBUTIONS

Hennie Kotzé and S.F. Mapolie

Poster Titled: ***Immobilization of pyridinyl-diimine metal complexes on silica supports and their future application in the selective oxidation of alcohols***

Catalysis Society of South Africa (CATSA), Cape Town (Goudini Spa), South Africa, 2009.

Hennie Kotzé and S.F. Mapolie

Poster Titled: ***Immobilized pyridinyl-diimine complexes on silica supports as possible alcohol oxidation catalysts: Synthesis and characterization***

International Symposium on Homogeneous Catalysis (ISHC), Poznan, Poland, 2010

TABLE OF CONTENT

Chapter four: *Preliminary studies on catalytic benzyl alcohol oxidation*

LIST OF FIGURES

Chapter one

Chapter two

Chapter three

Chapter four

LIST OF SCHEMES

Chapter one

Chapter two

Chapter three

Chapter four

LIST OF TABLES

Chapter two

Chapter three

ABBREVIATIONS

ºC	degrees Celsius
µM	micromolar
Å	Ångstrom
ABTS	2,2'-azino-bis(3-ethylbenzthiazoline-6-sulphonic acid)
acac	acetylacetone
ATH	asymmetric transfer hydrogenation
ATR	attenuated total reflectance
BET	Brunauer-Emmett-Teller
bipy	bipyridine
BJH	Barret-Joyner-Halenda
cm^{-1}	wavenumber
cod	cyclooctadiene
CTAB	cetyl trimethylammonium bromide
d	doublet
DCM	dichloromethane
ee	enantiomeric excess
FT-IR	Fourier Transform infrared spectroscopy

g	grams
GC	gas chromatography
h	hours
HPLC	high performance liquid chromatography
Hz	Hertz
ICP-AES	inductively coupled plasma atomic emission spectroscopy
m	multiplet
MCF	mesocellular silica foam
MCM	Mobil crystalline material
mL	milliliters
MLCT	metal-to-ligand charge transfer
min.	minute
mmol	millimole
mol	mole
MP	methyl-pyridine
MSU	Michigan State University
nm	nanometer
NMR	nuclear magnetic resonance

OMM	ordered mesoporous material
P	pyridine
PEG	polyethyleneglycol
ph	phenyl
ppm	chemical shift
Q	quinoline
s	singlet
SBA	Santa Barbara amorphous
SEM	scanning electron microscopy
t	triplet
TEOS	tetraethylorthosilicate
THF	tetrahydrofuran
TMOS	tetra-methylorthosilicate
TMKP	transition metal Keggin-type polyoxometalates
TGA	thermogravimetric analysis
TMSD	trimethylsilyl diazomethane
UV/Vis	ultraviolet/visible
XRD	X-ray diffraction

Chapter 1: Literature Review of Immobilized Catalyst

1. Introduction

The synthesis of numerous chemicals is facilitated by catalysis at some stage or another. Two of the biggest issues concerning catalysis are catalyst recovery and recyclability of catalysts. The impact of certain reactions or processes on the environment has become a telling factor in the design of catalyst systems and has an influence on their application in industry. The reusability of a particular catalyst is thus of great importance to minimize its effect on the environment. By increasing the reusability of a catalyst, one can increase the productivity of a chemical transformation and decrease the overall cost of such a process.

The production of fine chemicals is still mostly achieved by utilizing homogeneous catalyst systems.[1-3] The reason being that homogeneous catalysis gives high yields and better selectivity towards the major products. Unfortunately homogeneous systems are plagued by two major drawbacks. The first is the problem of separation of the catalyst from the product mixture. Since the catalyst and the products are in the same phase, it is virtually impossible to separate them to recover the catalyst. This leads to the second problem, the recovery of the catalyst. During the workup of the reaction mixture to obtain the major product, the catalyst is usually destroyed and this makes it almost impossible to recover the catalyst.[4] Another telling factor is the availability and cost of precious metals. The problem with the separation and recovery together with the catalyst cost forced researchers to investigate ways to overcome these problems.

One proposed approach, and which has been available for years, is to employ heterogeneous systems. This would solve the separation issue by making it possible to simply separate the catalyst from the product mixture with normal filtration techniques. This would make it possible to recover the catalyst and to regenerate it for further use. Although heterogeneous systems seem like a viable alternative, this approach also has a major drawback. These systems, compared to their homogeneous counterparts cannot compete with the conversion and selectivity accomplished by the homogeneous systems. An alternative approach that has received widespread interest over the past two decades is to take a homogeneous catalyst and to try and "heterogenize" it. By doing this one would expect to have the best characteristics of both homogeneous and heterogeneous catalysts. On the one hand one would have the ability to easily separate and recover the catalyst from the products after a chemical transformation, and on the other be able to get selectivities and conversions comparable to that of normal homogeneous systems. The easiest way to accomplish this is to immobilize the homogeneous catalyst onto an insoluble carrier. The insoluble material would give the catalyst its heterogeneous characteristics and would allow for easy separation. This process, by which a homogeneous catalyst is immobilized onto a solid support, is known as "heterogenization" and has had a big impact on the field of catalysis in recent times.[5,6]

1.1 Heterogenization of homogeneous catalysts

Over the past few decades, numerous approaches have been developed to immobilize homogeneous catalysts to try and facilitate its separation and reusability. Considerable interest has been shown by academia as well as industry for this reason and as a result numerous approaches have been developed to try and achieve heterogenization.

There are mainly three types of materials being employed to synthesize a "heterogenized" homogeneous catalyst. Inorganic, organic and so called hybrid materials have been employed as supports for homogeneous catalysts. Examples in the literature of inorganic and organic supports are respectively: silica, clay, zeolites, heteropolyacids (inorganic), dendrimers, carbon, polymeric ligands and polyelectrolytes (organic).[7-10] Methods of immobilization onto these supports vary. The immobilization can either occur covalently or noncovalently. The most widely used approach for immobilization of homogeneous catalysts on solid supports involves the covalent attachment of functionalized metal complexes. Covalent immobilization in ordered mesoporous materials is made possible by the presence of surface silanol groups which provides the reactive sites for functionalization.

1.1.1 Covalent interaction

The abovementioned silanol groups on the surface of ordered mesoporous silicas make it possible to functionalize the surface of the support by covalently binding the active species making use of these surface silanols. Scheme 1.1 shows the two distinct approaches used to bind the so called active species to the surface of the support.

These are known as the sequential and convergent approaches. Firstly, the convergent approach entails the synthesis of a so called functionalized ligand (containing a trimethoxy-or triethoxy-silyl group) with a carbon tether. The catalytic metal centre is then coordinated to the ligand to form the catalyst which is then immobilized onto the support. Sequential synthesis follows the exact opposite route. Here the carbon tether (e.g. 3-aminopropyltriethoxysilane) is firstly anchored on the support. The ligand is then subsequently attached to the tether followed by the coordination of the catalytic metal centre.[11,12]

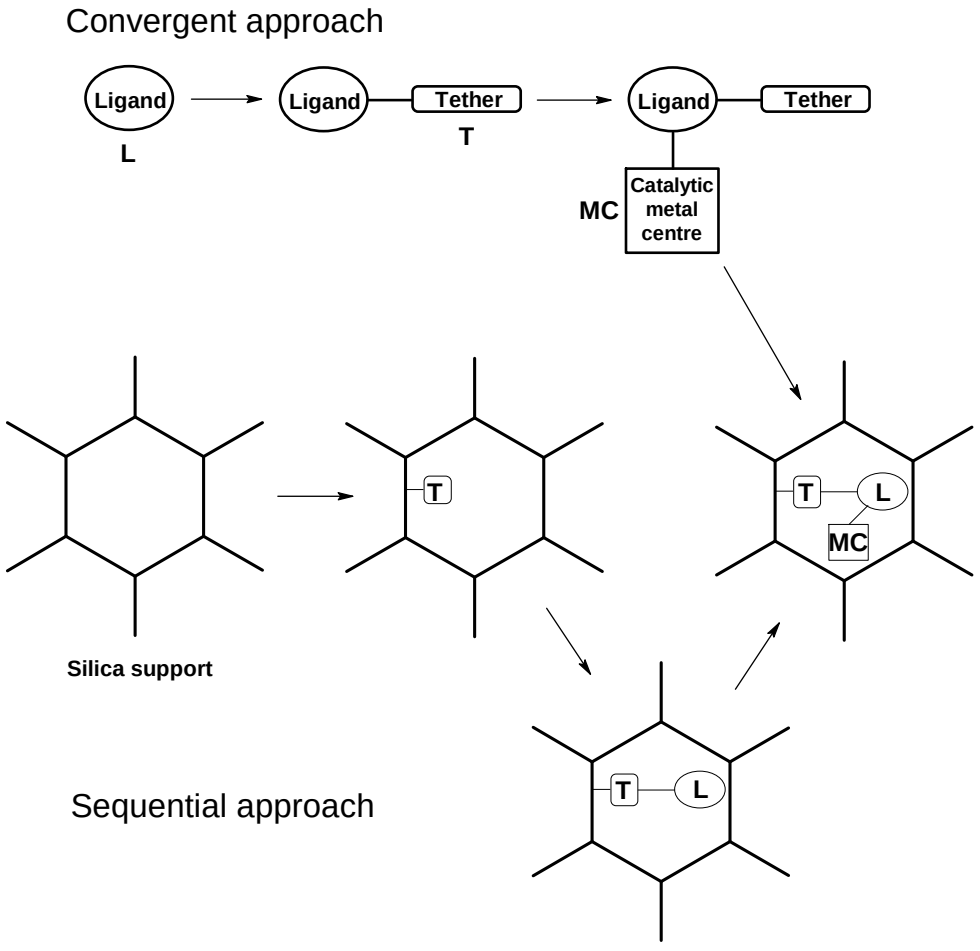

Scheme **1.1 Convergent and sequential heterogenization methods**[12]

1.1.2 Noncovalent interaction

Noncovalent catalyst immobilization is mostly achieved by adsorption, electrostatic interaction and encapsulation/entrapment.[11,13,14] An example of a noncovalently bound rhodium catalyst (Figure 1.1) used during hydroformylation was reported by Bianchini *et al*. [15]

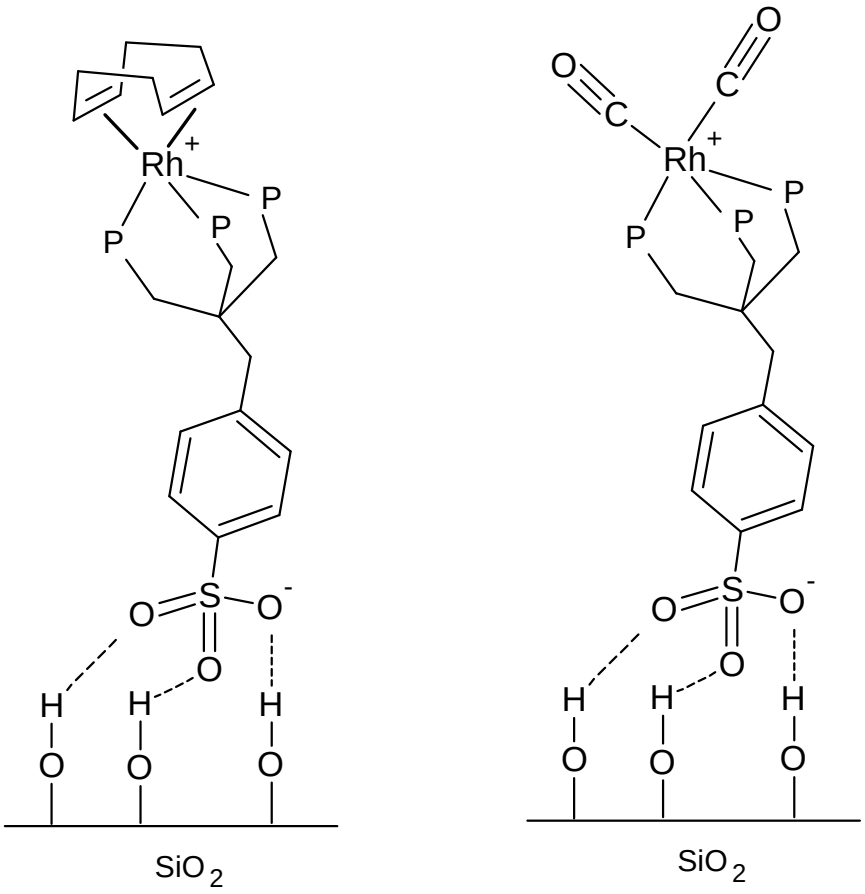

Figure 1.1 Left: non-covalently bound Rh(I) based molecular complex for hydroformylation immobilized on a silica surface. Right: catalytically inactive species that forms on prolonged exposure of the one on the left to syngas.[15]

1.1.2.1 Adsorption

Immobilization of catalysts by means of adsorption relies almost entirely on weak van der Waals interactions. These weak interactions cause leaching of the catalyst onto the support and into the reaction medium. By modifying the catalyst and the support to incorporate hydrogen bonding, the stability of the immobilized catalyst can be improved dramatically.[14] Adsorption is most widely used for the immobilization of enzymes onto solid supports. Denaturation of the enzymes are avoided seeing that no further treatment of the support is needed, thus ensuring the stability of the enzymes.

1.1.2.2 Electrostatic interaction

Immobilization of a catalyst onto a solid support making use of ionic interaction has been explored for years. Zeolites are surface-charged and it is easy to ionize the surface of other solid supports. It has been shown that the interaction between the homogeneous catalyst and the support is strong enough to minimize catalyst leaching.[14] There are two distinct methods to achieve this electrostatic interaction, shown in Scheme 1.2. Electrostatic interaction can only occur when cationic complexes need to be immobilized. The first case involves the direct cationic exchange of the complex which is preformed in solution. In this case the formed salt (CX) is formed from the compensating cation of the solid (C^+) and the counterion of the complex (X^-). This salt can then either be eliminated into the solution or remain absorbed on the solid, depending on the solvent that is used. The second method relies on the formation of the complex on a pre-exchanged metal center.[16]

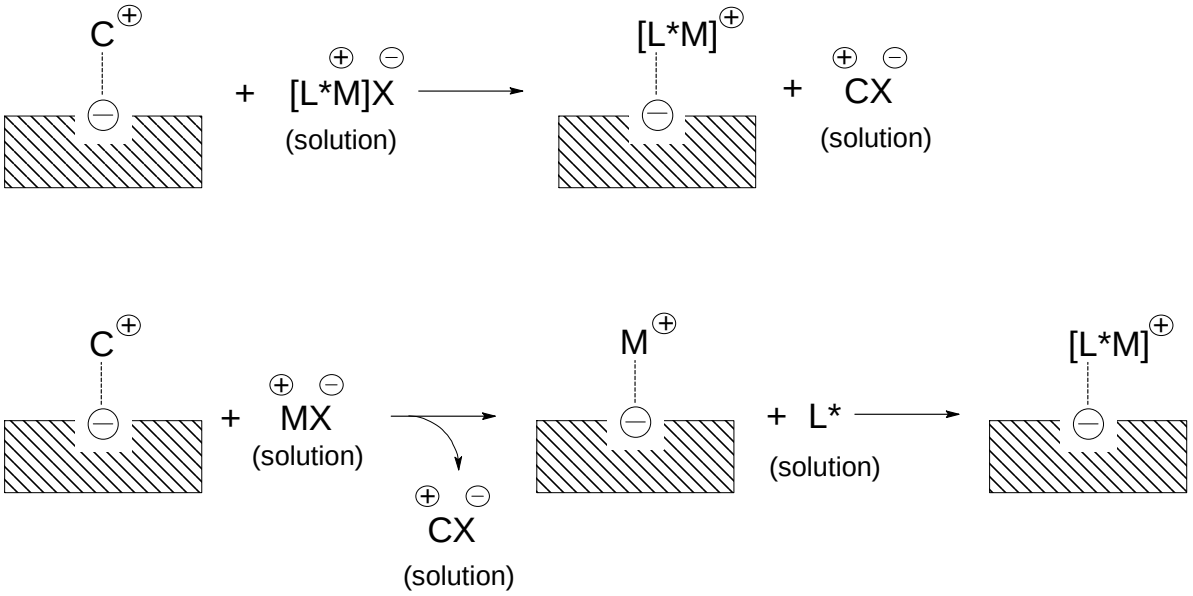

Scheme 1.2 Methodologies to obtain immobilization through electrostatic interactions[16]

1.1.2.3 Encapsulation/Entrapment

Encapsulation, as the name suggests, involves the enclosing of the catalyst within a certain pore space with the opening to the pore being smaller than the catalyst itself. This smaller pore opening is what would keep the catalyst trapped in the support and prevent leaching. This is not a widely used immobilization approach when it comes to ordered mesoporous silica (OMM) though, mainly due to the large pore sizes seen for OMMs. This method can however be applied for the immobilization of larger molecules such as enzymes, first reported by Balkus Jr. and Díaz[17].

Immobilization through encapsulation can be achieved by making use of three distinctly different methods. The two more widely reported methods are the assembly of the catalyst's individual building units into the pores (ship-in-a-bottle), by forming the solid

support around the catalyst and the coordination of the ligands of the final catalyst in the framework of the support.[5] Attention should be paid to the reaction conditions when the second approach is used, seeing that these conditions can have a influence on the structure and/or stability of the catalyst. When a catalyst's stability is a potential problem, the ship-in-a-bottle approach would be a viable substitution to maintain the structural integrity of the molecular catalyst.

The third and more recent method for encapsulation of a molecular catalyst was described by Gelman *et al*. [18] They were able to physically entrap/encapsulate [(BINAP)Ru(*p*-cymene)Cl]Cl, [(DIOP)Rh(cod)Cl] and [(BPPM)Rh(cod)Cl] complexes by making use of the sol-gel method using an appropriate silica precursor.

The sol-gel process, also known as chemical solution deposition, is a wet-chemical technique widely used in the fields of material science and ceramics. Such methods are used primarily for the fabrication of materials (typically a metal oxide) starting from a chemical solution (or ***sol***) which acts as the precursor for an integrated network (or ***gel***) of either discrete particles or network polymers. Typical precursors are metal alkoxides and metal chlorides, which undergo various forms of hydrolysis and polycondensation reactions. The preparation of one of these silicas (also known as silica glasses) begins with an appropriate metal alkoxide ($Si(OEt)_4$ for example) which is mixed with a suitable solvent. Two distinctly different sol-gel processes are known, aqueous and non-aqueous. The difference is the addition of water for the aqueous route as one of the solvents. Starting from a chemical solution (***sol***) the gel is subsequently formed. In the gelation step, alkoxide gel precursors in aqueous solution are hydrolyzed, and polymerize through alcohol or water producing condensations (Scheme 1.3). The gel

formed after the condensation consists of a three-dimensional network with nanometer sized pores.

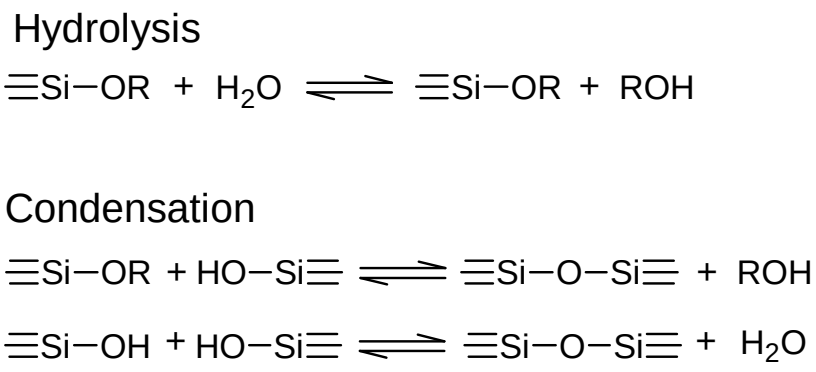

Scheme 1.3 Hydrolysis and condensation steps of the sol-gel process

A big question that arises though; where would the catalyst be in the formed silica structure? Three possible positions are known: inaccessible internal species, accessible internal species and external species. Zhang *et al.* [19] tried to get rid of external species by washing with dichloromethane but unfortunately leaching was observed when testing the catalyst for the hydrogenation of itaconic acid (2-methylidenebutanedioic acid) in THF. They deduced that the majority of their active catalyst was still on the surface, rather than inside the pores.

A similar situation was observed for the entrapment of a chiral Ru-porphyrin complex (Figure 1.2).[19] The same approach as described above was used and similar results were obtained when the immobilized catalyst was evaluated as an epoxidation catalyst. Diffusion restrictions were observed together with the total deactivation of the catalyst after only three runs.

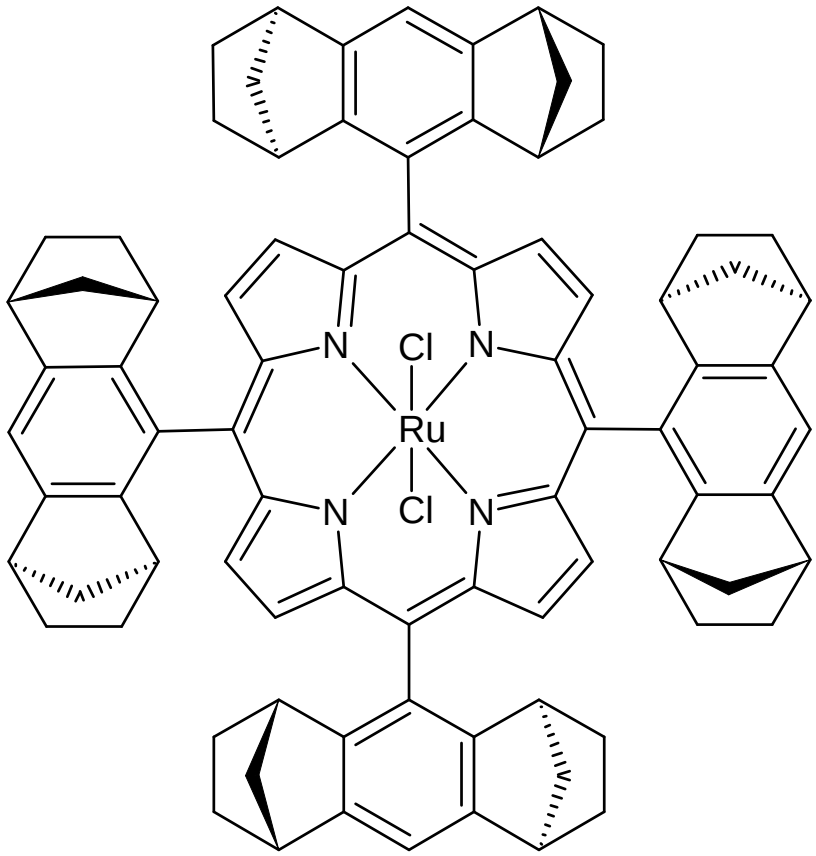

Figure 1.2 Ru-porphyrin complex entrapped in silica[19]

1.2 Ordered mesoporous silica

MCM-41 and SBA-15 are two of the most well known ordered mesoporous silicas. These materials have received considerable attention mainly because of their high surface area, large pore volumes and the well ordered arrangement of their uniformly sized mesopores.[20] These characteristics make them very useful for application as catalyst supports. MCM-41 and SBA-15 are inorganic materials which are synthesized in the presence of surfactants that act as templates for the polycondensation process of the silica. The silica species can originate from numerous sources for example: sodium

silicate, tetra-ethylortosilicate (TEOS) and tetra-methylorthosilicate (TMOS). The synthesis of these ordered mesoporous silicas is influenced by various reaction conditions. Surfactant type, pH, silica source, temperature and reaction time play a major role in the composition and type of material that is synthesized. These conditions influence the nano structure of the silica material and will determine the type of the mesostructure as well as the diameter and volume of the pores.[21,22]

The silanol surface functionalities on the mesoporous silica make it a versatile material for the heterogenization of homogeneous catalysts. Through the simple modification of the ligand of the molecular catalyst, one can covalently immobilize the homogeneous catalyst to give a heterogenized catalyst. In Figure 1.3 one can see that the silanols on the surface of the silica can be present in three different configurations. Ramírez *et al*. [18] proved that the content depended on the way in which the surfactants were removed from the mesoporous silica after its synthesis.

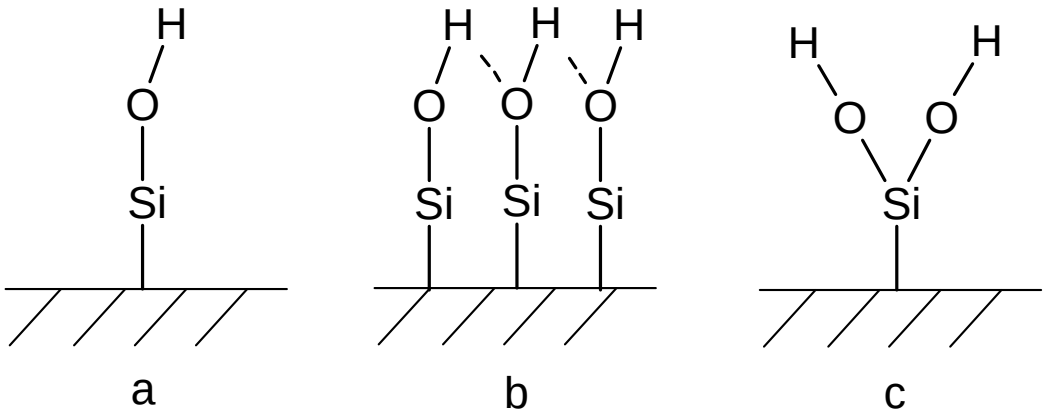

Figure 1.3 Different silanol groups on surface of a silica support: (a) single, (b) hydrogen bonded and (c) geminal silanol groups.[23]

1.2.1 Synthesis of ordered mesoporous silicas

In 1990, a group of researchers from Japan synthesized the first mesoporous silica nanoparticles.[24] Two years later, further research by Mobil Corporation laboratories produced periodic mesoporous silicate materials. These new mesoporous materials were named Mobil Crystalline Materials; MCM for short.[25,26] From then onwards, wide spread interest in surfactant templated synthesis of mesoporous materials have been shown mainly because of their applications in catalysis and separation technology.[25] MCM-41 is the most well-known of these mesoporous supports, but eight years after the discovery of MCM-type materials, researchers at the University of California in Santa Barbara synthesized silica nanoparcticles with larger pores. These materials were called Santa Barbara Amorphous type materials; SBA.[27] As seen in MCM-41, materials like SBA-15 also contain a hexagonal array of pores with large surface areas and pore volumes.[28] These two factors together with the high density of surface silanols provides the basis for an excellent support with numerous applications in chemistry.

The synthesis of mesoporous materials have been reported widely in the literature. A proposed method for the synthesis of MCM-41 is shown in Figure 1.4. The synthesis of the hexagonal silicate material relies on the hydrophobic and hydrophilic properties of the template molecule. When this template molecule (cetyl trimethylammonium bromide or CTAB) is dissolved in water, it arranges itself to form a micelle with the hydrophobic tails facing inwards. The hydrophilic heads form the outside of the micelle. These micelles are then believed to arrange themselves to form a micellar rod. Over time in solution these micellar rods arrange to form a hexagonal array of micellar rods. At this time in the synthesis process, a silicate source (eg. Tetra-methylorthosilicate) is

introduced into the reaction mixture and it forms a layer on the outside of the arranged micellar rods. After the reaction is completed, the formed white product is washed, dried and calcined at 500 to 600 ℃ to get rid of the template molecule.[29]

MCM-41 and SBA-15 synthesis differs only slightly. MCM-41 is synthesized under basic conditions whereas SBA-15 is synthesized under acidic conditions. A PEG (poly ethylene glycol) block copolymer is used as the templating agent, instead of CTAB.

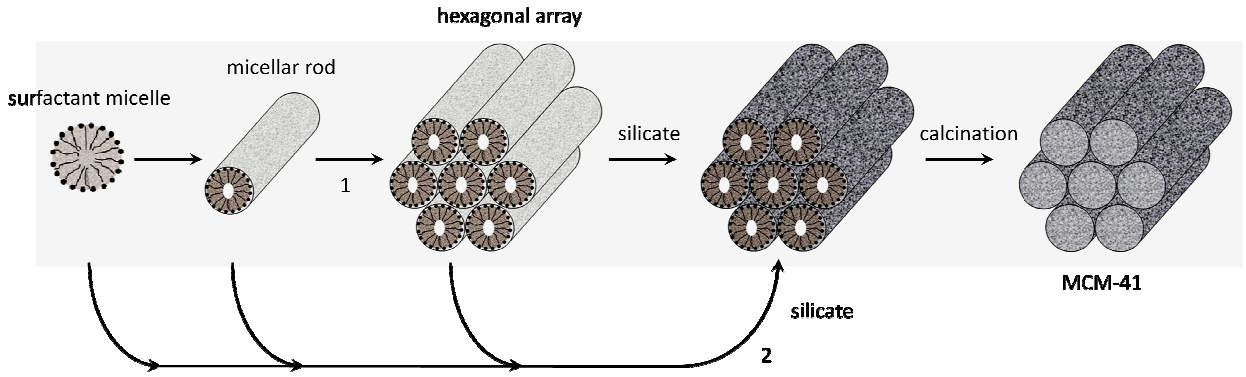

Figure 1.4 Possible pathway for the templated synthesis of mesoporous MCM-41[29]

1.2.2 Doping of mesoporous silicas

As stated earlier, mesoporous materials such as MCM-41 possess high surface areas, ordered pore structures and narrow pore size distributions. These three factors make them great candidates as potential catalysts or catalysts supports. By including other metals into the silica framework, the properties of the silica can be altered and significant changes in the activity of the silica can be observed when it is applied as a catalyst. Elements such as Ni[30], Ti[31] and Fe[32] have successfully been included in the

silicate framework and have been applied in the field of inclusion chemistry.[33,34] Much attention is focused on the substitution by Ti because of its successful application in the oxidation of larger types of materials when incorporated into a zeolite structure.

Metals can be introduced into the silica framework by making use of either direct synthesis or post-synthetic impregnation. Both of these methods are well studied and well defined for the introduction of a metal into the silica substructure. The only difference in these methods is the time when the Ti source is introduced.

In direct synthesis the Ti source is introduced during the synthesis of the mesoporous material. The preferred ratio of Si/Ti is prepared and added to the reaction mixture. Post-synthetic impregnation entails the synthesis of the mesoporous material by making use of the normal method. The only difference is that the silica is impregnated with the doping agent before it is calcined. A Ti source, eg. $Ti(OEt)_4$, in a suitable solvent is used to impregnate the pure uncalcined silica. The Ti-doped silica is then dried and calcined to afford the product.[35]

1.2.3 Applications of mesoporous materials

Mesoporous materials have found numerous uses in chemistry mainly because of their high surface areas and tunable pore sizes. These types of materials are applied in a wide field ranging from chemistry to biology. They are applied as stationary phases for liquid chromatography in the field of separation science, as catalysts, supports for the immobilization of biomolecules, as polymer reinforcements and as templates for the synthesis of mesoporous carbons.[36]

1.2.3.1 Stationary phases for high performance liquid chromatography (HPLC)

Mesoporous silica's high surface area and organized porous structure make them interesting materials for use as stationary phases in HPLC. Their thermal stability and surface silanol groups resembles the properties shown by precipitated silica. For application as RP-HPLC (reverse phase high performance liquid chromatography) stationary phases some post-synthesis modification is required (C8 and C18). C8 HPLC columns have packing material composed of silica particles attached to C8 carbon units while C18 HPLC columns will, of course, have packing materials coated with C18 hydrophobic units. Numerous groups have studied the effects of particle size and the use of different surfactant molecules on the quality and ease of separation using these types of stationary phases.[37,38]

1.2.3.2 Mesoporous silica as support for immobilization of bioactive molecules

By immobilizing drugs and enzymes onto a mesoporous material such as MCM-41, one is able to increase its activity, stability and selectivity. By increasing these parameters, it is very easy to facilitate its use in biological processes. The same immobilization techniques used to immobilize metal complexes are used for the immobilization of bioactive molecules. Silicates find widespread application as materials for controlled drug delivery seeing that they are biocompatible and inert in the human body. These characteristics also make them perfect candidates for enzyme immobilization for use as biosensors and in bioconversion processes.[36]

Izquierdo-Barba and his group[39] studied the influence of the mesoporous structure type on the controlled delivery of ibuprofen from MCM-48, SBA-15 and functionalized SBA-15. The process of loading of the ibuprofen onto the supports involved the soaking of preformed compacted disks in a solution of ibuprofen in hexane over a period of 4 days. The drug delivery studies involved the soaking of these disks in a solution which simulated body fluid. They made use of BET analysis, powder XRD, thermo gravimetric analysis, solid state NMR and elemental analysis to characterize their products. Their experiments showed no visible effect of the structure type on the release kinetics of the encapsulated drug. They did however see that the different pore sizes of the MCM and SBA materials affected the profiles from first order kinetics for MCM-48 to zero order kinetics for SBA-15. The functionalization of the SBA-15 material with a hydrophobic long chain hydrocarbon (C18) did however have an influence on the delivery of the ibuprofen from the support material. The decreased interaction of the ibuprofen with the modified material resulted in the faster delivery of the ibuprofen from the material. They successfully showed that mesoporous silica materials can easily be applied for controlled drug delivery and by just changing the functional groups on the surface, one can influence the speed of delivery of the drug.

1.2.3.3 Porous silica as hard template

The process for synthesizing carbon type materials with different pore sizes relies on the use of microporous and mesoporous materials as a so called hard template. Ryoo *et al.* [40] was the first to report the synthesis of ordered mesoporous carbon materials (CMK-1) by using MCM-48 as their hard template and sucrose to infiltrate inside the

mesoporous silica. Since then, different types of mesoporous silica materials have been employed as hard templates together with the use of different carbon sources to obtain mesoporous carbon with new compositions and different pore characteristics.

1.2.3.4 Mesoporous silica in catalysis

Porous materials are widely studied as catalysts and catalyst supports. There are three different types of porous materials; microporous (pore size <2 nm), mesoporous (2-50 nm) and macroporous (>50 nm).[41] One of the best known and actively studied porous materials are the zeolites. Due to their crystallographically defined pore structure, zeolites have a narrow and uniform microporous size distribution. Environmental and economic considerations have forced the petrochemical industry to look at other types of catalytic and/or modified catalytic processes. These would for instance require the petrochemical industry to substitute its liquid acid catalysts with solid materials to try and minimize the impact of catalyst disposal on the environment. Zeolites have attracted much attention as suitable substitutes for such acids. Their applications as either base or redox catalysts have made them really attractive for use as industrial catalysts. Unfortunately even zeolites have some limitations, mainly caused by the small pore size of its microstructure. When larger reactant molecules are involved (>2 nm), zeolites become less useful because access to the active sites within the micropores are limited. There have been many attempts to improve the diffusion of reactants to catalytic sites by modification of either the substructure of the zeolite (micropore sizes) or by surface modification.[42]

The introduction of mesoporous type materials in the 1990's solved this problem of accessibility of active sites by the introduction of a new type of mesoporous material called MCM-41. The increased pore size of MCM-41 (2-3 nm) made it a useful substitute as a solid catalyst for chemical transformation. Since then the application of mesoporous materials in catalysis has probably become one of the more actively studied fields in heterogeneous catalysis. Numerous reports of supported catalysts are reported in the literature. These are either synthesized through immobilization/heterogenization or through impregnation of the mesoporous material with a certain metal precursor. A few examples of recent reports will be shown to give an idea of the wide application of mesoporous catalysts in chemical transformations.

Mureşeanu and co-workers[43] synthesized a Cu(II) immobilized system for application as catalysts for biomimetic oxidations. Their suggested synthesis method for the immobilization of the Cu(II) complex onto the silica support is shown in Scheme 1.4 below. The HMS silica (hexagonal mesoporous silica) was firstly synthesized and then functionalized with 3-aminopropyltriethoxysilane by a post-synthesis method. This functionalized support was then used to immobilize two Cu(II) complexes, [Cu(acac)(phen)(H_2O)](ClO_4) and [Cu(acac)(Me_2bipy)](ClO_4), and laccase (copper-containing oxidase enzymes). The support and immobilized systems were characterized by XRD, N_2 adsorption/desorption, SEM, TGA, IR and UV-Vis spectroscopy.

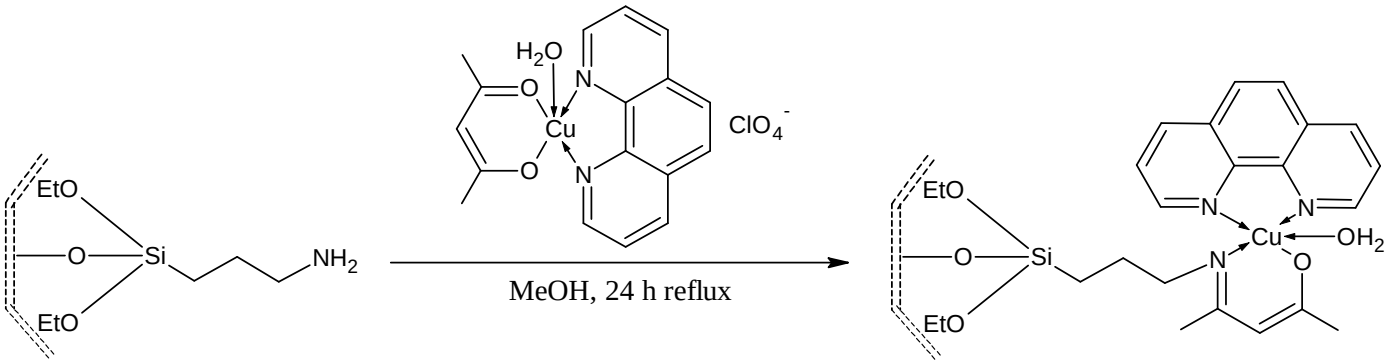

Scheme 1.4 Suggested model for the anchoring of $[Cu(acac)(phen)(H_2O)]ClO_4$ complex onto NH_2-HMS[43]

They tested their systems for the oxidation of ABTS with air. In biochemistry ABTS (2,2'-azino-bis(3-ethylbenzthiazoline-6-sulphonic acid)) is a chemical reagent used to evaluate the reaction kinetics of specific enzymes. They evaluated their results from the absorption band of an ABTS oxidation product at 424 nm using a Cu(II):ABTS ratio of 1:42. The initial rate values were used to compare the systems with each other. The calculated initial rate values for the normal complexes where found to be 0.48 and 0.50 µM min^{-1} respectively. For the immobilized systems this initial rate value increased to 18.85 and 28.81 µM min^{-1} respectively. They also tested a copper-substituted HMS silica and it also showed a very high initial rate value (25.23 µM min^{-1}). They ascribed this increase to the interaction of the substrate molecule with the inorganic support. These systems were also all found to be active as catalysts for the oxidation of aromatic hydrocarbons with hydrogen peroxide.

Lim *et al.* [44] made use of heterogenization to circumvent the problem of leaching and the high cost of ruthenium catalysts in ring-closing metathesis. They developed a novel

reactor system which made use of an immobilized catalyst in a continuous process by the circulation of the reaction mixture. This system facilitates the removal of by-products generated during the reaction process. Their immobilized system in showed in Scheme 1.5.

They found their immobilized catalyst to be very active as a ring-closing metathesis catalyst with high recyclability. Conversions, determined by GC analysis, were shown to be between 60 and 99% for certain substrates.

One of studies showed that even after 10 runs the conversion only dropped from 99 to 91% for a particular diene substrate. This showed that the immobilization increased the stability of the ruthenium catalyst and decreased leaching of metal from the catalyst.

Another example of the implementation of a silica-type catalyst for catalysis is the work done by Wang and his co-workers.[45] It is widely reported in the literature that metals such as Cr, Ti and Fe are incorporated into mesoporous silica to form catalytically active sites. They found little to no research devoted to the incorporation of bismuth (Bi) into the framework of mesoporous silica. To their knowledge, in 2007 when this paper was published, no report of bismuth incorporated into SBA-15 was found in the literature. They synthesized a Bi-containing SBA-15 mesoporous material by a direct hydrothermal method. The catalytic performance of their Bi-catalyst was then evaluated in the selective oxidation of cyclohexane in a solvent-free system with O_2 as oxidant.

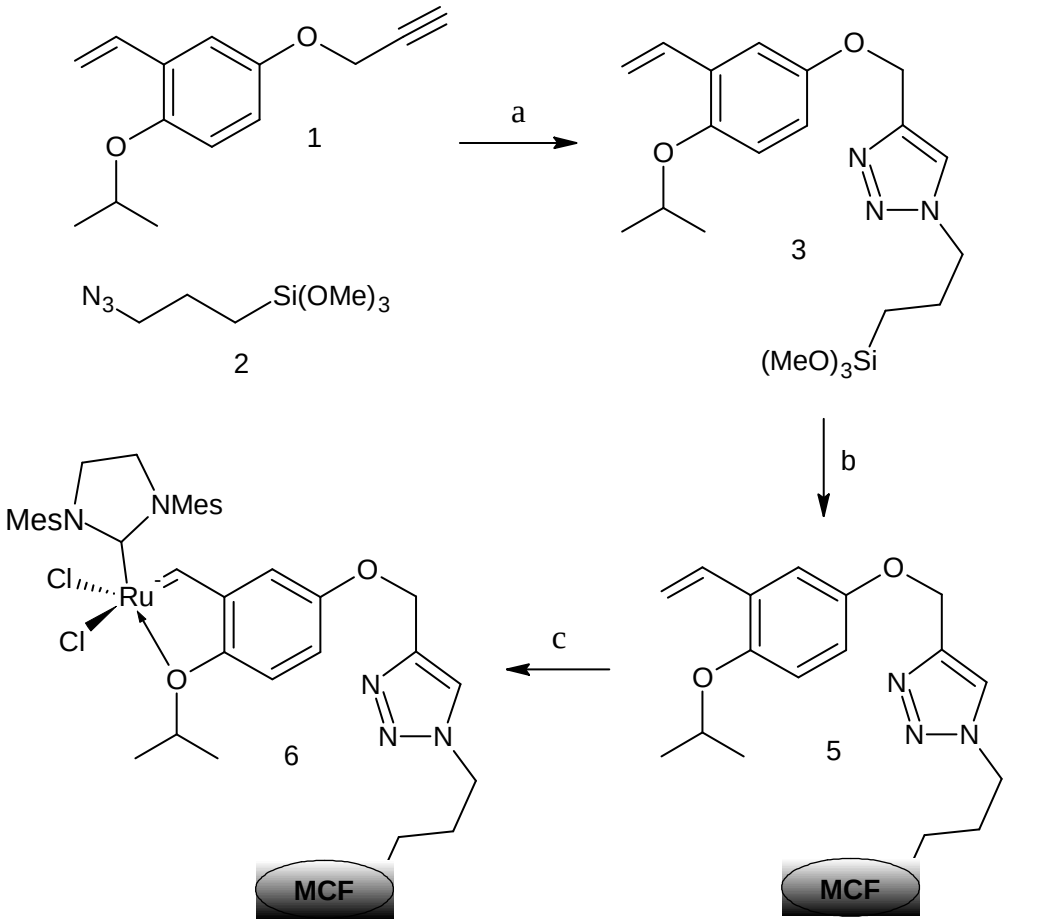

[a]CuI, DIPEA, THF, 25 °C. [b]TMS-MCF (**4**), toluene, 100 °C;HMDS, 80 °C
[c]Second generation Grubbs' catalyst, CuCl, DCM, 50 °C

Scheme 1.5 Synthesis of the immobilized catalyst 6 on mesocellular silica foam (MCF) support[44]

Compared to other similar reported systems, except those containing noble metals such as Au/SBA-15, a higher cyclohexane conversion (16.9 %, yield of 15.7 %) was observed for their immobilized catalyst system. They found that an increase in the conversion resulted in a decrease in the cyclohexanol selectivity. Reusability and stability of their Bi-SBA-15 catalyst was found to be very high compared to its homogeneous counterpart.

These few examples were selected to show the diverse applications of immobilized and/or metal impregnated metal catalysts and their application in chemical processes. In all of the cases higher conversions and selectivity where seen when compared to their respective homogeneous counterparts. Many more reports like these are available in the literature and mostly improved catalytic activity is seen when these systems are employed.

1.3 Immobilization of functionalized complexes

Covalent immobilization of a complex onto a silica support like MCM-41 makes use of the surface silanol groups that are present in mesoporous silica materials. By incorporating a triethoxysilane or similar functionality into the complex that needs to be immobilized, a simple condensation reaction leads to the formation of a covalent bond that affords the successful immobilization of the wanted complex. This results in the formation of the “heterogenized” catalyst. This immobilization does not only give the catalyst heterogeneous properties, but also improves the stability of the catalyst.

Numerous methods have been used to support metallic palladium species as heterogenized catalysts on materials such as: carbon, metal oxides, zeolites and mesoporous silica for application as Heck catalysts.[46] Unfortunately these types of catalysts suffered from a major drawback. The stability of the catalysts was poor under certain reaction conditions and resulted in the leaching of the metal. Dams *et al*. [47] and Zhao *et al*. [48] both reported the deactivation of palladium metal immobilized on mesoporous silica via leaching of the active metal species into solution under their reaction conditions. Oxidation of the palladium and the stabilization of the leached metal

in polar solvents played a big role for them to do research into other methods of heterogenization. Kosslick and his group[49] reported the successful immobilization of a palladium catalyst on MCM-41 which was appropriately functionalized to obtain an active catalyst for application in Suzuki coupling. They found that they could increase the stability of the palladium catalyst but could unfortunately not suppress the leaching caused by the oxidation of the phosphine ligands of the complex.

This problem of the oxidation of the palladium by the phosphine ligand has been overcome by replacing it with nitrogen chelating ligands. These types of ligands are also air stable, much cheaper and less toxic.

1.3.1 Immobilization methods

Numerous groups have reported on both the convergent and sequential methods for immobilization of metal complexes. Both these methods have been fully studied and can easily be applied to synthesize the required catalyst. The preferred method, and the one chosen for our investigation, is the convergent synthesis method. Both methods are explained and shown in Schemes 1.6 and 1.7. The reasoning for the selection of this method over the other will become clearer when one takes a closer look at the detailed synthesis methods involved.

1.3.1.1 Sequential immobilization

This method of immobilization, as shown in Scheme 1.6, involves the functionalization of the surface of the support with a spacer or linker (in this example a three carbon spacer). This spacer (3-aminopropyltriethoxysilane) then contains the amine

functionality which can react with a carboxaldehyde during a Schiff-base condensation reaction to afford the immobilized ligand. After this formation of the immobilized ligand, a metal salt, in this case $PdCl_2$, is added to form the immobilized metal catalyst.

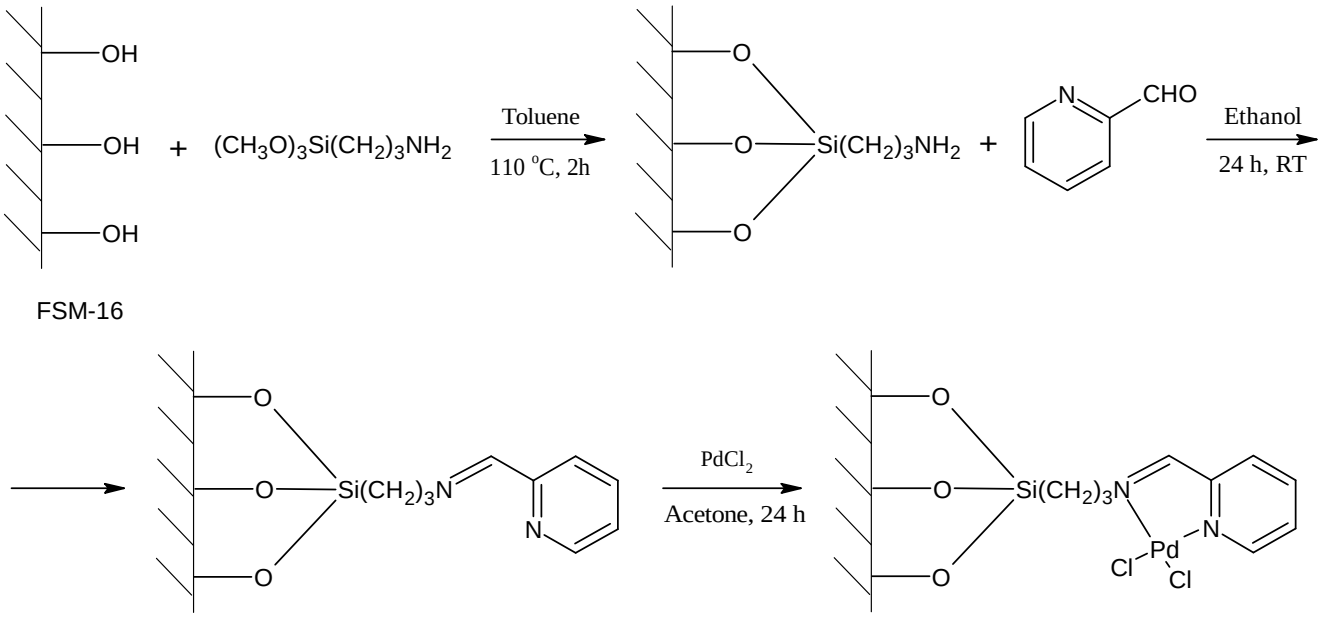

Scheme 1.6 Sequential immobilization method as used by Horniakova *et al*. [46]

Unfortunately it is not possible to know if all of the metal salt that is added reacts and is coordinated to the nitrogen-chelating ligand or if it is just simply physically adsorbed directly on the surface of the support or in the pores. This makes it difficult to fully characterize the catalyst and prove that the catalysis is facilitated by the metal complex or free metal salt. This is why the convergent approach was chosen for our study.

1.3.1.2 Convergent immobilization

Convergent immobilization follows the exact opposite route as seen for the sequential method. Here the functionalized metal complex is first synthesized and then immobilized (Scheme 1.7). The main difference here is that the metal salt or precursor is first coordinated to the nitrogen-chelating ligand to form the functionalized metal complex. This complex is then immobilized onto the silica support to form the catalyst. All of the active metal species is now associated with the discrete metal complex and one can say with certainty that no uncoordinated metal is present on the surface of the support material.

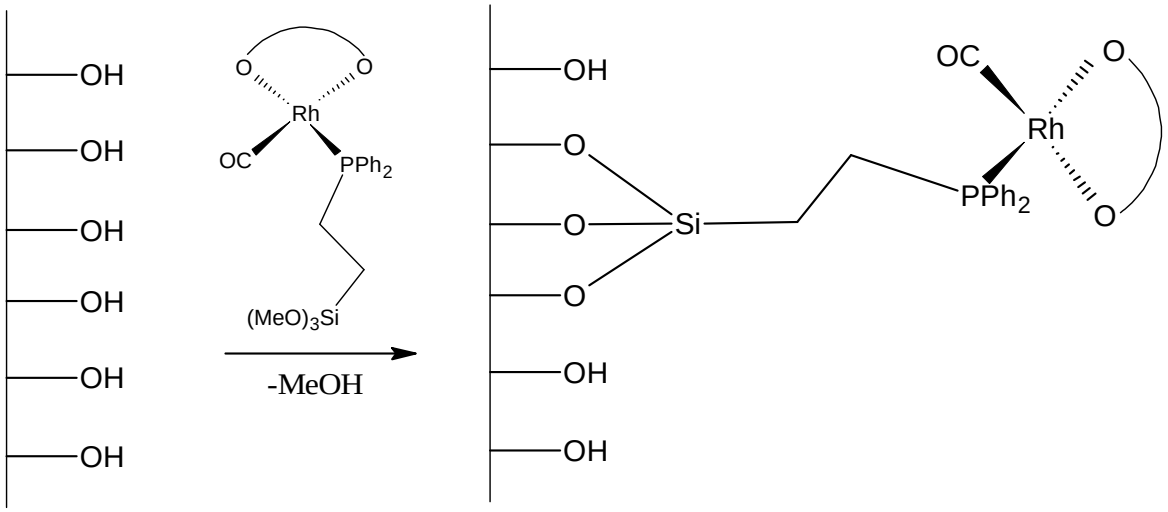

Scheme 1.7 Convergent immobilization as reported by Standfest-Hauser *et al.* [49]

1.3.2 Schiff-base ligands and their complexes

Nitrogen containing ligands have certain advantages when compared to their normal non-nitrogen containing counterparts. The abundance of nitrogen containing ligands

together with the rich chemistry of the nitrogen atom itself are the two main reasons why these types of ligands have received much attention recently. By using nitrogen containing starting materials, one is able to synthesize a wide range of different types of ligands with specific physicochemical properties. A wide range of ligands can be prepared and complexed to transition metals to form transition metal complexes which find wide application in catalysis.[50]

There are a few different types of ligand systems which are employed as ligands for the immobilization of metals such as palladium. The easiest way to synthesize a ligand that is suitable to form a metal complex for immobilization is to make use of a method called Schiff-base condensation. In 1864, Hugo Schiff described the reaction between an aldehyde and an amine and this led to the class of compounds being known as Schiff bases. Schiff bases are able to coordinate metals through the imine nitrogen and another heteroatom. This heteroatom can be oxygen, nitrogen or phosphine and normally forms part of the original aldehyde molecule. Salicylaldimines are examples of Schiff base complexes. These complexes are formed by the condensation of a primary amine with a hydroxybenzaldehyde group. The so-called Salen type ligand can just as easily be formed using a diamine instead of a mono-functionalized amine. In salicylaldimine complexes the metal coordinates to the imine and a phenol group situated on the aldehyde. This leads to so-called N, O chelating complexes. A phosphine can be used in the same way as nitrogen to form a unidentate or bidentate ligand to coordinate to the metal.[51]

The ligand system that was employed in this study is called a *N*,*N*' diimine ligand. Coordination in the *N*,*N*' diimine complexes differs only slightly from that seen in the

salicylaldimine complexes. Instead of the phenol oxygen group on the aldehyde coordinating to the metal, the nitrogen in the pyridine ring of the aldehyde coordinates together with the imine formed by Schiff base formation. This stabilizes the metal to form the metal complex. In Figure 1.5 some different types of Schiff-base ligands are shown.

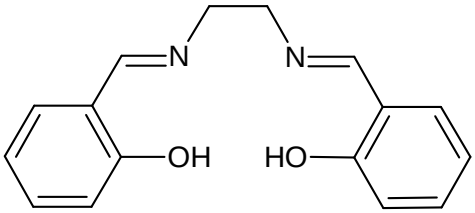

Salen Ligand

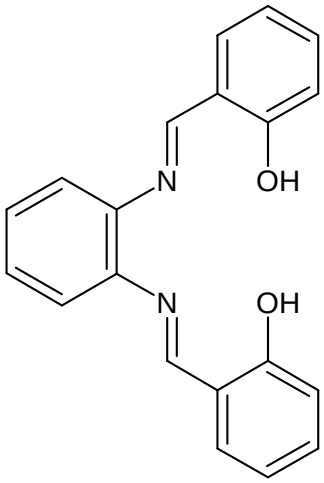

Salophen Ligand

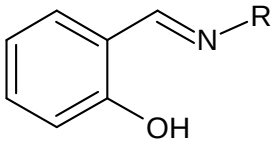

R = alkyl or aryl

Salicylaldimine Ligand

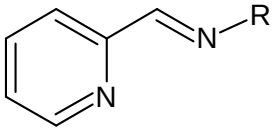

Pyridine diimine Ligand

Figure 1.5 Examples of different types of Schiff-base ligands

Metal complexes of these ligands are widely reported in the literature and find application as catalysts for numerous chemical transformations. Schiff base type ligands are especially widely studied because of the enhanced solubility it gives to the

homogeneous catalyst, at the same time being able to improve the stability of the heterogeneous counterpart.

1.4 Conclusions and Project objectives

1.4.1 Conclusions

Diimine Schiff base ligands are suitable ligand systems to coordinate transition metal complexes. The tunability and ease of synthesis of Schiff base ligands makes them ideal for the immobilization of transition metal complexes. Mesoporous silicas are widely employed as either supports for heterogenized catalysts or as catalysts themselves. Their varying pore sizes, high thermal stability and large surface areas make them very attractive for use as catalyst supports.

1.4.2 Project objectives

The aim of this project was to synthesize a range of *N,N*' diimine ligands, both model and siloxane functionalized, and to employ them to coordinate the appropriate palladium and copper salts to form the respective complexes. The synthesized model and functionalized Pd(II) and Cu(I) complexes were then fully characterized making use of various techniques. The functionalized complexes of Pd(II) and Cu(I) were immobilized on different silica supports and tested as oxidation catalysts.

Chapter one serves as a summary of work done on diimine ligand systems and their application as *N,N*' coordinating ligands to various metal salts. A thorough investigation

into the synthesis and applications of various mesoporous materials is done and ways of heterogenization of homogeneous complexes are investigated.

Chapter two deals with the synthesis of model and functionalized ligands through Schiff base condensation. All ligands were fully characterized by ^{1}H NMR and FT-IR spectroscopy. The complexation of the ligands to two different metal salts follows to produce Pd(II) and Cu(I) complexes. Model complexes are only characterized by ^{1}H NMR and FT-IR spectroscopy seeing that they were previously synthesized by another member of our group. The new functionalized ligands were also characterized by ^{13}C NMR spectroscopy.

In **Chapter three** the synthesis and characterization of the supports and immobilized catalysts are discussed. Various solid state techniques were employed to fully characterize the synthesized silica supports. Functionalized complexes of both palladium and copper were immobilized onto native, MCM-41 and SBA-15, as well as Ti-doped supports to produce the heterogenized catalysts. These were fully characterized and full characterization data is described.

The final chapter, **Chapter four**, focuses on the application of these synthesized catalysts in the oxidation of benzyl alcohol to benzaldehyde. Both the model and immobilized catalysts were tested and the results compared. ^{1}H NMR spectroscopy was employed to follow the reactions and calculate the various conversions.

Chapter five serves as a summary of the thesis and highlights the most important characterization information and results that were obtained for the alcohol oxidation reactions.

1.5 References

1 Stinson, S. C. *Chem. Eng. News*, **2001**, 79.

2 Johnson, N. B.; Lennon, I. C.; Moran, P. H.; Ramsden, J. A. *Acc. Chem. Res.* **2007**, 40, 1291.

3 Klingler, F. D. *Acc. Chem. Res.* **2007**, *40*, 1367.

4 Barbaro, P.; Liguori, F. *Chem. Rev*. **2009**, 109, 515.

5 McMorn, P.; Hutchings, G. *J. Chem. Soc. Re*v. **2004**, *33*, 108.

6 Jones, M. D.; Raja, R.; Thomas, J. M.; Johnson, B. F. G. *Top. Catal.* **2003**, *25*

7 Anderson, S.; Yang, H.; Tanielyan, S. K.; Augustine, R. L. *Chem. Ind.* **2001**, *82*, 557.

8 Song, C. E.; Lee, S. G. *Chem. Rev.* **2002**, *102*, 3495.

9 De Vos, D. E.; Dams, M.; Sels, B. F.; Jacobs, P. A. *Chem. Rev.* **2002**, *102*, 3615.

10 Van Heerbeek, R.; Kamer, P. C. J.; Van Leeuwen, P. W. N. M.; Reek, J. N. H. *Chem. Rev.* **2002**, *102*, 3717.

11 Hodge, P. *Chem. Soc. Rev.,* **1997**, *26*, 417.

12 Thomas, J. M.; Johnson, B. F. G.; Raja, R.; Sankar, G.; Midgley, P. A. *Acc. Chem. Res.* **2003**, 36, 20

13 Bein, T. *Curr. Opin. Solid State Mater. Sci.* **1999**, *59*, 73.

14 Zhao, X. S.; Bao, X. Y.; Guo, W.; Yin Lee, F. *Mater. Today* **2006**, 9, 33-38

15 Bianchini, D. G.; Burnaby, Evans, J.; Frediani, P.; Meli, A.; Oberhauser, W.; Psaro, R.; Sordelli, L.; Vizza, F. *J. Am. Chem. Soc*. **1999**, 121, 5961.

16 Fraile, J. M.; García, J. I.; Mayoral, J. A. *Chem. Rev.* **2009,** *109,* 360.

17 Díaz, J. F.; Balkus K. J. *J. Mol. Catal. B: Enzym*. **1996,** 2, 115

18 Gelman, F.; Avnir, D.; Schumann, H.; Blum, J. *J. Mol. Catal. A* **1999**, *146*, 123.

19 Zhang, R.; Yu, W.-Y.; Wong, K.-Y.; Che, C.-M. *J. Org. Chem.* **2001**, *66*, 8145.

20 Li, Y.; Feng, Z.; van Santen, R.; Hensen, E.; Li, C. *J. Catal.* **2008**, *255, 190.*

21 Di Renzo, F.; Testa, F.; Chen, J. D.; Cambon, H.; Galarneau, A.; Plee, D.; Fajula, F. *Micropor. Mesopor. Mater*. **1999**, 28, 437.

22 Tanev, P.; Pinnavaia, T. J. *Chem. Mater*. **1996**, 8, 2068.

23 Ramírez, A.; Lopez, B. L.; Sierra, L. *J. Phys. Chem. B* **2003**, 107, 9275.

24 Yanagisawa, Tsuneo; Shimizu, Toshio; Kuroda, Kazuyuki; Kato, Chuzo *Bull. Chem. Soc. Jpn.,* **1990**, 63, 988.

25 Beck, J. S.; Vartuli, J. C.; Roth, W. J.; Leonowicz, M. E.; Kresge, C. T.; Schmitt, K. D.; Chu, C. T.-W.; Olson, D. H.; Sheppard, E. W.; McCullen, S. B.; Higgins, J. B.; Schlenkert, J. L. *J. Am, Chem, Soc.* **1992**, 114, 10834.

26 Trewyn, B. G.; Slowing, I. I.; Giri, S.; Chen, H.-T.; Lin, V. S.-Y. *Acc. Chem. Res.* **2007**, 40, 846.

27 Zhao, D.; Feng, J.; Huo, Q.; Melosh, N.; Fredrickson, G. H.; Chmelka, B. F.; Stucky, G. D., *Science*, **1998**, 279, 548.

28 Zhao, X. S.; Lu, G. Q.; Millar, G. J.; Whittaker, A.J.; Zhu, H. Y., *J. Phys. Chem. B*. **1997**, 101, 6525.

29 Kresge, C. T.; Leonowicz, M. E.; Roth, W. J.; Vartuli, J. C.; Beck, J. S. *Nature,* **1992**, 359, 710.

30 Jung, J. S.; Chae, W. S.; McIntyre, R.A.; Seip, C. T.; Wiley, J. B.; O'Connor, C. J. *Mater. Res. Bull*. **1999**, 34, 1353.

31 Hsien, M.; Sheu, H. T.; Lee, T.; Cheng, S.; Lee, J.F. *J. Mol. Catal. A:-Chem*. **2002**, 181, 189.

32 Luo, Y.; Lu, G .Z.; Guo, Y. L.; Wang, Y.S. *Catal. Commun*. **2002**, 3, 129.

33 Brunel, D. *Micropor. Mesopor. Mater*. **1999**, 27, 329.

34 Moller, K.; Bein, T. *Chem. Mater*. **1998**, 10, 2950.

35 Zhang, A.; Li, Z.; Li, Z.; Shen, Y.; Zhu, Y. *Appl. Surf. Sci.* **2008**, 254, 6298.

36 Giraldo, L. F.; Lopez, B. L.; Pérez, L.; Urrego, S.; Sierra, L.; Mesa, M. *Macromol. Symp.* **2007**, 258, 129.

37 Inagaki, S. O.; Goto, S.; Fukushima, Y. *Stud. Surf. Sci. Catal*. **1998**, 117, 65.

38 Gallis, K. W.; Eklund, A. G.; Jull, S. T.; J Araujo,. T. J.; Moore, G.; C. Landry, C. *Stud. Surf. Sci. Catal*. **2000**, 129, 747.

39 Izquierdo-Barba, I.; Sousa, E.; Doadrio, J. C.; Doadrio, A. L.; Pariente, J. P.; Martínez, A.; Babonneau, F.; Vallet-Regi, M. *J. Sol-Gel Sci. Technol.* **2009**, 50, 421.

40 Ryoo, R.; Joo, S. H.; Jun, S. *J. Phys. Chem. B* **1999**, 103, 7743.

41 Sing, K. S. W.; Everett, D. H.; Haul, R. A. W.; Moscou, L.; Pierotti, R. A.; Rouquerol, J.; Siemieniewska, T. *Pure Appl. Chem*. **1985,** 57, 603.

42 Taguchi, A.; Schüth, F. *Micropor. Mesopour. Mat.* **2005**, 77, 1.

43 Mureşeanu, M.; Pârvulesc, V.; Ene, R.; Cioateră, N.; Pasatoiu, T. D.; Andruh, M. *J. Mater. Sci.* **2009**, 44, 6795.

44 Lim, J.; S. Lee, S.; Ying, J. Y. *Chem. Commun*. **2010**, 46, 806.

45 Wang, H.-L.; Li, R.; Zheng, Y.-F.; Chen, H.-N.; Jin, J.; Wang, F.-S.; Ma, J.-T. *Helv. Chim. Acta.* **2007**, 90, 1837.

46 Horniakova, J.; Raja, T.; Kubota, Y.; Sugi, Y. *J. Mol. Catal. A: Chem.*, **2004**, 217, 73.

47 Dams, M.; Drijkoningen, L.; Pauwels, Van Tondeloo, B.; De Vos, G. D.E.; Jacobs, P.A. *J. Catal*. **2002**, 209, 225.

48 Zhao, F.; Shirai, M.; Ikushima, Y.; Arai, M. *J. Mol. Catal. A: Chem.* **2002**, 180, 211.

49 Standfest-Hauser, C. M.; Lummerstorfer, T.; Schmid, R.; Hoffmann, H.; Kirchner, K.; Puchberger, M.; Trzeciak,A. M.; Mieczyńska, E.; Tylus, W.; Ziółkowski J. J. *J. Mol. Catal. A: Chem.* **2004**, 210, 179

50 González-Arellano, C.; Corma, A.; Iglesias, M.; Sánchez, F. *Catal. Today.* **2005**, 362, 107.

51 Liang, L.; Chien P.; Huang, M. *Organometallics,* **2005**, 24, 353.

Chapter 2: Synthesis and Characterization of Schiff Base Ligands and Complexes

2. Introduction

Schiff bases, also known as azomethine derivatives, are compounds that contain a carbon-nitrogen double bond with the nitrogen being bonded to an aryl or alkyl group. These types of compounds can easily coordinate transition metals and have found a wide range of applications in chemistry. Schiff base ligands are typically formed by the condensation of primary amines and aldehydes. The formed imine can bind metal ions via the lone pair electrons on the nitrogen. Ketones can just as easily be applied to form a Schiff base ligand but react much less readily when compared to their aldehyde counterparts.[1]

Schiff base condensation allows for the design of new ligand systems which are selective to specific metal ions. This makes them suitable to be applied as metal extracting agents in liquid-liquid or solid phase extraction techniques.[2,3] It is in catalysis though where these types of ligands have come into their own either as homogeneous or heterogeneous catalysts. Metal complexes of Schiff base ligands have found application in catalysis as precursors for ethylene polymerization, in Heck-type reactions and in the selective oxidation of styrene to benzaldehyde to name but a few examples.[4-7]

The ease of formation of Schiff base ligands make them ideal as suitable precursors to prepare catalyst systems where homogeneous catalysts need to be “heterogenized”. A good example of the versatility of Schiff base ligands was reported by Guo and his

group.[7] They used the ease of Schiff base condensation to synthesize a range of monosubstituted transition metal Keggin-type polyoxometalates (mono-TMKPs) impregnated on the mesoporous silica material, SBA-15. By employing successive grafting procedures of SBA-15 silica with 3-aminopropyltrimethoxysilane, benzaldehyde, and mono-TMSP they were able to easily synthesize the required compounds. Scheme 2.1 shows the condensation of the surface silanols of the SBA-15 with the 3-aminopropyltrimethoxysilane, followed by the Schiff base condensation reaction between the primary amine on the support with benzaldehyde. Examples where these types of ligands are complexed with transition metal and subsequently employed in catalysis or chemical transformations are plentiful.

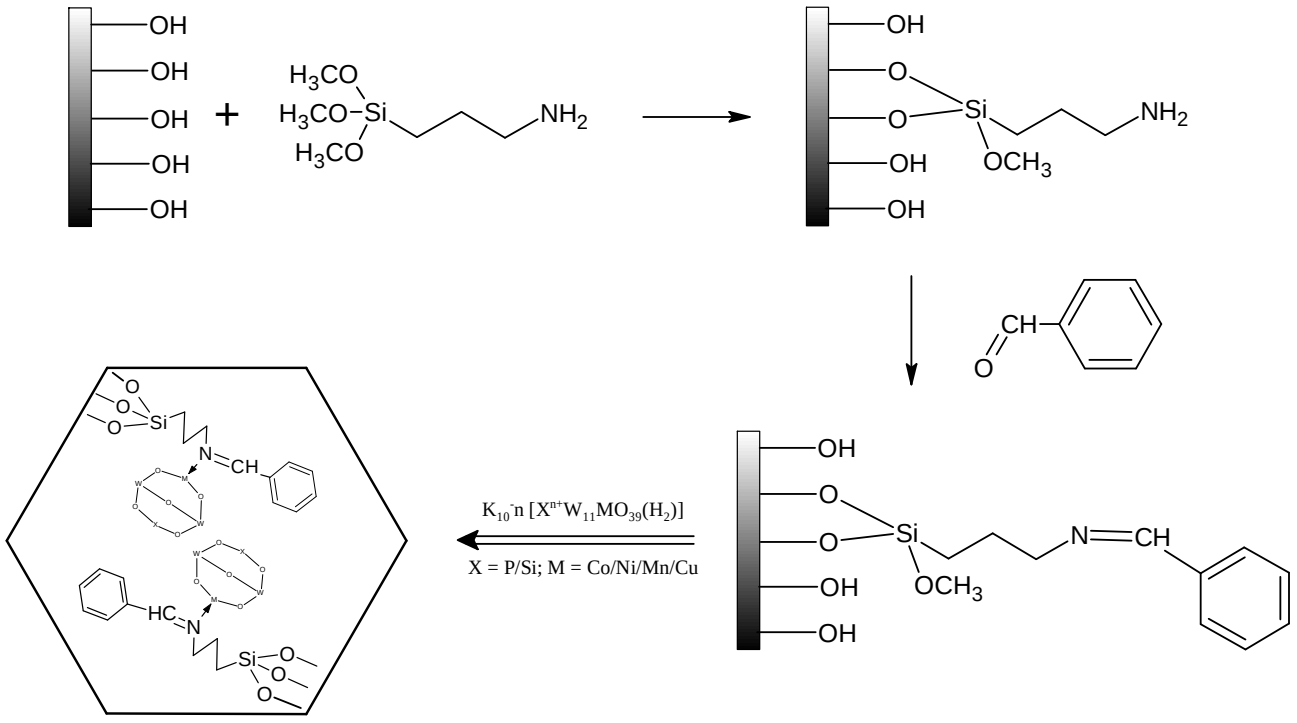

Scheme 2.1 Pathway of preparation of Schiff base-modified ordered mesoporous silica materials incorporated with mono-TMKPs.[7]

Murphy *et al.* [8] reported on novel ways to effectively immobilize transition metal complexes on inert inorganic supports like silica. Two distinctly different approaches for ligand synthesis, convergent and sequential, were investigated by them and are shown in Scheme 2.2.

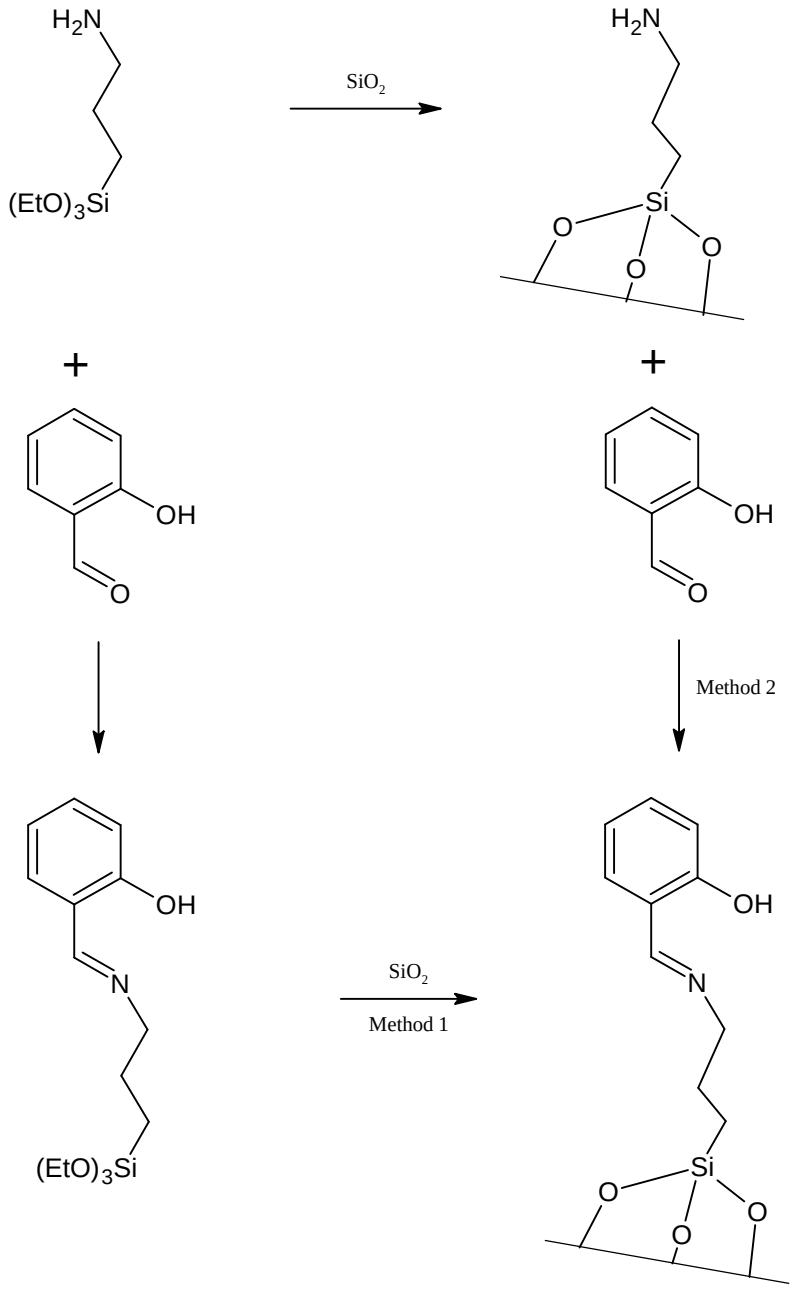

Scheme 2.2 Preparation and immobilization routes of salen HSi[8]

Method 1 involves the reaction between the aldehyde and 3-aminopropyltriethoxysilane followed by the subsequent condensation of the functionalized imine with SiO_2. The second method involves the reaction (condensation) between SiO_2 and 3-aminopropyltriethoxysilane followed by the Schiff base condensation of the immobilized *n*-propylamine with the aldehyde. These different synthetic methods on face value do not seem to be that different, but a possible problem presents itself when one wants to complex a metal to the ligand. When the functionalized ligand is firstly synthesized, and the metal complex formed from it, there is no doubt that when the complex is immobilized, that all of the metal salt is coordinated in the ligand. For this reason the first approach was followed in our study; formation of the functionalized metal complex, followed by immobilization on the silica supports.

Different types of Schiff base ligands are known and have been widely reported in the literature. The diimine ligand system was chosen for this study because of its ease of synthesis and coordination of transition metal ions. The mesoporous silicas, MCM-41 and SBA-15, were used as inorganic supports.

2.1 Synthesis and characterization of model ligands and siloxane functionalized ligands

The synthesis of pyridinyl and quinolyl diimine ligands was adapted from work previously reported in literature.[4,12,13] All ligands were synthesized by making use of normal Schlenk techniques under nitrogen atmosphere. Ligand **L1** was synthesized as

previously reported and the same synthetic procedure was employed for the synthesis of all the other ligands.[11] Ligands **L1**-**L3** (model ligands) were synthesized by the condensation of either pyridine-2-carboxaldehyde or quinoline-2-carboxaldehyde with *n*-propylamine in a 1:1 ratio (diethyl ether as solvent and anhydrous $MgSO_4$ to remove any formed water). Synthesis of functionalized ligands **L4**-**L6** was achieved via a modified method where *n*-propylamine was replaced with 3-aminopropyltriethoxysilane. All of these ligands were isolated as either yellow or colorless oils. A general synthetic procedure is shown in Scheme 2.3.

The model ligands **L1**-**L3** were found to be very stable in air and in solution and no hydrolysis of the imine bond was observed. For ligands **L4**-**L6** hydrolysis of the siloxane tail occurred when these ligands were left in air for extended periods of time and they were therefore stored in a glovebox.

2.1.1 Characterization of ligands

All ligands were characterized by ^{1}H NMR and FT-IR spectroscopy.

2.1.1.1 Characterization of ligands by means of ^{1}H NMR spectroscopy

^{1}H NMR spectra of all of the synthesized diimine ligands **L1**-**L6** show the expected resonances for both the aliphatic (0.55 – 3.85 ppm) and the aromatic (8.56 – 7.19 ppm) regions. For the siloxane functionalized pyridinyl ligand **L4**, Figure 2.1, five resonances are expected for the aromatic as well as the aliphatic region. The H-1 protons (corresponding to 9 protons) of the methyl group on the siloxane functionality resonates as a triplet (δ 1.17 ppm) while methylene (H-2) protons (corresponding to 6 protons)

resonates as a quartet at δ 3.77 ppm. The methylene protons are deshielded by the oxygen atom bound to the silica and results in a shift to the downfield region.

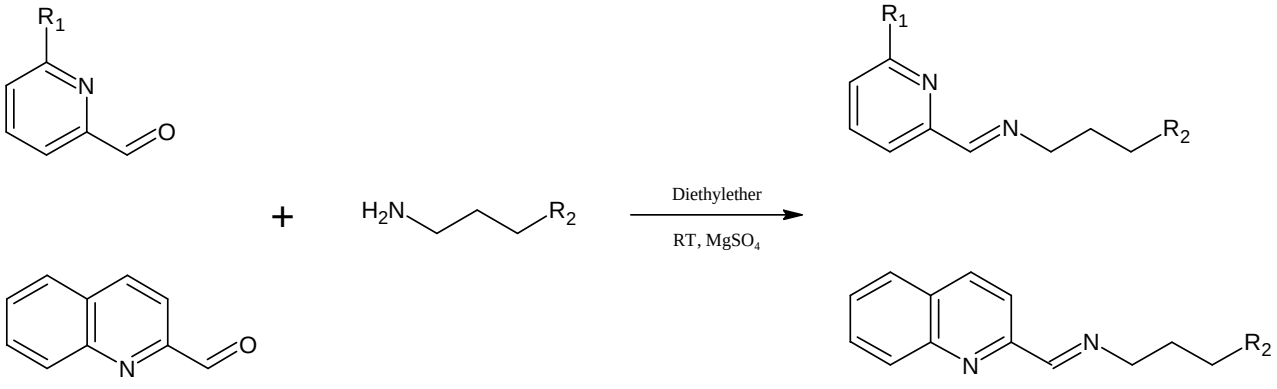

L1; $R_1 = R_2 = H$

L2; $R_1 = CH_3$, $R_2 = H$

L3; $R_2 = H$ (Quinoline)

L4; $R_1 = H$, $R_2 = Si(OEt)_3$

L5; $R_1 = CH_3$, $R_2 = Si(OEt)_3$

L6; $R_2 = Si(OEt)_3$ (Quinoline)

Scheme 2.3 General reaction scheme for the synthesis of model and functionalized ligands

The methylene protons of the propyl chain are found at δ 0.64 (H-3), δ 1.81 (H-4) and δ 3.63 (H-5) ppm respectively. The most downfield of these is the triplet of the H-5 protons because of the deshielding by the nitrogen atom of the imine. Of the four aromatic resonances, H-11 is found the furthest downfield at δ 8.59 ppm (doublet) being deshielded more by the nitrogen of the pyridine ring than the other protons. The other three resonances are found at δ 7.94 (doublet), δ 7.68 (triplet) and δ 7.26 ppm (triplet)

respectively. An important resonance is the singlet found at 8.32 ppm corresponding to the imine proton formed during the Schiff base condensation reaction.

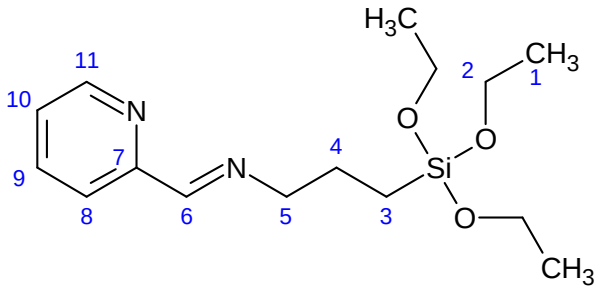

Figure 2.1 Siloxane functionalized pyridine ligand (L4)

The full ^{1}H NMR spectra for ligand **L4** is shown in Figure 2.2. The sample was run in chloroform-*d*. The resonance at 5.25 ppm corresponds to a small amount of DCM that was trapped in the oil after workup.

The complete ^{1}H NMR data for ligands **L1**-**L6** are summarized in Table 2.1.

2.1.1.2 Characterization of ligands by means of FT-IR (ATR) spectroscopy

The Schiff base condensation reaction to synthesize the ligands was followed by FT-IR spectroscopy. The disappearance of the aldehyde stretch of the carboxaldehyde and the subsequent formation of the imine during the condensation reaction were used to follow the reaction progress. The aldehyde stretch, depending on the carboxaldehyde used, appears at around 1700-1720 cm^{-1}, whereas the formed imine is found in the region of 1645-1659 cm^{-1}.

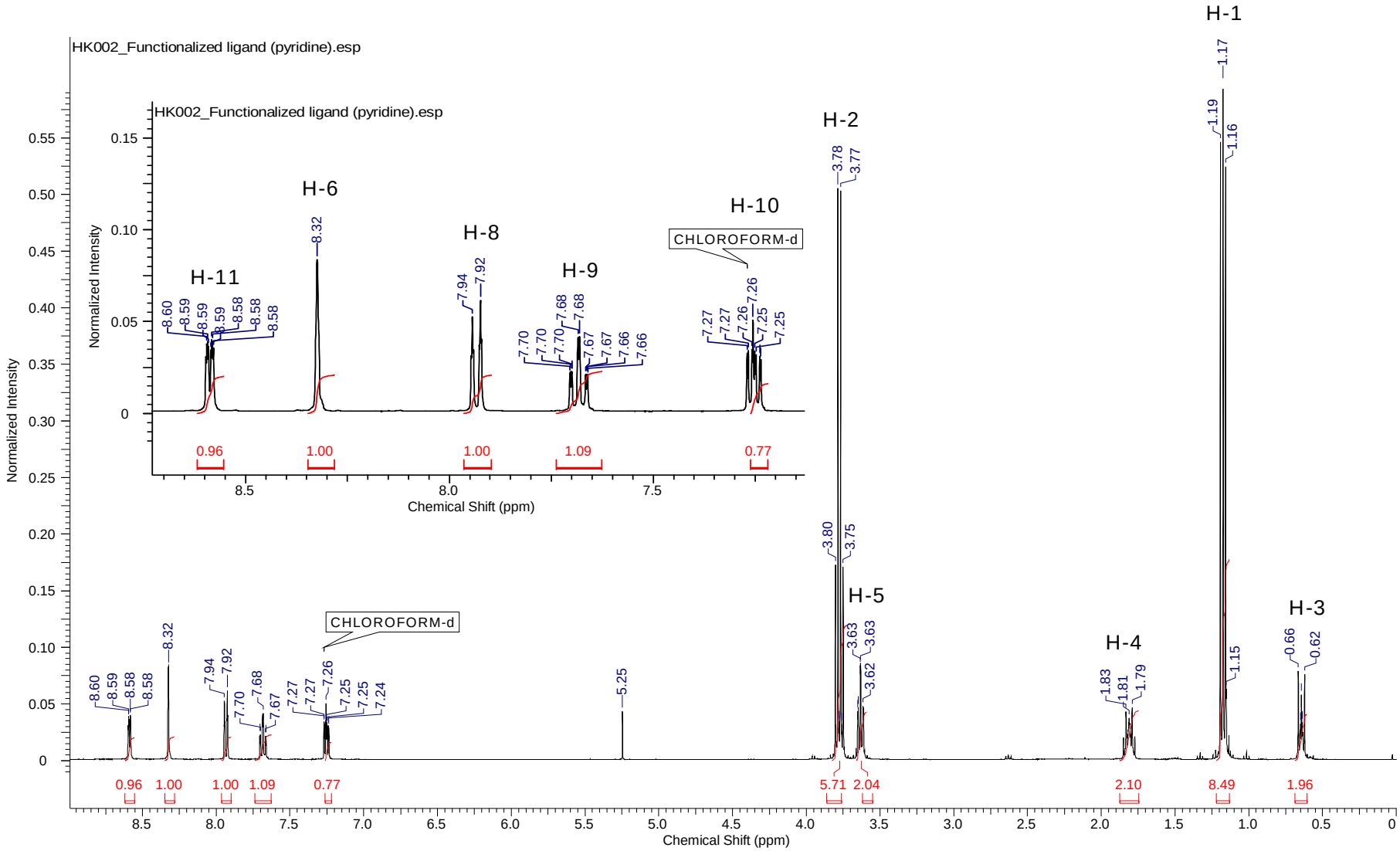

Figure 2.2 ^{1}H NMR spectra of L4 (functionalized pyridinyl ligand)

Table 2.1 ^{1}**H NMR data for model and siloxane functionalized ligands L1-L6**[c]

Ligand	-O-CH_2-CH_3	-Si-O-CH_2-	[a]-CH_2-CH_3 [b]-CH_2-Si-	[a]-CH_2-CH_2-CH_3 [b]-CH_2-CH_2-Si	-N-CH_2-CH_2-	Ar-H	Ar-CH_3	-N=CH-
L1[a]			0.86 (t, *J* = 6 Hz)	1.65 (m)	3.54 (t, *J* = 6 Hz)	8.54 (d, *J* = 3 Hz) 7.88 (d, *J* = 9 Hz) 7.62 (t, *J* = 6 Hz) 7.19 (t, *J* = 6 Hz)		8.27 (s)
L2[a]			0.93 (t, *J* = 6 Hz)	1.72 (m)	3.60 (t, *J* = 6 Hz)	7.77 (d, *J* = 6 Hz) 7.59 (t, *J* = 9 Hz) 7.14 (d, *J* = 9 Hz)	2.56 (s)	8.33 (s)
L3[a]			1.00 (t, *J* = 4 Hz)	1.80 (m)	3.73 (t, *J* = 8 Hz)	8.20 (d, *J* = 9 Hz) 8.16 (d, *J* = 4 Hz) 8.14 (d, *J* = 8 Hz) 7.85 (d, *J* = 8 Hz) 7.75 (t, *J* = 8 Hz) 7.58 (t, *J* = 8 Hz)		8.56 (s)
L4[b]	1.17 (t, *J* = 6 Hz)	3.78 (m)	0.64 (t, *J* = 9 Hz)	1.81 (m)	3.63 (t, *J* = 6 Hz)	8.59 (d, *J* = 6 Hz) 7.92 (d, *J* = 6 Hz) 7.68 (t, *J* = 9 Hz) 7.26 (t, *J* = 9 Hz)		8.32 (s)

L5[b]	1.14 (t, *J* = 9 Hz)	3.74 (m)	0.55 (t, *J* = 9 Hz)	1.47 (m)	3.85 (t, *J* = 6 Hz)	7.71 (d, *J* = 9 Hz) 7.54 (t, *J* = 9 Hz) 7.09 (d, *J* = 6 Hz)	2.52 (s)	8.26 (s)
L6[b]	1.23 (t, *J* = 8 Hz)	3.84 (m)	0.73 (t, *J* = 8 Hz)	1.90 (m)	3.76 (t, *J* = 4 Hz)	8.19 (d, *J* = 8 Hz) 8.15 (d, *J* = 8 Hz) 8.13 (d, *J* = 8 Hz) 7.85 (d, *J* = 8 Hz) 7.74 (t, *J* = 8 Hz) 7.58 (t, *J* = 8 Hz)		8.55 (s)

[c] Measured in Chloroform-*d*

Other stretches of importance are found between 1586-1696 cm^{-1} and between 1560-1573 cm^{-1} for the *υ*(C=N) and *υ*(C=C) vibrations of the pyridine ring respectively. For the siloxane functionalized ligands **L4**-**L6**, very intense stretches are observed at 1072-1100 cm^{-1} and 751-791 cm^{-1}. These vibrations correspond to the Si-O which forms part of the siloxane tail of the functionalized ligands. Table 2.2 gives a summary for all of these important vibrations of ligands **L1**-**L6**. A typical IR spectra for the siloxane functionalized ligand, **L4** is shown in Figure 2.3.

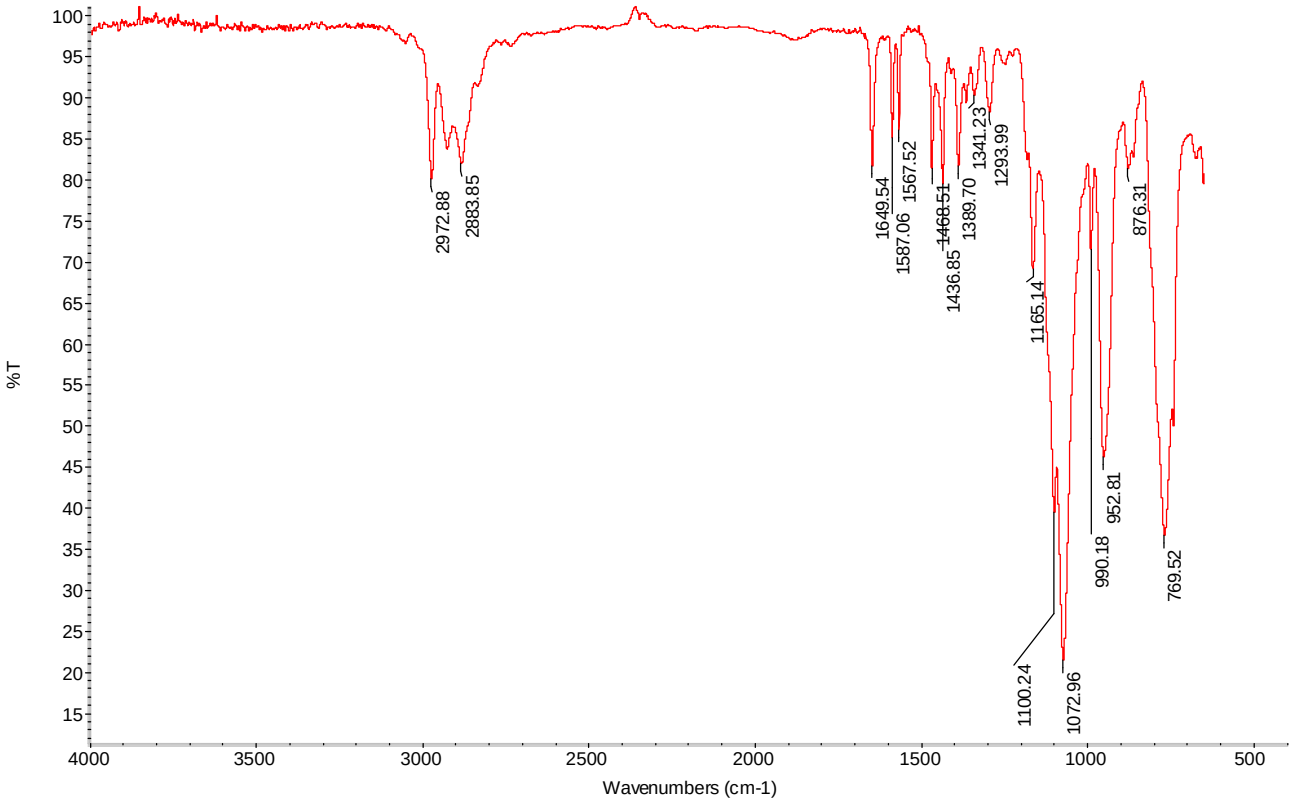

Figure 2.3 FT-IR(ATR) spectra for siloxane functionalized ligand L4

Table 2.2 Summary of IR vibrations of model and siloxane functionalized ligands[a]

Ligand	*u*(C=N) cm^{-1}	Pyridine ring		*u*(Si-O-Si) cm^{-1}	*u*(Si-OH) cm^{-1}
		u(C=N) cm^{-1}	*u*(C=C) cm^{-1}		
L1	1649	1586	1567	-	-
L2	1649	1591	1573	-	-
L3	1645	1596	1561	-	-
L4	1649	1587	1567	1073-1100	770
L5	1649	1590	1573	1072-1100	766-791
L6	1645	1596	1560	1073-1100	751

[a] Oils recorded as neat samples using ATR accessory

2.2. Synthesis and characterization of model and siloxane functionalized Pd(II) complexes

Numerous examples of palladium pyridinyl and quinolyl diimine complexes have been reported in the literature, including previous work done by our research group.[5,6,9] Synthesis of the siloxane functionalized complexes, making use of the convergent approach, however is not widely seen. The synthesis of immobilized catalysts on supports is mostly reported by making use of the sequential synthesis method. Horniakova *et al.* [5,6] have reported the synthesis of both the pyridine and quinoline derived immobilized complexes of palladium. Scheme 2.4 shows the route followed for the synthesis of the immobilized pyridine complex making use of the sequential approach.

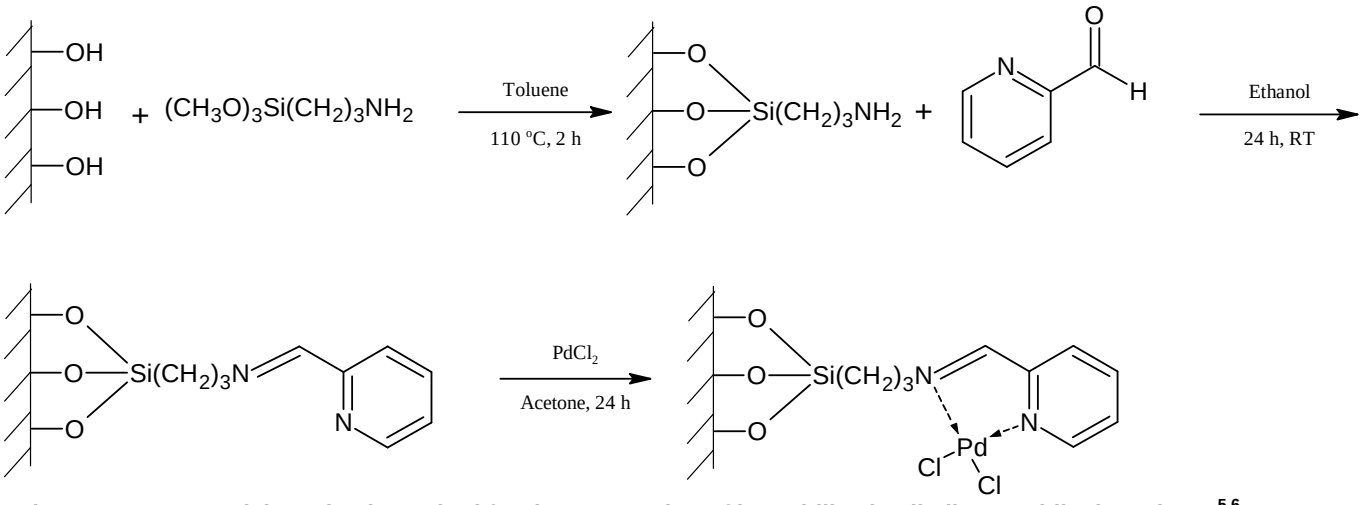

Scheme 2.4 Sequential synthesis method for the preparation of immobilized palladium-pyridinyl catalysts.[5,6]

Cloete[4] and Mketo *et al* [10] reported the synthesis of model-and dendritic complexes utilizing the same type of ligand systems. This synthetic procedure was adapted for the synthesis of the functionalized complexes reported here.

Both the model and functionalized metal complexes of palladium were synthesized by reacting the palladium precursor $Pd(CH_3CN)_2Cl_2$ with the ligands in a 1:1 mol ratio in dichloromethane as solvent for 3-8 hours under nitrogen atmosphere. After the allotted reaction time, the solvent was removed and a solid was obtained as product. The products ranged from pale yellow powders to bright orange needle like crystals. All of the complexes were purified by washing the formed solid in a suitable solvent (one in which the ligand is soluble and the complex not) to remove any unreacted ligand. A general reaction scheme for the synthesis of the model and functionalized complexes is given in Scheme 2.5.

2.2.1 Characterization of Pd(II) complexes

All complexes were characterized by FT-IR (ATR) spectroscopy, thermal analysis, ^{1}H NMR and $^{13}C\{^{1}H\}$ NMR spectroscopy (functionalized complexes).

2.2.1.1 Characterization of Pd(II) complexes by means of FT-IR (ATR) spectroscopy

IR spectroscopy was also used to prove successful complexation of the metal to the ligand. An average shift of 45-50 cm^{-1} in the imine vibration to lower wave number was observed for all the complexes compared to the ligands. This shift, brought on by the change in double bond character of the imine, proved coordination of the palladium to the ligand. A summary of these shifts is shown in Table 2.3.

Model complexes **C1**-**C3** were found to be very stable and had melting points between 190-233 ℃.

No other significant shifts in wave numbers are observed for any of the major vibrations. The bands of the silica vibrations of the functionalized complexes were still visible and confirmed that no hydrolysis of the siloxane functionality occurred.

Functionalization of the complexes (**C4**-**C6**) had a dramatic effect on the thermal stability of the complexes with an increase in melting point of between 30-60 ℃.

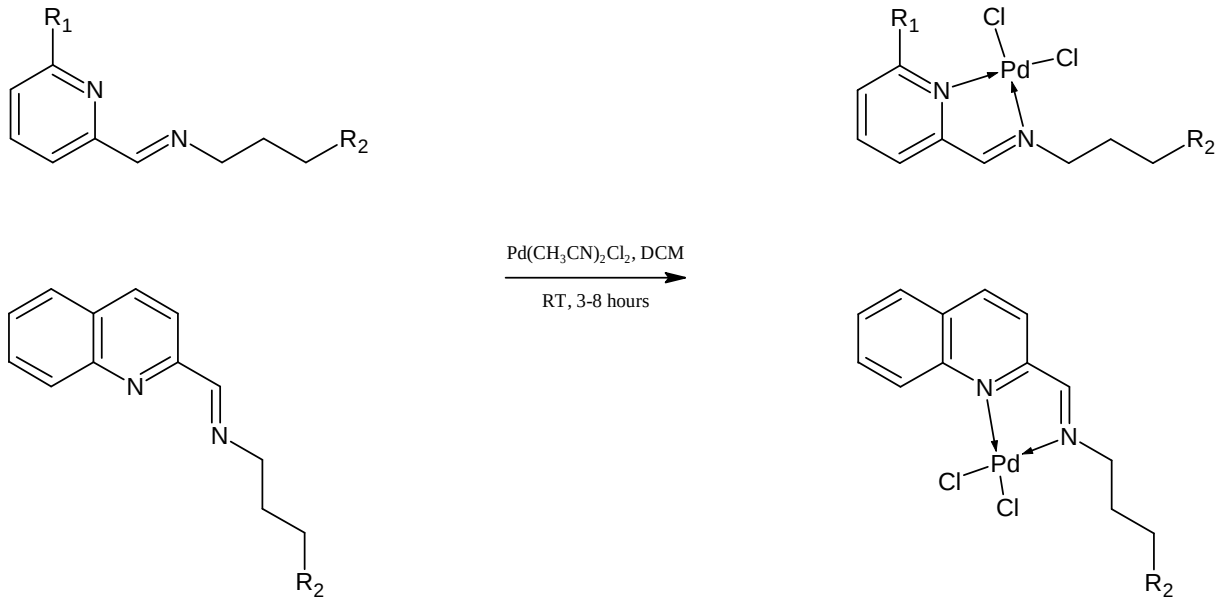

C1; $R_1 = R_2 = H$

C2; $R_1 = CH_3$, $R_2 = H$

C3; $R_2 = H$ (Quinoline)

C4; $R_1 = H$, $R_2 = Si(OEt)_3$

C5; $R_1 = CH_3$, $R_2 = Si(OEt)_3$

C6; $R_2 = Si(OEt)_3$ (Quinoline)

Scheme 2.5 General synthesis scheme for the synthesis of model and functionalized Pd(II) complexes

Table 2.3 Summary of shifts for imine vibrations (ATR)[a]

L/C	*u*(C=N) cm^{-1}		Melting point of complexes (℃)
	Ligand	Complex	
1	1649	1601	219-222
2	1649	1603	190-193
3	1645	1597	233-235
4	1649	1601	289-291
5	1649	1602	291-292
6	1645	1592	265-267

[a] Oils recorded as neat samples using ATR accessory

2.2.1.2 Characterization of Pd(II) complexes by means of ^{1}H NMR spectroscopy

All complexes were mainly characterized by making use of ^{1}H NMR spectroscopy. All of the model complexes have been previously synthesized and fully characterized by members of our group.[10] The siloxane functionalized complexes differ only slightly from their model counterparts and ^{1}H NMR spectroscopy proved sufficient to confirm successful synthesis. Table 2.4 gives a summary of the ^{1}H NMR data for complexes **C1**-**C6** with their appropriate assignments. The most important resonance is found between 8.57-8.88 ppm for the complexes. This resonance corresponds to that of the imine formed during the Schiff base condensation. A shift in this resonance is observed for all the complexes and provides proof that successful complexation occurred. An example is the downfield shift from 8.27 ppm for ligand **L1** to 8.60 ppm for complex **C1**. This shift is attributed to the change in double bond character of the imine caused by the ligand coordinating to the metal.

Table 2.4 ^{1}**H NMR data for model and siloxane functionalized Pd(II) complexes C1-C6**[c]

Complex	-O-CH_2-CH_3	-Si-O-CH_2-	[a]-CH_2-CH_3 [b]-CH_2-Si-	[a]-CH_2-CH_2-CH_3 [b]-CH_2-CH_2-Si	-N-CH_2- CH_2-	Ar-H	Ar-CH_3	-N=CH-
C1[a]			0.88 (t, *J* = 6 Hz)	1.77 (m)	3.67 (t, *J* = 6 Hz)	8.97 (d, *J* = 6 Hz) 8.34 (t, *J* = 6 Hz) 8.08 (d, *J* = 9 Hz) 7.86 (t, *J* = 6 Hz)		8.60 (s)
C2[a]			0.91 (t, *J* = 6 Hz)	1.85 (m)	3.76 (t, *J* = 9 Hz)	8.18 (t, *J* = 9 Hz) 7.95 (d, *J* = 6 Hz) 7.67 (d, *J* = 9 Hz)	3.05 (s)	8.58 (s)
C3[a]			0.91 (t, *J* = 6 Hz)	1.87 (m,)	3.74 (t, *J* = 6 Hz)	8.95 (d, *J* = 9 Hz) 8.16 (d, *J* = 9 Hz) 8.13 (d, *J* = 9 Hz) 8.08 (d, *J* = 9 Hz) 7.94 (t, *J* = 6 Hz) 7.83 (t, *J* = 6 Hz)		8.81 (s)
C4[b]	1.16 (t, *J* = 6 Hz)	3.76 (m)	0.55 (t, *J* = 9 Hz)	1.85 (m)	3.68 (t, *J* = 6 Hz)	8.96 (d, *J* = 6 Hz) 8.34 (t, *J* = 6 Hz) 8.08 (d, *J* = 9 Hz) 7.86 (t, *J* = 6 Hz)		8.57 (s)

C5[b]	1.14 (t, *J* = 9 Hz)	3.76 (m)	0.55 (t, *J* = 3 Hz)	1.84 (m)	3.68 (t, *J* = 6 Hz)	7.71 (d, *J* = 9 Hz) 7.54 (t, *J* = 9 Hz) 7.09 (d, *J* = 6 Hz)	2.52 (s)	8.57 (s)
C6[b]	1.19 (t, *J* = 9 Hz)	3.83 (m)	0.64 (t, *J* = 9 Hz)	1.90 (m)	3.92 (t, *J* = 6 Hz)	9.82 (d, *J* = 9 Hz) 8.90 (d, *J* = 6 Hz) 8.25 (d, *J* = 9 Hz) 8.18 (d, *J* = 9 Hz) 7.91 (t, *J* = 6 Hz) 7.84 (t, *J* = 6 Hz)		8.86 (s)

[c] Measured in Chloroform-*d*

2.2.1.3 Characterization of Pd(II) complexes by means of ^{13}C NMR

Model complexes and ligands were synthesized and fully characterized by a member of our group and thus only functionalized complexes were characterized with ^{13}C NMR spectroscopy. Unfortunately we were unable to obtain ^{13}C NMRs for the functionalized Cu(I) complexes. A summary of the chemical shifts of important signals are shown in Table 2.5. An average downfield shift in the imine resonance of the functionalized Pd(II) complexes from 161-172 ppm was observed.

2.3. Synthesis and characterization of model and siloxane functionalized Cu(I) complexes

Copper complexes were synthesized by reacting the model and siloxane functionalized ligands with an appropriate copper precursor in a 2:1 ligand to metal ratio. These reactions were carried out in dichloromethane as solvent, under nitrogen at room temperature being stirred for 3-8 hours, depending on the ligand. Complexes **C7**, **C8**, **C10** and **C11** were obtained as dark brown solids, whereas complexes **C9** and **C12** were obtained as bright purple solids after workup. The workup of these complexes was slightly more difficult than complexes **C1**-**C6** and required more time to solidify the products.

The three model copper complexes **C7**-**C9** only required the removal of some of the DCM used as solvent followed by the addition of diethyl ether.

Table 2.5 Summary of $^{13}C\{^{1}H\}$ NMR resonances of functionalized ligands and Pd(II) complexes

Ligand and complex	Siloxane tail		Imine	Aromatic region	Propyl linker
	-O-$\underline{C}H_2$-CH_3	-O-CH_2-$\underline{C}H_3$	($\underline{C}$H=N)		
L4[a]	58.31	18.23	161.85	154.56, 149.30, 136.46, 124.54, 121.11	64.04, 24.05, 8.02
L5[a]	58.13	18.35	162.27	158.03, 153.95, 136.76, 124.28, 118.17, 27.04 (Ar-$\underline{C}H_3$)	64.08, 27.04, 9.90
L6[a]	58.74	18.66	162.82	155.24, 148.13, 136.83, 130.10, 129.93, 129.08, 128.04, 127.68, 118.73	64.56, 24.52, 8.48
C4[b]	57.27	17.68	170.73	155.35, 149.46, 140.69, 127.90, 121.47	61.01, 23.21, 6.34
C5[b]	59.00	18.80	171.57	167.59, 156.93, 140.90, 131.85, 126.71, 27.53 (Ar-$\underline{C}H_3$)	62.88, 25.12, 8.12
C6[b]	58.17	18.12	169.04	159.56, 140.84, 130.75, 130.75, 129.27, 126.32, 123.43, 120.37, 117.75	72.14, 23.53, 14.95

[a] Measured in Chloroform-*d*

[b] Measured in Acetone-d_8

The dark brown or purple mixtures were left in a fridge overnight and formed brown and purple solids respectively and were filtered off.

For the siloxane functionalized complexes the same route was attempted without any success. The adapted approach relied on the addition of a small amount of hexane to the mixture of DCM and ether before any solid products could be obtained. The complexes were obtained in yields ranging from 60-74%. These complexes were all successfully characterized by ^{1}H NMR and FT-IR (ATR) spectroscopy.

A general synthetic procedure is shown in Scheme 2.6.

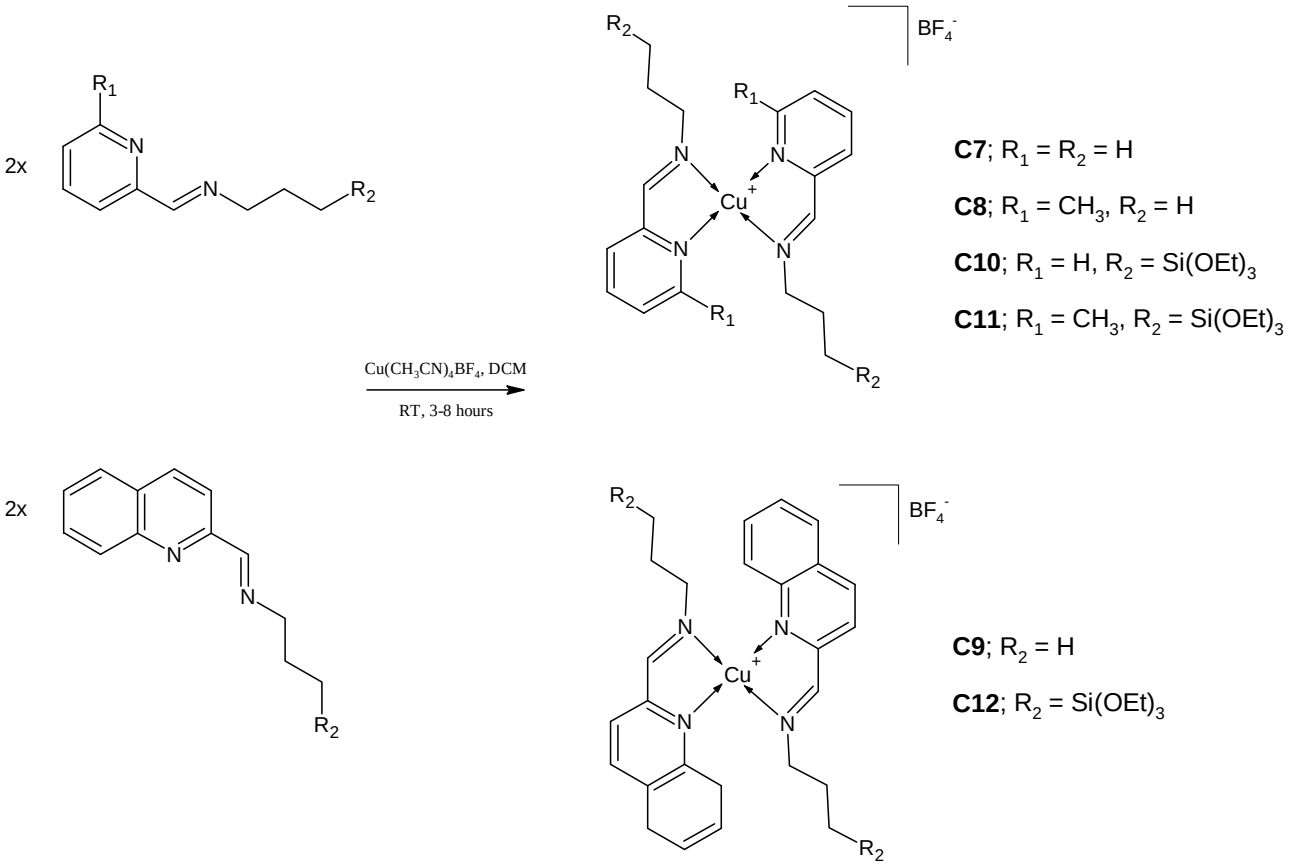

Scheme 2.6 Synthesis of model and functionalized Cu(I) complexes

2.3.1 Characterization of Cu(I) complexes

All complexes were characterized by ^{1}H NMR and FT-IR (ATR) spectroscopy, thermal analysis and UV/Vis spectroscopy.

2.3.1.1 Characterization of Cu(I) complexes by means of FT-IR(ATR) spectroscopy and thermal analysis

IR spectroscopy proved to be a valuable tool to confirm successful complexation of the copper precursor to the ligands. A general trend for the vibrations of the imine functionality was observed. A shift to lower wave numbers for the imine stretch was seen for complexes **C7**-**C12**. The absence of the imine stretch of the ligand confirmed that the obtained solid was pure and contained no unreacted ligand. A summary of these shifts are shown in Table 2.6. No other significant shifts in wave numbers are observed for any of the major vibrations.

Table 2.6 Summary of shifts for imine vibrations (ATR)[a]

L/C	*u*(C=N) cm^{-1}		Melting Point (℃)
	Ligand	Complex	
L1/C7	1649	1593	115-117
L2/C8	1649	1592	93-96
L3/C9	1645	1591	110-113
L4/C10	1649	1603	293-295
L5/C11	1649	1594	275-278
L6/C12	1645	1591	270-272

[a] Oils recorded as neat samples using ATR accessory

The model Cu(I) complexes were found to have much lower melting points when compared to their Pd(II) counterparts. The melting points of complexes **C7**-**C9** varied between 93-115 ℃. This showed that the model Pd(II) complexes were much more stable at higher temperatures compared to their Cu(I) counterparts. The functionalization of the complexes with the siloxane tail had a massive influence on the thermal stability of these complexes and caused an increase in melting point up to 295 ℃.

2.3.1.2 Characterization of Cu(I) complexes by means of ^{1}H NMR spectroscopy

Synthesis of complexes **C7**-**C12** was confirmed by ^{1}H NMR spectroscopy. The resonances observed differ only slightly from those observed for complexes **C1**-**C6**. The shift in the imine proton resonance for all of the complexes to the downfield region by between 25-50 ppm confirmed successful complex synthesis. An example of this imine shift is the downfield shift from 8.32 ppm for **L4** to 8.64 ppm for **C10**. The resonances for the model complexes are very similar to work previously done by Mketo *et al*.[10] For the functionalized complexes the same general trend was observed and the complexes could easily be characterized. Full ^{1}H NMR data for complexes **C7**-**C12** are shown in Table 2.7.

Table 2.7 ^{1}**H NMR data for model and siloxane functionalized Cu(I) complexes C7-C12**

Complex	-O-CH_2-CH_3	-Si-O-CH_2-	[a]-CH_2-CH_3 [b]-CH_2-Si-	[a]-CH_2-CH_2-CH_3 [b]-CH_2-CH_2-Si	-N-CH_2-CH_2-	Ar-H	Ar-CH_3	-N=CH-
C7[a]			0.81 (t, *J* = 6 Hz)	1.62 (m)	3.80 (t, *J* = 6 Hz)	8.87 (d, *J* = 6 Hz) 8.19 (t, *J* = 6 Hz) 8.02 (d, *J* = 9 Hz) 7.73 (t, *J* = 6 Hz)		8.53 (s)
C8[a]			0.85 (t, *J* = 9 Hz)	1.55(m)	3.85 (t, *J* =*6* Hz)	8.09 (t, *J* = 9 Hz) 7.88 (d, *J* = 6 Hz) 7.68 (d, *J* = 9 Hz)	2.83 (s)	8.86 (s)
C9[a]			0.81 (t, *J* = 9 Hz)	1.67 (m)	3.98 (t, *J* = 6 Hz)	8.89 (d, *J* = 9 Hz) 8.26 (d, *J* = 9 Hz) 8.17 (d, *J* = 9 Hz) 7.82 (d, *J* = 9 Hz) 7.70 (t, *J* = 6 Hz) 7.61 (t, *J* = 6 Hz)		9.22 (s)
C10[b]	1.25 (t, *J* = 4 Hz)	3.82 (m)	0.57 (t, *J* = 6 Hz)	1.59 (m)	3.73 (t, *J* = 6 Hz)	8.42 (d, *J* = 4 Hz) 8.03 (t, *J* = 8 Hz) 7.90 (d, *J* = 8 Hz) 7.61 (t, *J* = 4 Hz)		8.64 (s)

C11[b]	1.06 (t, *J* = 6 Hz)	3.54 (m)	0.55 (t, *J* = 3 Hz)	2.01 (m)	3.42 (t, *J* = 6 Hz)	8.17 (d, *J* = 6 Hz) 7.90 (t, *J* = 3 Hz) 7.70 (d, *J* = 6 Hz)	2.52 (s)	8.86 (s)
C12[b]	0.97 (t, *J* = 9 Hz)	3.52(m)	0.55 (t, *J* = 9 Hz)	2.04 (m)	4.06 (t, *J* = 6 Hz)	8.90 (d, *J* = 9 Hz) 8.28 (d, *J* = 9 Hz) 8.17 (d, *J* = 6 Hz) 7.80 (d, *J* = 9 Hz) 7.69 (t, *J* = 6 Hz) 7.59 (t, *J* = 6 Hz)		9.24 (s)

[a] Measured in Chloroform-*d*

[b] Measured in Acetone-d_8

2.3.1.3 Characterization of Cu(I) complexes by means of UV/Vis spectroscopy

Electronic absorption spectra of model complexes **C7**-**C9** are shown in Figure 2.4. These samples were all obtained in DCM solutions with concentrations of $2.5x10^{-5}$ M at room temperature. Solubility of the functionalized Cu(I) complexes proved to be problematic and data were subsequently not recorded.

Three distinctly different adsorption bands are seen for all three of the complexes. The first band in the region of 240-250 nm are attributed to the intramolecular (π-π^*) ligand transitions of the pyridine and quinoline rings. The π-π^* transitions for similar systems are widely reported to be found at <350 nm.[14-16] The transitions attributed to the n-π^* azomethine chromophore is found at 280-325 nm and correlates well with work previously reported.[15,16] A third transition is observed at lower energy (475-540 nm) and is attributed to the metal-to-ligand charge transfer transition typical for Cu(I) systems.[17]

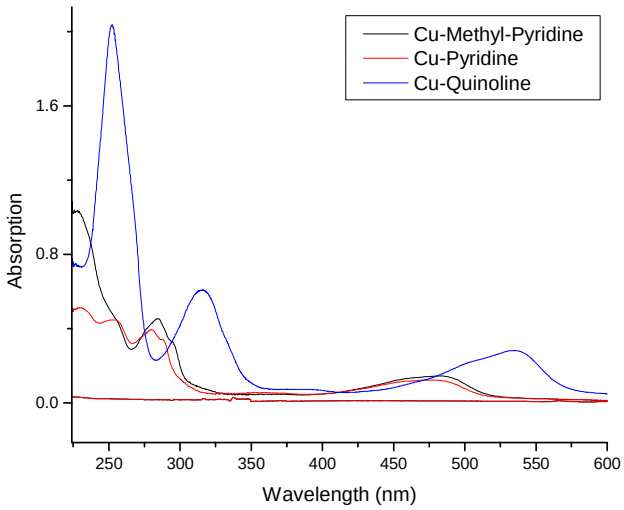

Figure 2.4 Electronic absorption spectra of functionalized Cu(I) complexes (2.5 x 10^{-5} M DCM)

2.4 Concluding remarks

Six model and functionalized ligands were prepared by Schiff base condensation reactions. By the complexation of these ligands with the appropriate palladium and copper precursors we were able to synthesize a range of Pd(II) and Cu(I) complexes (both model and siloxane functionalized). Model complexes of both palladium and copper were found to be very stable in air and in solution. These complexes were characterized by ^{1}H NMR, FT-IR (ATR) and UV-Vis spectroscopy and the results correlated well with work previously done by a member of our group. Model Pd(II) complexes were found to have better thermal stability than their Cu(I) counterparts. Functionalization of the complexes with a siloxane tail had a big influence on the thermal stability of both the Pd(II) and Cu(I) complexes. Siloxane functionalized complexes were slightly less stable in air and hydrolysis of the siloxane tail was observed and these were therefore stored in a glovebox to prevent any decomposition. Characterization by means of ^{1}H NMR spectroscopy was the main method to confirm successful complexation of the functionalized complexes and compared well to the ^{1}H NMR spectra obtained for the model complexes.

2.5 Experimental section

2.5.1 General remarks and instrumentation

All reactions were carried out under nitrogen making use of standard Schlenk techniques. Highly air sensitive materials were stored in a nitrogen purged glovebox and all manipulations with these materials were carried out in the glovebox to prevent decomposition or oxidation. IR spectra were recorded using an ATR accessory on a Nicolet Avatar 330 FT-IR spectrometer. NMR spectra were recorded on a Varian Unity Inova instrument at 300, 400 and 600 MHz for ^{1}H and 75 ,100 and 150 MHz for ^{13}C.

2.5.2 Materials

Reagents were purchased from Sigma-Aldrich and used as received; these include 2-pyridinecarboxaldehyde, 2-quinolinecarboxaldehyde, 6-methyl-2-pyridinecarbox-aldehyde, *n*-propylamine and 3-aminopropyltriethoxysilane. Solvents were purchased from Sigma-Aldrich and Kimix Chemicals and were dried by refluxing them over the appropriate drying agents. Dichloromethane and acetonitrile were dried over phosphorous pentoxide, hexane and pentane over sodium wire and diethyl ether, tetrahydrofurane and toluene over sodium wire with added benzophenone. Dimethyl sufloxide was left standing over molecular sieves. The $Pd(CH_3CN)_2Cl_2$ precursor was prepared by refluxing $PdCl_2$ in acetonitrile for 3-4 hours. $Cu(CH_3CN)_4BF_4$ was used as received from Sigma-Aldrich and was stored in a glovebox to keep it from oxidizing to Cu(II).

2.6 Synthesis of model and functionalized *N*,`*N* donor ligands

2.6.1 Model [*N*-(*n*-propyl)-(2-pyridyl and quinolyl)] ligands L1-L3

Model ligands were prepared using a procedure similar to that described by Cloete *et al.* [4] and Chen *et al*.[12] For ligand **L1** 2-pyridinecarboxaldehyde (0.403 g, 3.73 mmol) was dissolved in dry diethyl ether (10 mL) in a 100 mL round bottomed flask. To this stirring solution, *n*-propylamine (0.223 g, 3.73 mmol) was added followed by the addition of a small amount of $MgSO_4$. This solution was allowed to stir at room temperature for a further 3 hours and was filtered to remove the $MgSO_4$. The solvent was removed on a rotor evaporator and a yellow oily product was obtained. This oil was dissolved in minimal amount of DCM and washed with distilled water (2x20 mL) to remove any unreacted aldehyde. The organic layer was separated from the water layer and dried over $MgSO_4$ and filtered. The DCM was removed and the purified yellow oil was obtained. Ligands **L2** and **L3** were prepared in a similar way and were also isolated as yellow/orange oils. These ligands were characterized by FT-IR (ATR) and ^{1}H NMR spectroscopy.

2.6.2 Siloxane functionalized [*N*-(3-aminopropyltriethoxysilane)-(2-pyridyl and quinolyl)] ligands, L4-L6

Siloxane functionalized ligands were synthesized by slightly modifying the method used for model ligand synthesis. Instead of n-propylamine, 3-aminopropyltriethoxysilane was used. For ligand **L6,** 2-quinolinecarboxaldehyde (0.418 g, 2.66 mmol) was dissolved in dried diethyl ether (10 mL) and added to a 100 mL round bottomed flask. To this stirring solution 3-aminopropyltriethoxysilane (0.583 g, 2.66 mmol) was added followed by the

addition of a small amount of $MgSO_4$. This solution was allowed to stir at room temperature for a further 8 hours and was filtered to remove the $MgSO_4$. The solvent was removed on a rotor evaporator and a yellow/orange oil was isolated as product. No further purification of the ligand was carried out and FT-IR was used to confirm that no aldehyde was left in the oil obtained. Ligands **L4** and **L5** were also isolated as yellow/orange oils. These ligands were characterized by FT-IR (ATR), ^{1}H NMR and ^{13}C NMR spectroscopy.

Summaries of the NMR and IR data for all the ligands are found in Tables 2.1 and 2.2 respectively.

2.7 Synthesis of model and functionalized Pd(II) complexes

2.7.1 Model [*N*-(*n*-propyl)-(2-pyridyl and quinolyl)] $PdCl_2$ complexes, C1-C3

The complexes were prepared using the same procedure employed by Chen[12] and Cloete.[4] For preparation of **C2**, the model methyl-pyridine ligand **L2** (0.150 g, 0.925 mmol) was dissolved in DCM (10 mL) in a round bottomed flask purged with nitrogen. $Pd(CH_3CN)_2Cl_2$ (0.240 g, 0.925 mmol) was dissolved in DCM (10 mL) (bright red color) and added to the stirring solution of the ligand. The color of the almost colorless solution immediately changed to a bright orange and the mixture was stirred at room temperature for a further 3 hours. After the allotted time, an orange precipitate was observed and filtered off. The solid was washed with DCM to remove any

unreacted ligand that might be present and the product was dried under vacuum. Complexes **C1** and **C3** were isolated as yellow and orange powders respectively and all were characterized by ^{1}H NMR and FT-IR (ATR) spectroscopy.

2.7.2 Siloxane functionalized [*N*-(3-aminopropyltriethoxysilane)-(2-pyridyl and quinolyl)] $PdCl_2$ complexes, C4-C6

For **C5**, the siloxane functionalized methyl-pyridine ligand, **L5** (0.486 g, 1.5 mmol) was dissolved in DCM (10 mL) in a round bottomed flask purged with nitrogen. $Pd(CH_3CN)_2Cl_2$ (0.388 g, 1.5 mmol) was dissolved in 10 mL DCM (bright red color) and added to the stirring solution of the siloxane functionalized methyl-pyridine ligand. The color of the colorless solution immediately changed to bright orange and the mixture was stirred at room temperature for a further 6 hours. The solvent was removed under vacuum and an orange solid was isolated. The solid was dissolved in minimal amount of DCM and diethyl ether (10 mL) was added. An oily precipitate formed and was filtered off (unreacted ligand). 20 mL of hexane was then added to the orange filtrate which was kept in the fridge overnight. Very fine needle like crystals were formed and recovered. Unfortunately the crystals were not suitable for single crystal analysis. Complexes **C4** and **C6** were isolated as yellow and orange powders respectively and all were characterized by ^{1}H NMR, ^{13}C NMR and FT-IR (ATR) spectroscopy.

Full NMR characterization data of all the complexes is shown in Table 2.4. FT-IR imine shifts are summarized in Table 2.3.

2.8 Synthesis of model and functionalized Cu(I) complexes

2.8.1 Model Bis [*N*-(*n*-propyl)-(2-pyridyl and quinolyl)] Cu(I) tetrafluoroborate complexes, C7-C9

Cu(I) complexes were synthesized making use of the same method employed for Pd(II) complex synthesis. For **C7** model pyridine ligand (0.258 g, 1.74 mmol) was dissolved in DCM (10 mL) in a round bottomed flask purged with nitrogen. $Cu(CH_3CN)_4BF_4$ (0.274 g, 0.87 mmol) was dissolved in 10 mL DCM (colorless) and added to the stirring solution of the methyl-pyridine ligand (2:1 ligand to precursor ratio). The dark brown solution was stirred at room temperature for a further 4 hours. After this allotted time, the solvent was reduced to a small volume. Diethyl ether (20 mL) was added to the dark brown solution and a precipitate started to form. The mixture was left at -5 ℃ over night and the solvent was decanted. Hexane was added and the solid brown solid was filtered off and dried under vacuum. Complexes **C8** and **C9** were isolated as brown and purple powders respectively and all were characterized by ^{1}H NMR and FT-IR (ATR) spectroscopy.

2.8.2 Siloxane functionalized Bis [N-(3-aminopropyltriethoxysilane)-(2-pyridyl and quinolyl)] Cu(I) tetrafluoroborate complexes

For **C11**, the siloxane functionalized methyl-pyridine ligand, **L5** (0.972 g, 3 mmol) was dissolved in DCM (10 mL) in a round bottomed flask purged with nitrogen. $Cu(CH_3CN)_4BF_4$ (0.388 g, 1.5 mmol) was dissolved in 10 mL DCM (colorless) and added to the stirring solution of the methyl-pyridine ligand (2:1 ligand to precursor ratio). The dark brown solution was stirred at room temperature for a further 4 hours. After the

allotted time, the solvent was reduced to a minimal amount. Diethyl ether (20 mL) was added to the dark brown solution resulting in a precipitate forming. The mixture was left at -5 ℃ over night and the solvent was decanted. Hexane was added and the solid brown solid was filtered off and dried under vacuum. Complexes **C10** and **C12** were isolated as brown and purple solids respectively and all were characterized by ^{1}H NMR and FT-IR (ATR) spectroscopy.

Full NMR characterization data of all the complexes is shown in Table 2.7. FT-IR imine shifts are shown in Table 2.6.

2.9 References

1 Gupta, K.C.; Sutar, A. K. *Coord. Chem. Rev.* **2008**, 252, 1420.

2. Hirayama, H.; Takeuchi, I.; Honjo, T.; Kubono, K.; Kokusen, H. *Anal. Chem*. **1997**, 69, 4814.

3. Shamspur, T.; Sheikhshoaie, I.; Mashhadizadeh, M.H. *J. Anal. At. Spectrom*. **2005**, 20, 476.

4. Cloete, J.; Mapolie, S. F. *J. Mol. Catal., A: Chem.* **2006**, 243 221.

5. Horniakova, J.; Raja, T.; Kubota, Y.; Sugi, Y. *J. Mol. Catal., A: Chem.* **2004**, 217, 73.

6. Horniakova, J.; Nakamura, H.; Kawase, R.; Komura, K.; Kubota, Y.; Sugi, Y. *J. Mol. Catal., A: Chem.* **2005**, 233, 49.

7. Hu, J.; Li, K.; Li, W.; Ma, F.; Guo, Y. *Appl. Catal., A*, **2009**, 364, 211.

8 Murphy, E. F.; Ferri, D.; Baiker, A. *Inorg. Chem.* **2003**, *42*, 2559.

9 Smith, G. S.; Mapolie, S. F. *J. Mol. Catal A: Chem.* **2004**, 213 187.

10 Mketo, N. Palladium and Copper Complexes based on Dendrimeric and Monofunctional N, N' Chelating Ligands as Potential Catalysts in the Oxidative Carbonylation of Alcohols, **2010**, Stellenbosch University

11 Cozzi, P. G. *Chem. Soc. Rev.* **2004**, 33, 410.

12 Chen, R.; Bacsa, J.; Mapolie, S. F. *Polyhedron*. **2003**, 22, 2855.

13 Murphy, E. F.; Baiker, D. F. A. *Inorg. Chem*. **2003**, 42, 2559.

14 Wang, W.-J.; Lim, C.-H.; Tang, S.-W. *Mol. Cryst .Liq .Cryst*. **2006**, 456, 209.

15 Yang, P.; Yang, X.-J.; Wu, B. *Eur .J .Inorg. Chem*. **2009**, 2951.

16 Chen, Y.; Chen, J.-S.; Gan, X.; Fu, W.-F. *Inorg. Chim. Acta*, **2009**, 362, 2492.

17 Massa, W.; Dehghanpour, S.; Jahani, K. *Inorg. Chim*. **2009**, 362, 2872.

Chapter 3: Synthesis and Characterization of Immobilized Catalysts

3. Introduction

In the 1990's a considerable amount of effort was dedicated towards the synthesis of new mesoporous materials with pore sizes greater than 20 Å. Back then, the largest available mesoporous-type materials were ($AlPO_4$)-8,[1] VPI-5[2] and cloverite[3] which had pore sizes ranging between 8-13 Å. There was great interest shown in various fields of chemistry to synthesize higher pore diameter materials and in 1992 Beck and his group[4] at the Mobil Research and Development Corporation reported the synthesis of a new type of mesoporous silicate material. This new family of mesoporous silicate/aluminosilicate molecular sieves was designated as M41S. MCM-41 (Mobil Crystalline Material), probably one of the most well known and widely studied silicate materials of this family, exhibited a hexagonal array of uniform mesopores in which pore sizes ranged in diameter from 15 Å to more than 100 Å. Their application of the liquid crystal templating technique (LCT) coupled with the use of the correct templating agent or surfactant made it possible for them to synthesize a whole range of mesoporous materials with varying physical properties.

Since then the field of mesoporous silicate synthesis has grown exponentially. SBA-15 (Santa Barbara University) and MSU-X (Michigan State University) materials soon followed with both expanding the field dramatically.[5,6] These materials have found application in numerous fields of chemistry which include: stationary phases for high performance liquid chromatography (HPLC), immobilization of bioactive molecules,

polymer reinforcement and most importantly catalysis.[7] The tunability of the pore sizes and ease of functionalization of the surface of these materials made them really attractive for use as either a support for catalysis or as catalysts in their own right.

An excellent example to demonstrate the versatility of these silica materials is shown in work done by Li *et al*.[8] They reported asymmetric transfer hydrogenation making use of a recoverable ruthenium catalyst immobilized onto a magnetic mesoporous silica. This Ru-TsDPEN (TsDPEN=*N*-(*p*-toluenesulfonyl)-1,2-diphenylethylene-diamine) species is air-sensitive and thus separation of the catalyst from the reaction mixture through filtration can be very problematic. They synthesized a magnetic support to immobilize this catalyst to afford a heterogeneous catalyst that can be separated from the reaction mixture by applying a magnetic field. Scheme 3.1 gives a short synthetic procedure to obtain a magnetic siliceous mesocellular foam support. They successfully applied this catalyst in the asymmetric transfer hydrogenation (ATH) reaction and were able to recover the magnetic catalyst quantitatively. They reported 99 % yield for each of their 9 runs (recovering catalyst after each run) with only a small drop in ee (%) from 94 % for the first run to 90 % for the 9th recycled run.

Given the large surface area (>650 m^2/g) of these materials, one can understand why they are so intensively studied and used as a support material for immobilization. Chmielarz and his group[9] used this large surface area to their advantage and effectively supported oxides of Cu and Fe by deposition on MCM-48, SBA-15 and Mesocellular silica foam (MCF). A wet impregnation technique was employed to deposit the transition metal oxides onto the supports making use of aqueous solutions of $Cu(NO_3)_2 \cdot 3H_2O$ or

$Fe(NO_3)_3 \cdot 9H_2O$. These modified catalysts were effectively employed as catalysts in the selective reduction of NO with ammonia.

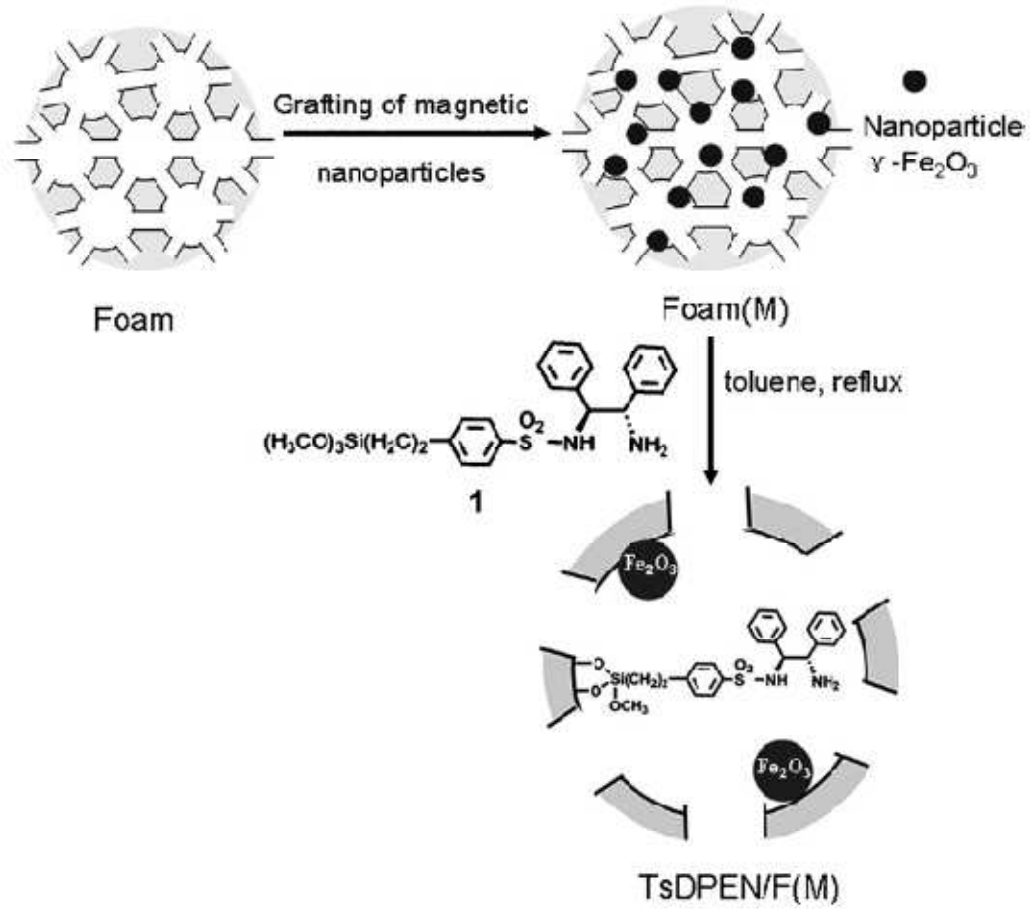

Scheme 3.1 Schematic description of preparation of hybrid ligand, TsDPEN/F(M).[8]

The synthesis of mesoporous silica materials (MCM-41 and SBA-15) has been widely reported in literature. A simplified reaction scheme for the synthesis of MCM-41 is shown in Scheme 3.2. An inorganic precursor is added to a solution (either acidic or basic) containing an appropriate surfactant molecule which leads to the formation of the hexagonal array of cylindrical pores.[10]

The same technique applies for the synthesis of other types of mesoporous materials such as SBA-15. The synthetic procedure differs only slightly viz. in the selection of the surfactant molecule used.

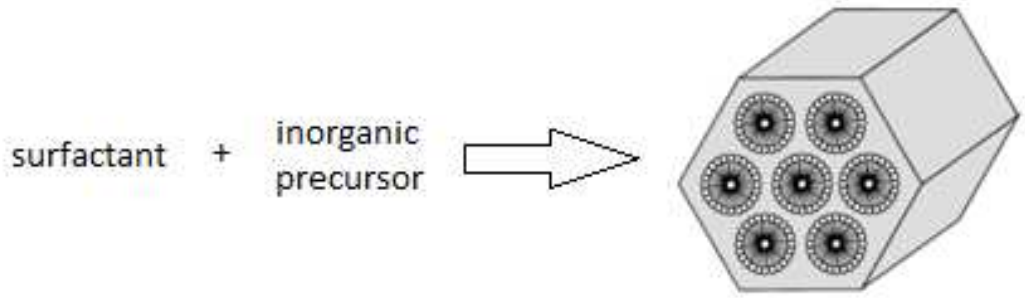

Scheme 3.2 Schematic representation of the general formation of MCM-41[10]

Three different types of surfactant molecules have been reported for the synthesis of the above-mentioned supports. For the synthesis of MSU-X, MCM-41 and SBA-15 type materials a neutral (Triton X-100), cationic (cetyl trimethylammonium bromide) and a polymeric (tri-block copolymer) co-surfactant were respectively used for the synthesis of these silicas.[11-13] The choice of surfactant molecule has a significant effect on the pore sizes and surface area of the formed support. Other factors such as reaction temperature, pH and reactant concentrations also play a major role in determining the microstructure of the final product. A lot of work has been focused on the synthesis and characterization of these types of silicas and their synthesis has been widely reported in the literature.[14-17]

3.1 Synthesis and Characterization of Silica Supports, MCM-41 and SBA-15

The synthetic procedure used for the synthesis of the chosen MCM-41 and SBA-15 supports was adapted form work previously done by the groups of Cai[18] and Zhao.[19]

MCM-41 was synthesized by using cetyl trimethylammonium bromide as surfactant in a basic solution (pH ~ 12). After the surfactant was totally dissolved the silica source, tetra-orthosilicate, was added to form a white slurry.

For SBA-15 the surfactant molecule was changed to poly(ethyleneglycol)-block-poly(propyleneglycol)-block-poly(ethyleneglycol) (PEG) in acidic conditions. After the formed silicas were filtered, washed with water and dried the white powders were calcined at 550 ℃ to get rid of the templating mol ecule used for their synthesis.

3.1.1 Characterization of MCM-41 and SBA-15

MCM-41 and SBA-15 were characterized by X-ray diffraction, infrared spectroscopy, scanning electron microscopy (SEM), thermal gravimetric analysis (TGA) and BET surface area analysis.

3.1.1.1 Characterization of MCM-41 and SBA-15 by means of FT-IR spectroscopy

IR spectra for MCM-41 and SBA-15 were recorded as nujol-mulls. The spectra obtained are shown in Figure 3.1 for MCM-41 and Figure 3.2 for SBA-15. For MCM-41 the band at 3384 cm^{-1} is a characteristic band of the Si–O and water molecules adsorbed; the band at 1623 cm^{-1} is from the vibration of water molecules adsorbed; the bands at 1239

and 1082 cm^{-1} are due to Si–O–Si vibrations. The same bands are observed for SBA-15 and compare well with that reported in the literature.[20]

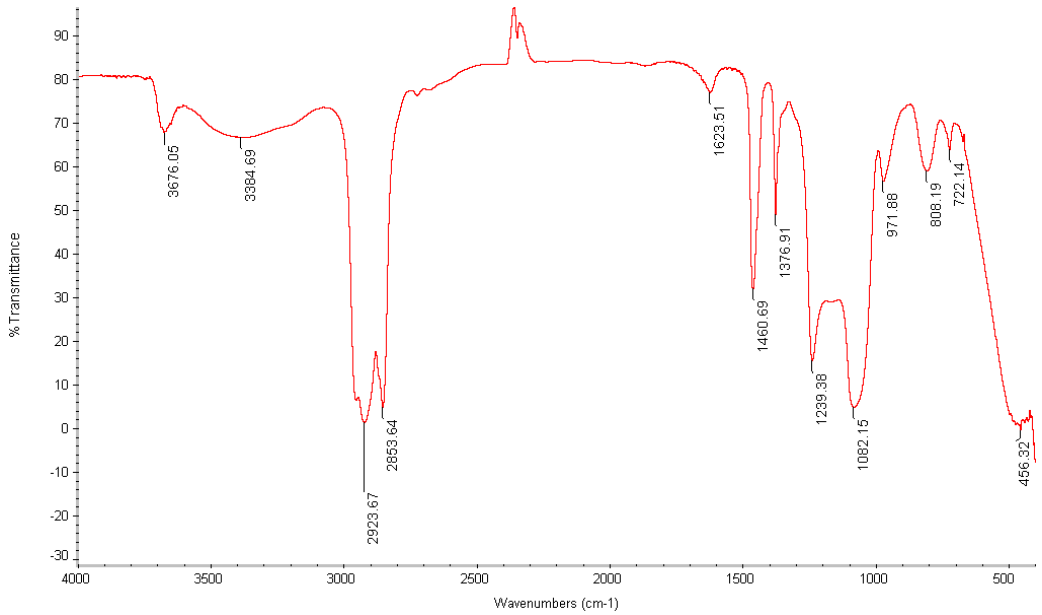

Figure 3.1 FT-IR spectra of MCM-41 (nujol: 2923, 2853, 1460, 1376 cm^{-1})

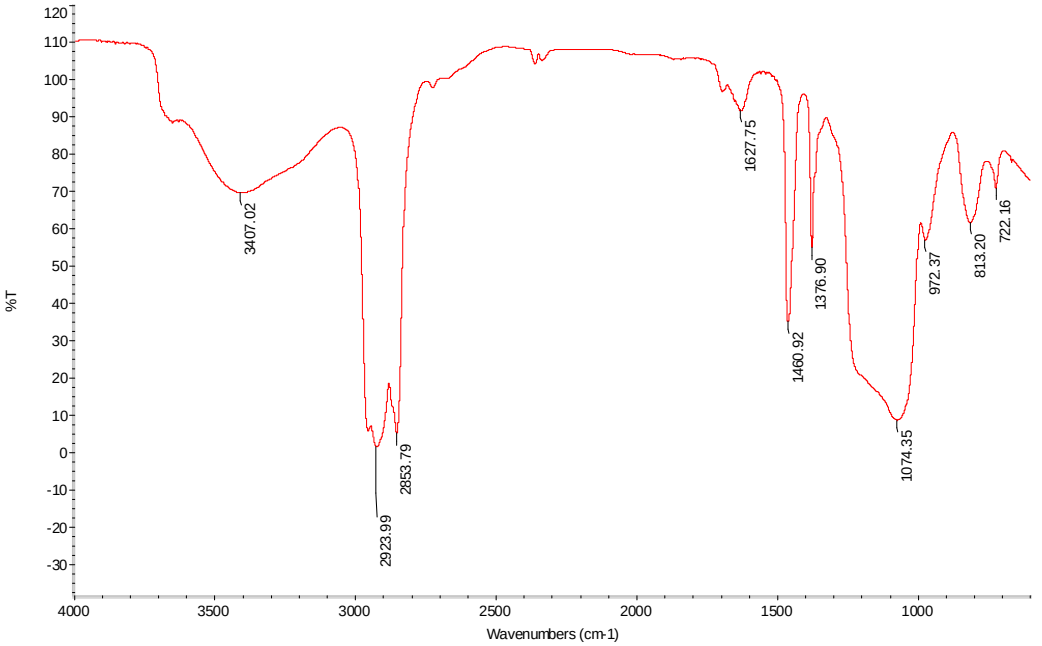

Figure 3.2 FT-IR spectra of SBA-15 (nujol: 2923, 2853, 1460, 1376 cm^{-1})

3.1.1.2 Characterization of MCM-41 and SBA-15 by means of BET (Brunauer Emmett Teller) analysis

BET analysis was used to determine the surface area and average pore diameter of the synthesized supports. The samples were degassed at 230 ℃ for 18 hours to ensure that the samples were completely dry and solvent free. The relative pressure was increased from 0 to 1 relative pressure (P/P_o) and the amount of nitrogen adsorbed was measured.

There are different types of nitrogen adsorption isotherms and they are classified by the adsorption profile they follow. The types range from I-V and the difference between each of them is shown in Figure 3.3. The type of material and the micropore structure would determine which isotherm profile or type will be observed for a certain material.

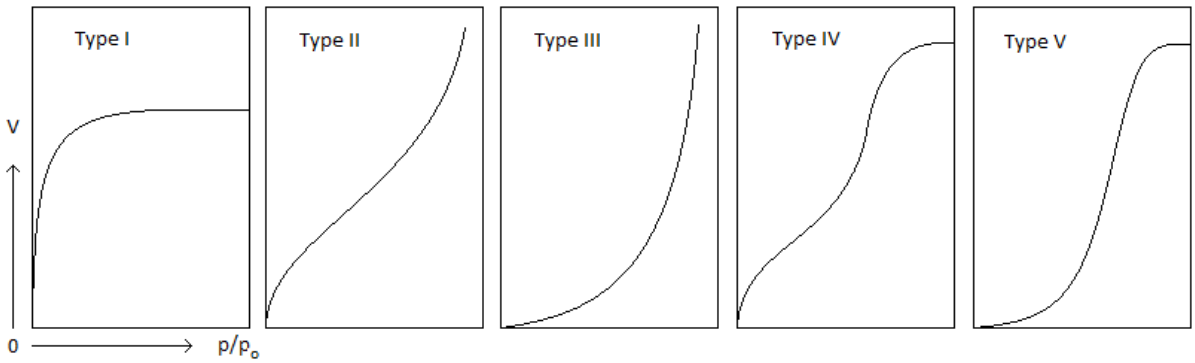

Figure 3.3 Different types of isotherm plots

The isotherm plots of the MCM-41 and SBA-15 produced are shown in Figure 3.4. Characteristic isotherm plots were observed for both the MCM-41 and the SBA-15. In

both cases the isotherms are of type IV and a H1 hysteresis loop, typical of materials with pores of constant cross-section (cylindrical or hexagonal), is observed.[16]

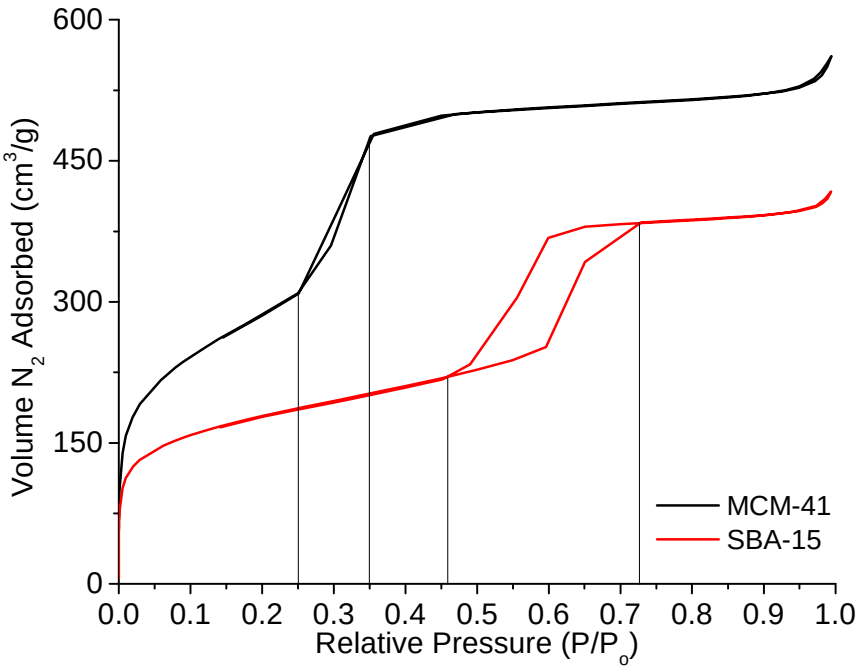

Figure 3.4 Isotherm plots for MCM-41 and SBA-15

A higher total volume of nitrogen adsorbed is observed for MCM-41 than for SBA-15. It can be concluded that the MCM-41 has a higher surface area than SBA-15. From this one can assume that SBA-15 would have thicker silica walls as wall thickness is inversely proportional to surface area.[22]

The pore-filling step of the MCM-41 and SBA-15 occurs at P/P_o 0.25-0.35 and 0.45-0.73 relative pressures respectively. The pores of MCM-41 are filled over a smaller range than that of SBA-15 and from this one can conclude that MCM-41 would have a much narrower pore size distribution than SBA-15. This can also be seen in Figure 3.5 where

the pore volume is plotted against the pore diameter for both of the supports. The pore diameter is calculated by making use of Barret-Joyner-Halenda (BJH) calculations ($t = 3.5400 \times [-5.0000 / \ln(P/P_o)]0.3330$) and desorption data.

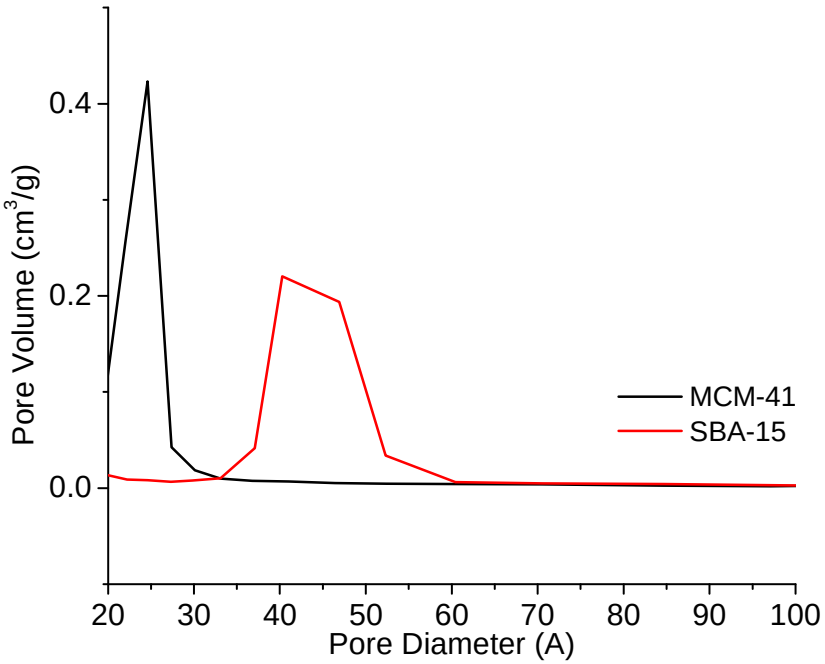

Figure 3.5 Pore size distribution plot of MCM-41 and SBA-15

Table 3.1 summarizes the calculated BET surface areas and average pore diameters of the MCM-41 and SBA-15 samples.

Table 3.1 BET surface area and average pore diameters of MCM-41 and SBA-15

Material	Surface Area (cm^2/g)	Pore Diameter (Å)
MCM-41	1035.16	26.06
SBA-15	633.54	49.78

MCM-41 shows a much higher surface area than SBA-15 (~400 cm^2/g greater). SBA-15 on the other hand has much larger pores than MCM-41. These results are consistent with results reported in literature.[15-17]

3.1.1.3 Characterization of MCM-41 and SBA-15 by means of Powder XRD

The X-ray diffraction patterns of the MCM-41 and SBA-15 produced are shown in Figure 3.6 and these are typical for these types of silica materials.[4,23] Both the MCM-41 and SBA-15 show three well resolved peaks that can be well indexed as (100), (110) and (200) diffractions associated with a 2-D hexagonal symmetry, indicating a well-ordered mesostructure. For MCM-41 a fourth peak of much lower intensity can just be seen, corresponding to the (210) diffraction. The presence of this fourth and sometimes fifth peak (300) indicates that the material is of good quality.[24] A summary of the diffraction peaks of MCM-41 and SBA-15 is shown in Table 3.2.

Table 3.2 Powder XRD diffractions of MCM-41 and SBA-15

Material	(100)	(110)	(200)	(210)
MCM-41	2.60°	4.40°	5.11°	6.70°
SBA-15	0.98°	1.65°	1.89°	2.71°

It can be seen that the diffraction peaks of SBA-15 occurs at much lower angles than that of MCM-41. This is typical for SBA-15 and illustrates the influence of synthetic methods (different templating agent and pH) on the meso-structure of the silica support formed. In this case SBA-15 has a much lower surface area than MCM-41, but much

larger average pore diameters (confirmed with BET analysis). This brings about the shift to lower angles in the XRD, characteristic of materials with larger pore diameters.[23]

The interplanar spacing of the materials (*d* spacing value) for the reflection plane (100) was calculated using Bragg's equation, $2d\sin\theta = n\lambda$, where $\lambda = 1.540598$ Å (*n* for $d_{100} = 1$).

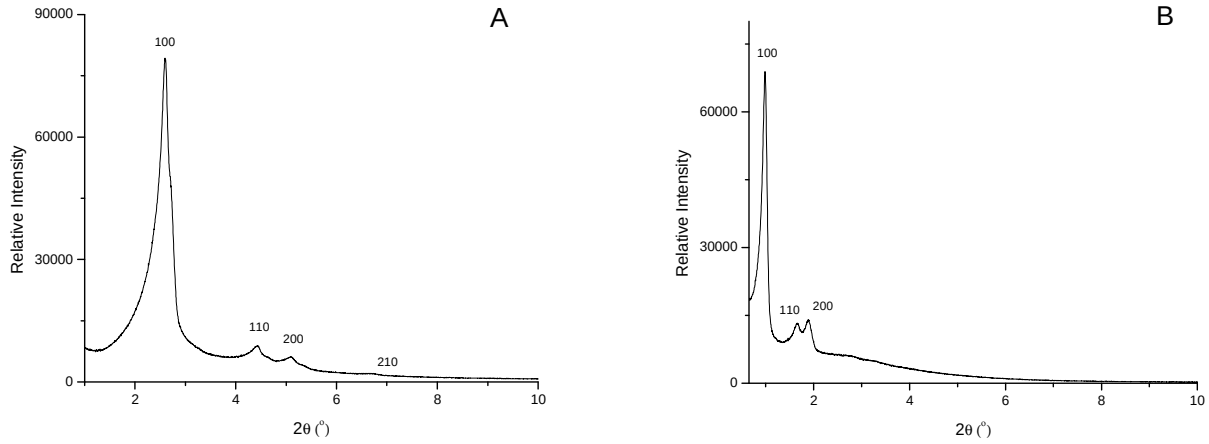

Figure 3.6 Powder XRD plot of MCM-41 (A) and SBA-15 (B)

The calculated *d* spacing for the reflection plane d_{100} was found to be 34.0 Å for MCM-41 and 90.7 Å for SBA-15. From this one is able to calculate the hexagonal lattice parameter *a* ($a = 2d_{100}/\sqrt{3}$).[25] The hexagonal lattice parameter for MCM-41 and SBA-15 was calculated as 39.2 Å and 104.7 Å respectively.

3.1.1.4 Characterization of MCM-41 and SBA-15 by means of thermal gravimetric analysis (TGA)

Both supports were analyzed using TGA to determine if the silica supports are thermally stable at temperatures up to 600 ℃. For both MCM-41 and SBA-15 a rather large weight loss below 100 ℃ is observed and can be ascribed to the evaporation of water absorbed onto the supports during storage. From 100 ℃ to 600 ℃ though, less than 2 weight % loss is observed proving that the support undergoes no decomposition and still retains its structure (Figure 3.7).

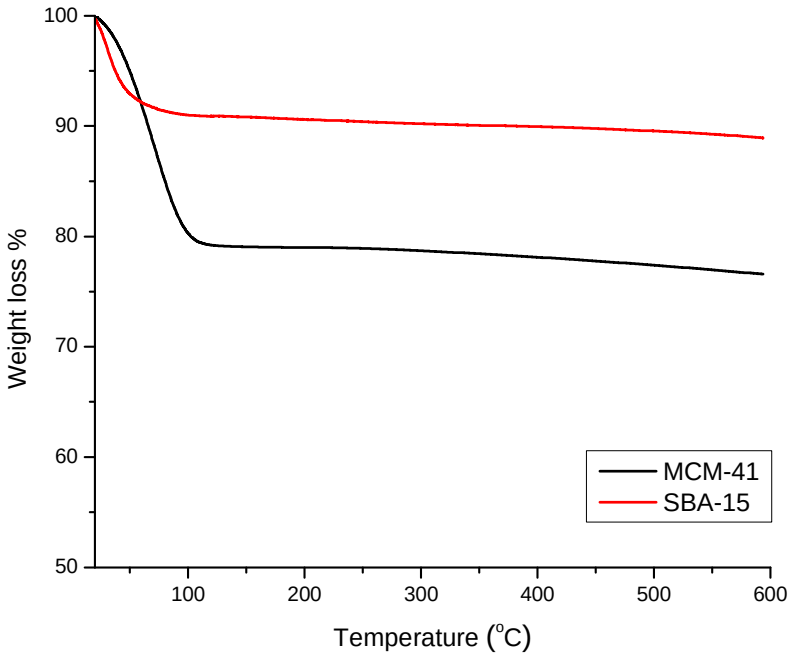

Figure 3.7 TGA analysis of native MCM-41 and SBA-15

A higher initial weight loss is observed for MCM-41 when compared to SBA-15. This means that more water had likely adsorbed onto the surface of MCM-41 and can be ascribed to the higher surface area of MCM-41.

3.1.1.5 Characterization of MCM-41 and SBA-15 by means of scanning electron microscopy (SEM)

The two silica supports were also characterized by scanning electron microscopy (SEM) to verify the morphology of the materials. SEM gives a detailed image of the morphology of the individual silica particles and also provides a good indication of the particle sizes (Figure 3.8).

Characteristic SEM micrographs were obtained for both MCM-41 and SBA-15 with the former showing more compact hexagonal structures in nature, with the latter displaying longitudinal cylinders.[4,23]

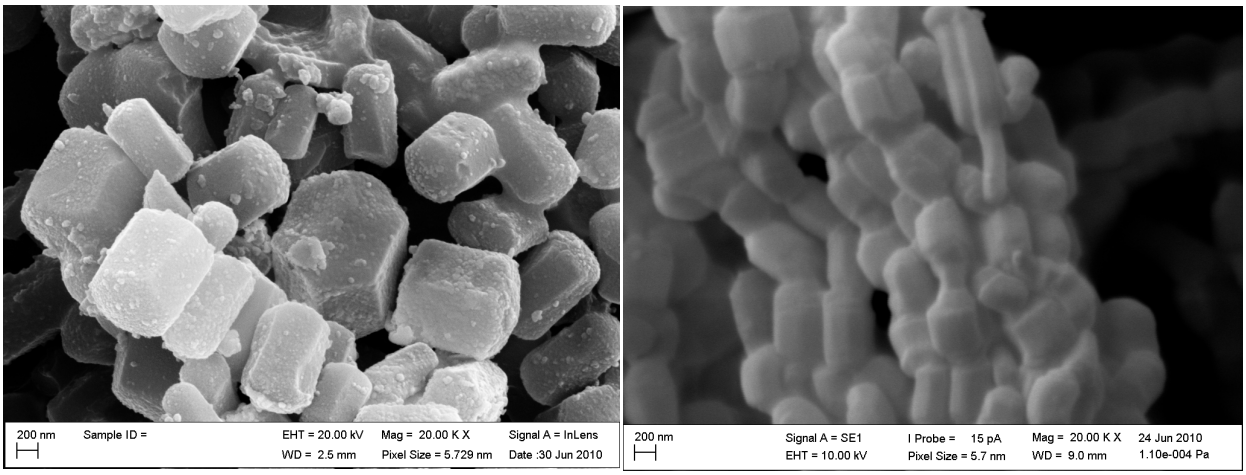

Figure 3.8 SEM micrographs of native MCM-41 (top) and SBA-15 (bottom)

3.2 Synthesis and Characterization of Titanium Doped Silica Supports

The doping of silica supports can be achieved through numerous strategies such as direct synthesis and post synthetic treatment. Direct synthesis entails the addition of an appropriate metal source together with the Si source. Post synthetic treatment involves the initial synthesis of the silica and subsequent impregnation thereof (after calcination) with a chosen metal source. Both methods can be successfully applied to introduce metals like Al, Ni, Cr, Fe, Mn, Ti, Au or Pb into the silica framework. These approaches to introduce a metal into the support aim to improve the stability, hydrophobicity and most importantly the catalytic activity of the supports.[26]

Zhang *et al.* [25] reported on the change brought about in the stability and microstructure of the silica supports with increased amounts of Ti. They found that the mesoporous ordering of MCM-41 species synthesized using both methods i.e. direct synthesis and post synthetic treatment, decreased with increasing degree of Ti doping. These authors noted an overall decrease in BET surface area for both methods with an increase in the pore size of the support synthesized using the direct synthesis method. These supports were however synthesized with very high Ti/Si ratios whereas much lower ratios were chosen for our doped supports.

For this study titanium isopropoxide was employed as titanium source. The direct synthesis method was used and doped supports with different mol ratios of Ti/Si were synthesized. The same synthetic procedure was followed as described for MCM-41 and SBA-15 to synthesize Ti-MCM-41 and Ti-SBA-15 respectively. The mol ratio of Ti/Si

was varied from 1-3 mol %. The obtained white powders were calcined at 550 ℃ until they were white again (times varied and were longer than the non-doped supports).

3.2.1 Characterization of Titanium Doped Supports

Ti-doped supports were characterized by X-ray diffraction, infrared spectroscopy, scanning electron microscopy (SEM), thermal gravimetric analysis (TGA) and BET surface analysis.

3.2.1.1 Characterization of Ti-MCM-41 and Ti-SBA-15 by means of FT-IR spectroscopy

Exactly the same FT-IR spectra were obtained for Ti-MCM-41 and Ti-SBA-15 when compared to the native supports MCM-41 and SBA-15. Only when very high Ti doping is used are any noteworthy changes in the IR is observed.[25] With such low doping (3 mol %) no significant difference is observed.

3.2.1.2 Characterization of Ti-MCM-41 and Ti-SBA-15 by means of BET (Brunauer Emmett Teller) analysis

BET analysis was employed to see what the influence of Ti-doping had on the surface characteristics of the supports. Figure 3.9 and Figure 3.10 shows the isotherm plots for Ti-doped MCM-41 and SBA-15 respectively.

For Ti-MCM-41 supports a general trend is seen for the amount of nitrogen adsorbed with an increase in Ti loading. It is seen that the volume of nitrogen adsorbed onto the support decreases with an increase of Ti from 0-3 mol %. This is however consistent

with what is reported in the literature. Zhang and his group[25] found that with an increase in the concentration of Ti, a decrease in the surface area with an increase in the pore diameter is observed. They ascribed this decrease in surface area and increase in pore diameter to the difference in the ionic radius of Ti and Si. Ti has a larger ionic radius than Si and leads to the partial collapse of the structure of Ti-MCM-41 which causes a decrease in the surface area. This however causes an increase in the average pore size (larger ionic radius of Ti) which results in the larger pore diameter.

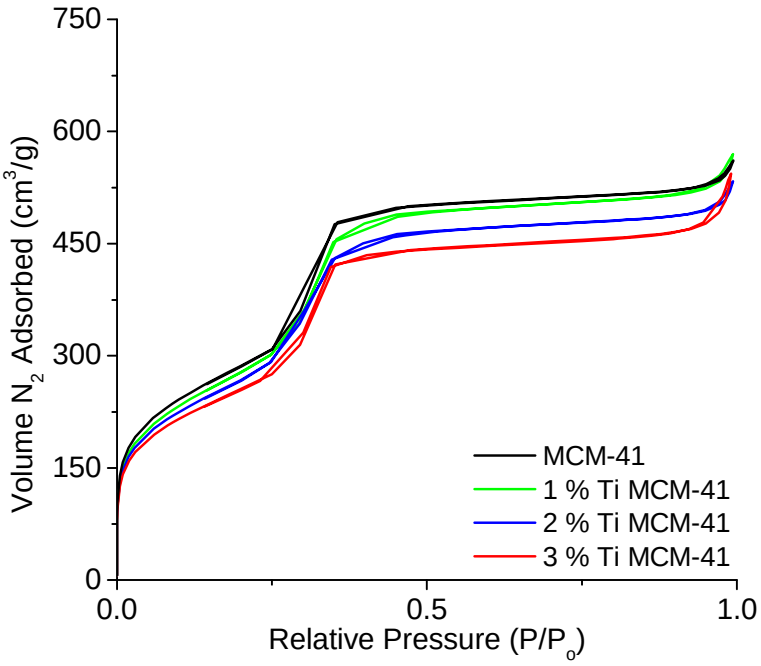

Figure 3.9 Isotherm plots for doped MCM-41

For Ti-SBA-15 though, exactly the opposite trend is seen with an increase in Ti loading leading to an increase in the surface area (volume adsorbed) of the support. An increase in the pore diameter is also observed and a summary for the surface areas and pore diameters of the supports is shown in Table 3.3. This increase in surface area for

Ti-SBA-15 is not consistent with that reported for other doped SBA-15 materials. However literature only reports on very high Ti doping for SBA-15 silicas, whereas we used low levels of Ti-doping.

The type of material obtained during doping is determined by the reaction conditions employed. In the case of MCM-41, synthesis is carried out in very basic conditions, whereas SBA-15 synthesis is carried out in a very acidic solution.

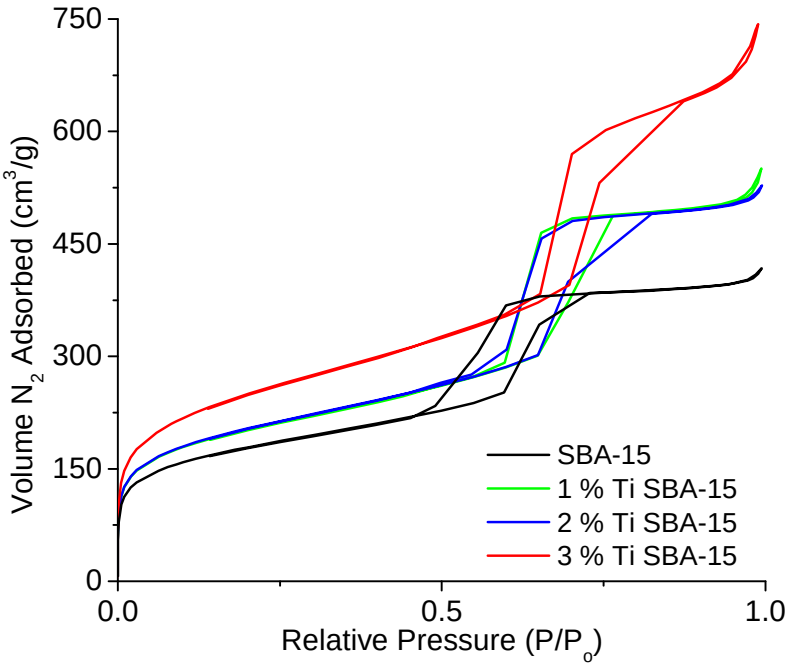

Figure 3.10 Isotherm plots for doped SBA-15

It is a known that Ti-isopropoxide is hydrolyzed faster than the TEOS used as silica source. It is believed that this leads to the condensation of the Ti precursor with itself, rather than with the Si precursor leading to the formation of TiO_2 clusters which could lead to an increase in the surface area of the resulting material.

Table 3.3 Summary of surface areas and pore diameters of MCM-41 and SBA-15 doped supports

Material	Surface Area (m^2/g)	Pore Diameter (Å)
MCM-41	1035	32.33
1 % Ti-MCM-41	1005	33.37
2 % Ti-MCM-41	965	32.58
3 % Ti-MCM-41	922	34.11
SBA-15	633	39.49
1 % Ti-SBA-15	721	44.48
2 % Ti-SBA-15	724	43.70
3 % Ti-SBA-15	892	49.20

3.2.1.3 Characterization of Ti-MCM-41 and Ti-SBA-15 by means of Powder XRD

Powder XRD was used to see if the original silica structure was maintained during the doping process. All reflections are well resolved and no major differences are observed when compared to the native supports. For doped MCM-41 (Figure 3.11) a shift to lower angles is observed with an increase in the doping. The intensity of the reflections also increases and this suggests a more ordered system with a higher degree of crystallinity.

For the doped SBA-15 system not much change is observed and only a slight shift to lower angles is observed (Figure 3.12). There is, as is the case with MCM-41, an increase in the intensity of the reflections. The supports seem to be intact and still have the characteristic mesoporous silica reflections.

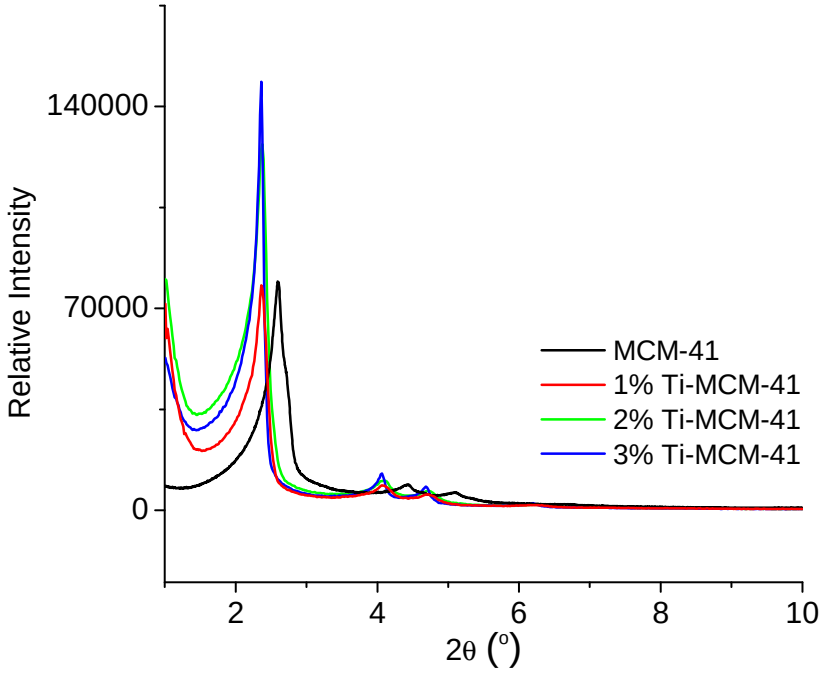

Figure 3.11 Powder XRD plot of doped MCM-41

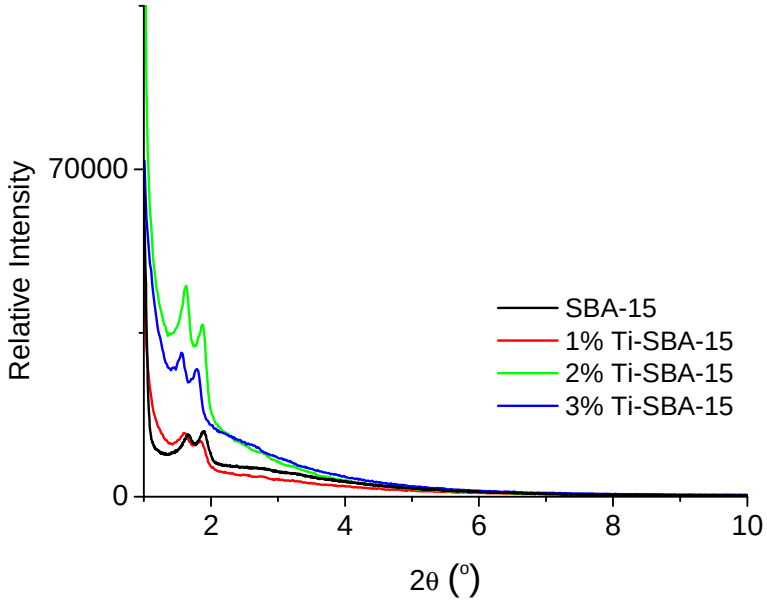

Figure 3.12 Powder XRD plot of doped SBA-15

3.2.1.4 Characterization of Ti-MCM-41 and Ti-SBA-15 by means of thermal gravimetric analysis (TGA)

All Ti-doped supports (MCM-41 and SBA-15) were analyzed with TGA. No significant weight loss (<2 weight %) was observed for all of the doped supports. They showed high thermal stability up to the measured temperature of 600 ℃.

3.2.1.5 Characterization of Ti-MCM-41 and Ti-SBA-15 by means of scanning electron microscopy (SEM)

SEM micrographs were taken of the Ti-doped supports and were found to look exactly the same as the native MCM-41 and SBA-15. Characteristic SEM micrographs for Ti-MCM-41 and Ti-SBA-15 are shown in Figure 3.13.

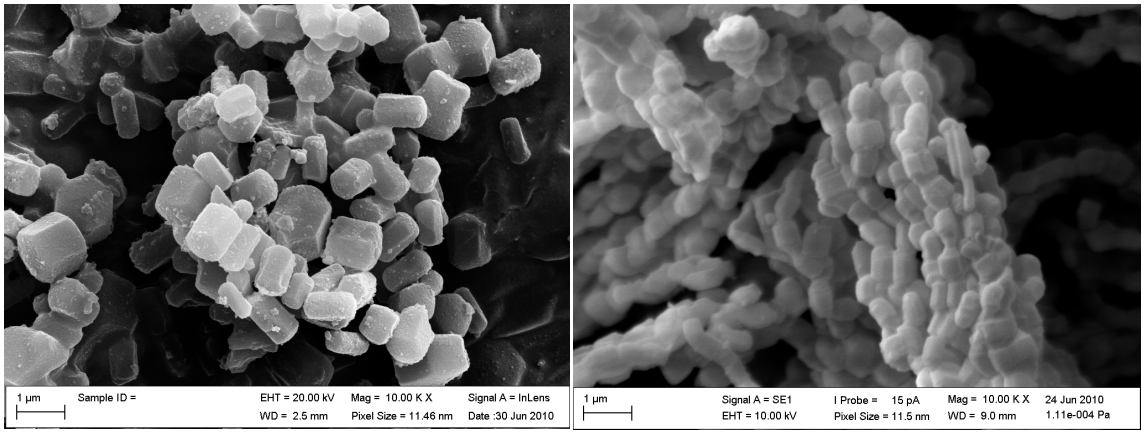

Figure 3.13 SEM micrographs of 1% Ti-MCM-41 (left) and 1% Ti-SBA-15 (right)

3.3 Synthesis and Characterization of Immobilized Catalysts

The immobilization of the siloxane functionalized complexes onto the different silica supports is achieved by the condensation of the surface silanol (Si-OH) groups of the support with the siloxane (Si-$(OEt)_3$) group of the complex. This condensation results in the formation of the covalently bound immobilized catalyst.

For our study 10 weight % complex was utilized to produce the immobilized catalyst. This reaction was carried out in toluene as solvent while being refluxed. A synthetic procedure for the synthesis of the Pd-Pyridine immobilized catalyst is shown in Scheme 3.3.

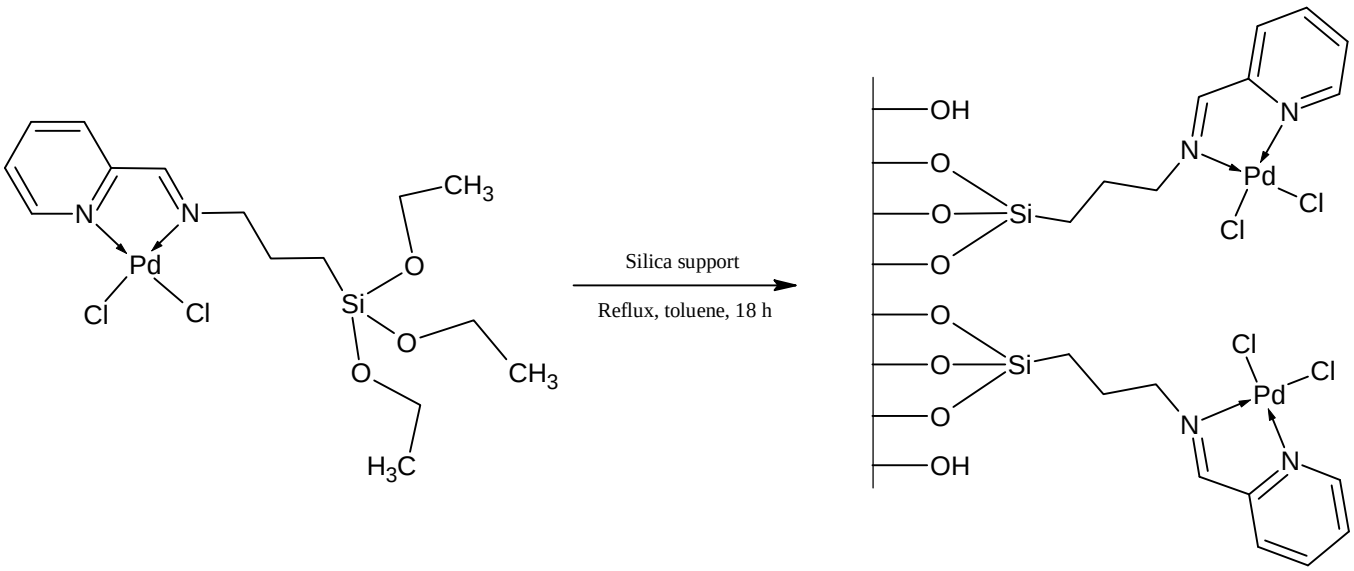

Scheme 3.3 Synthetic route towards Pd-Pyridine immobilized catalyst

Off-white (Pd complexes) or light purple/brown (Cu complexes) powders were recovered as products after the reaction was left to run for 18 hours. The powders were dried

under vacuum to remove any residual toluene. All immobilized catalysts were stored in a glove box until further use.

3.3.1 Characterization of Immobilized Catalysts

Immobilized catalysts were characterized by IR spectroscopy (nujol), BET analysis, powder X-ray diffraction, scanning electron microscopy (SEM), thermal gravimetric analysis (TGA), ICP and solid state $^{13}C\{^{1}H\}$ NMR spectroscopy.

3.3.1.1 Characterization of immobilized Pd(II) and Cu(I) catalysts by means of FT-IR spectroscopy

Characterization of the immobilized catalyst by IR spectroscopy was attempted but proved unsuccessful. Seeing that the immobilization involves only using a 10 weight % complex the expected complex vibrations would be too low in intensity to be seen together with the very intense silica vibrations. This resulted in acquiring exactly the same IR that was observed for the native supports.

3.3.1.2 Characterization of immobilized Pd(II) and Cu(I) catalysts by means of BET (Brunauer Emmett Teller) analysis

BET analysis was used to visualize the expected decrease in surface area after the immobilization of the functionalized complexes onto the different supports. Figure 3.14 shows that there is a significant decrease in the volume of nitrogen adsorbed onto the surface of the immobilized catalysts with the Pd-Quinoline-MCM-41 catalyst showing the lowest adsorption and thus having the lowest surface area. This change in the volume of nitrogen adsorbed is as one would expect. By

immobilizing the functionalized complex onto the supports, the surface of the support where nitrogen can adsorb becomes less and causes the decrease in the total volume that can be adsorbed.

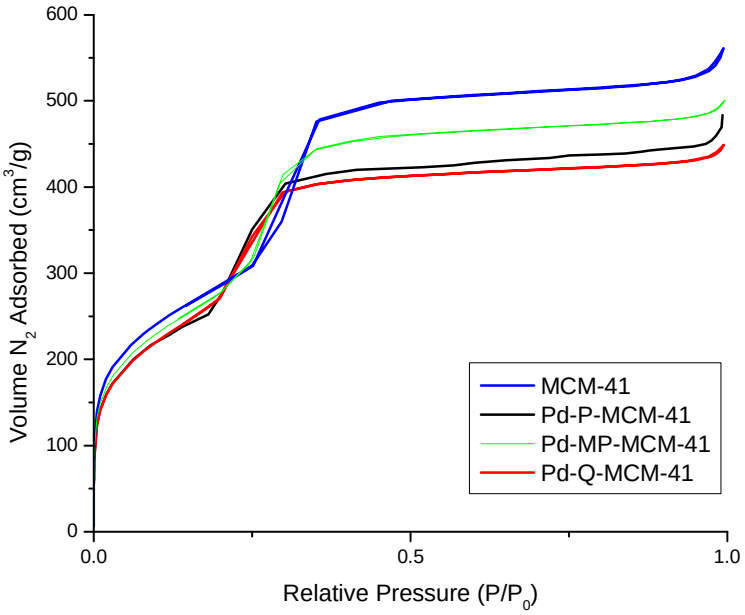

Figure 3.14 Isotherm plots of immobilized Pd(II) catalysts (non-doped supports) MCM-41

The same decrease in volume of nitrogen adsorbed onto the surface of SBA-15 is seen for the immobilized catalysts (Figure 3.15). For SBA-15 immobilized catalysts the Pd-Methyl-Pyridine-SBA-15 catalyst shows the lowest volume of nitrogen adsorbed.

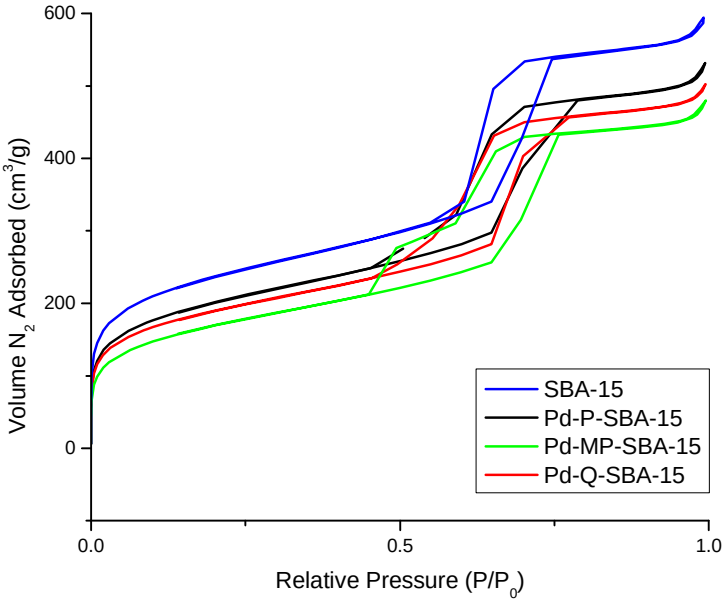

Figure 3.15 Isotherm plots of immobilized Pd(II) catalysts (non doped supports) SBA-15

For the Cu(I) immobilized MCM-41 catalysts, a very large change in the volume of nitrogen adsorbed is observed when compared to the native MCM-41. The isotherm plots for MCM-41 Cu(I) catalysts are shown in Figure 3.16. These isotherms showed very low nitrogen adsorption and it is apparent that the immobilization of the functionalized Cu(I) complexes had an influence on the morphology of the MCM-41 support. This is seen when comparing the surface areas and average pore diameters of the immobilized catalysts with that of the native MCM-41 (Table 3.4). A dramatic increase in the pore diameter is observed, especially for Cu-P-MCM-41 catalyst which pore diameter increases from 26.15 Å for the native support to 88.38 Å for the immobilized catalyst.

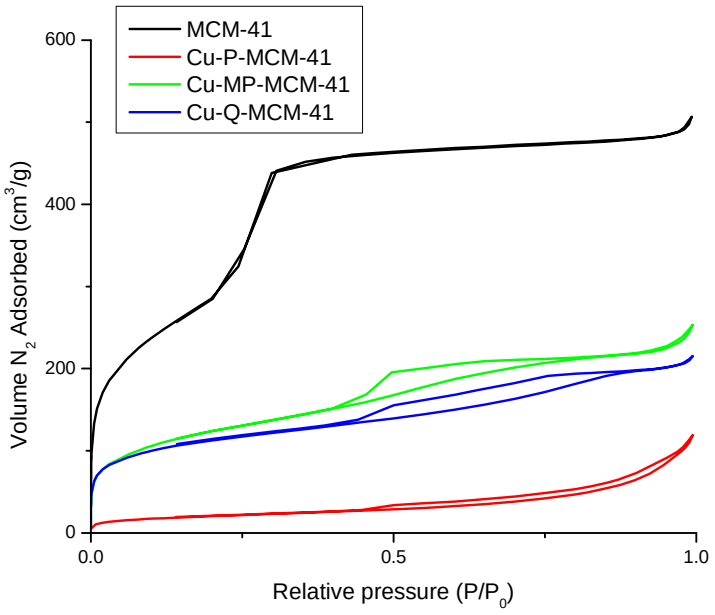

Figure 3.16 Isotherm plots of immobilized Cu(I) catalysts (non doped supports) MCM-41

A similar trend is observed for the methyl-pyridine and quinoline analogues. Powder XRD analysis was employed to determine whether the structural integrity of the support stayed intact and is discussed in the next section.

Isotherm plots obtained for complexes immobilized on SBA-15 show more uniform decreases in the amount of nitrogen adsorbed onto the immobilized catalysts (Figure 3.17). The largest change is observed for Cu-P-SBA-15 with Cu-Q-SBA-15 showing the lowest change in volume. Compared to the MCM-41 immobilized Cu(I) catalyst systems, it seems that much more stable catalysts are obtained. This would be as one would expect seeing that SBA-15 has thicker pore walls than MCM-41 and would thus be thermally and structurally more stable. No major change in the pore diameters

of the Cu(I) SBA-15 catalysts are observed with Cu-P-SBA-15 having the lowest surface area.

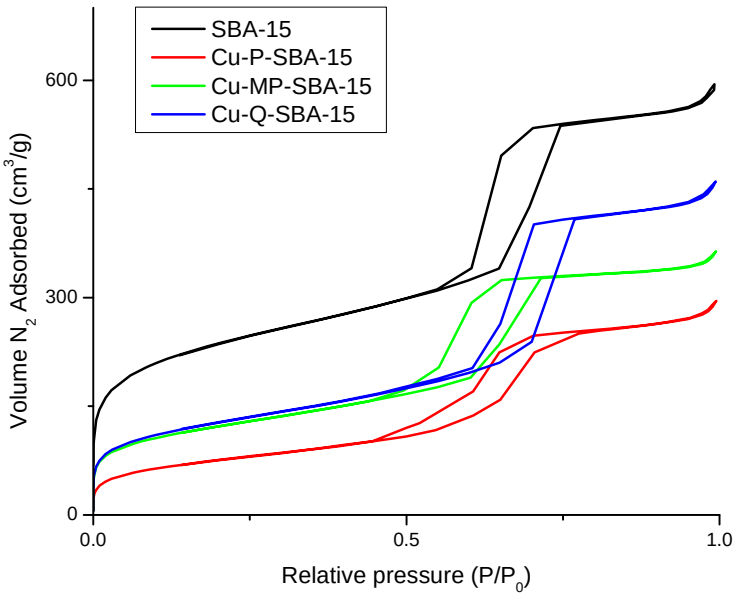

Figure 3.17 Isotherm plots of immobilized Cu(I) catalysts (non doped supports) SBA-15

A summary of the surface areas and the pore diameters of the MCM-41 and SBA-15 immobilized catalysts are shown in Table 3.4.

From the surface areas of the immobilized catalysts it is clear that successful immobilization of the functionalized complexes was obtained. There is a decrease, as expected and is seen for all of the immobilized catalysts. The pore diameter for the MCM-41 and SBA-15 immobilized catalysts compared to the native supports do not differ that much.

Table 3.4 Summary of BET surface area and pore diameter results for MCM-41 and SBA-15 immobilized catalysts

Material	Surface Area (cm^2/g)	Pore diameter (Å)
MCM-41	1038	26.14
Pd-P-MCM-41[a]	979	25.57
Pd-MP-MCM-41[b]	1004	26.37
Pd-Q-MCM-41[c]	984	25.81
Cu-P-MCM-41	74	88.38
Cu-MP-MCM-41	447	39.12
Cu-Q-MCM-41	400	42.71
SBA-15	842	58.21
Pd-P-SBA-15	718	56.98
Pd-MP-SBA-15	606	59.41
Pd-Q-SBA-15	676	57.35
Cu-P-SBA-15	275	53.67
Cu-MP-SBA-15	436	49.14
Cu-Q-SBA-15	456	61.02

[a] Pyridine, [b] Methyl-Pyridine, [c] Quinoline

A change in surface area of between 30-60 cm^2/g and 130-240 cm^2/g is seen for the MCM-41 and SBA-15 immobilized catalysts respectively. These results are consistent with work done by Malumbazo.[27] From the larger change in surface area observed for SBA-15 supported catalysts one can deduce that much more complex overall was

immobilized onto the support. The reason for this is the significant difference in the pore volume between MCM-41 and SBA-15. If one compares the pore diameter of MCM-41 and SBA-15, it can be clearly seen that the complex could enter the pores of SBA-15 more easily than is the case for the MCM-41. A range of functionalized Pd-Pyridine complexes immobilized on the doped supports were also characterized making use of BET analysis (Table 3.5).

Table 3.5 Summary of surface areas and pore diameters of functionalized Pd-Pyridine complex immobilized on Ti-doped supports

Material	Surface Area (cm^2/g)	Pore diameter (Å)
1 % Ti-MCM-41	1005	33.37
2 % Ti-MCM-41	965	32.58
3 % Ti-MCM-41	922	34.11
Pd-P-1% Ti-MCM-41	825	30.20
Pd-P-2% Ti-MCM-41	897	30.45
Pd-P-3% Ti-MCM-41	805	31.30
1 % Ti-SBA-15	721	44.48
2 % Ti-SBA-15	724	43.70
3 % Ti-SBA-15	892	49.20
Pd-P-1% Ti-SBA-15	566	52.83
Pd-P-2% Ti-SBA-15	624	51.45
Pd-P-3% Ti-SBA-15	740	59.93

The expected decrease in the surface area was observed for both Ti-MCM-41 and Ti-SBA-15 showing that immobilization of the functionalized Pd-Pyridine complex was successful. The largest change in surface area is once again seen for the SBA-15 supports and is ascribed to the larger pore diameters which would facilitate the immobilization of the complex.

3.3.1.3 Characterization of immobilized Pd(II) and Cu(I) catalysts by means of Powder XRD

The immobilized Pd(II) catalysts were also characterized with powder XRD diffraction. The diffraction pattern of the immobilized catalysts does not differ much from the native MCM-41 and SBA-15. This means that the support was not significantly altered during the immobilization process and that it retained its high degree of crystallinity. XRD plots of the immobilized catalysts are shown in Figure 3.18 for MCM-41 and in Figure 3.19 for SBA-15.

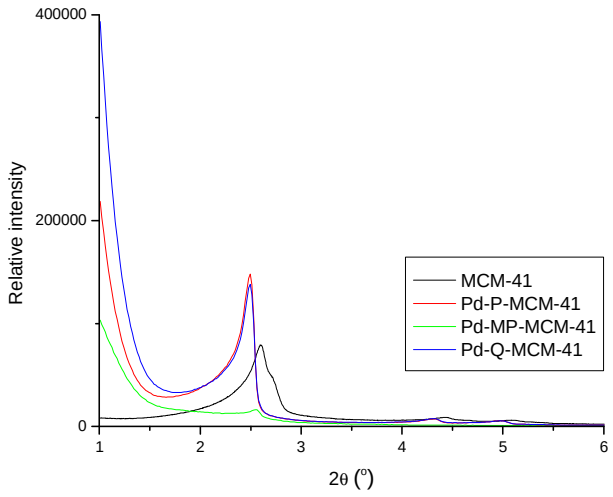

Figure 3.18 Powder XRD plots of Pd immobilized MCM-41 catalysts

A drop in the intensity of the reflections of the Pd-Methyl-Pyridine-MCM-41 catalyst is seen, however the characteristic three inflections observed for MCM-41 are retained. This decrease in the inflection intensity is a result of the decrease in the degree of ordering of the silica material brought about by the immobilization process. A slight shift to lower angles is also observed for the immobilized catalysts when compared to MCM-41.

For SBA-15 immobilized catalysts both the Pd-Methyl-Pyridine-SBA-15 and Pd-Q-SBA-15 catalyst showed lower intensities for their inflections. The respective reflection peaks can be seen despite the lowered intensity.

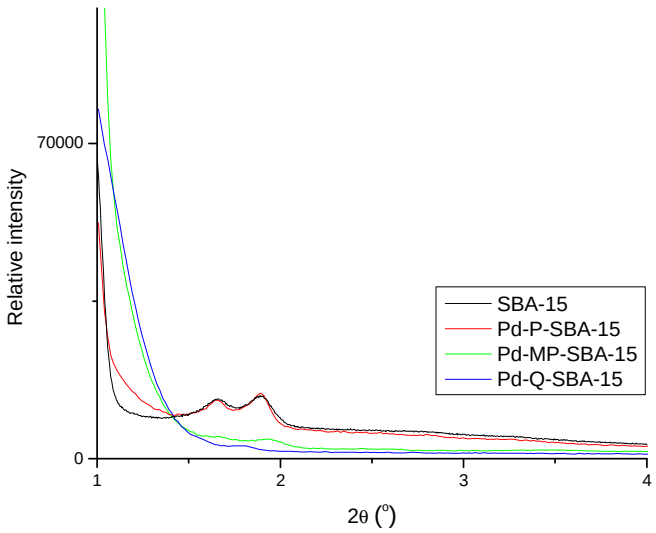

Figure 3. 19 Powder XRD plots of Pd immobilized SBA-15 catalysts

This lowering in the intensity of the reflections is however expected as one is modifying the support by the immobilization of the functionalized complexes. Powder XRD

provides proof that the morphology of the silica material remains intact after the immobilization of the Pd(II) complexes.

Powder XRD was employed to try and determine if the structural integrity of the MCM-41 immobilized Cu(I) catalysts were in fact compromised. XRD results confirm what was observed for BET results and showed that the inflection peaks of the immobilized catalysts disappeared (Figure 3.20). This confirms that the MCM-41 support material is structurally compromised with loss of its crystallinity. The Cu(I) complexes contains a tetra-fluoroborate counter ion and thermal analysis showed that the Cu(I) complexes are thermally not as stable as the Pd(II) counterparts, which did not show similar results for BET and powder XRD. The conditions employed for immobilization probably resulted in the partial decomposition of the copper complexes. This decomposition together with the present counter ion could have resulted in the disintegration of the MCM-41 support material.

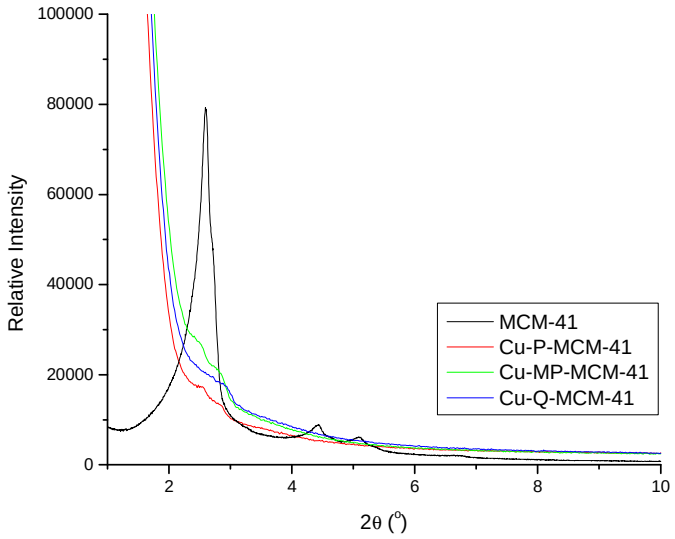

Figure 3.20 Powder XRD plots of Cu immobilized MCM-41 catalysts

This effect, especially on MCM-41, has been observed by members of our group for other immobilized systems and suggests that the conditions of immobilization (100 ℃) together with the counter ion of the complex play a major role in the stability of the support. For SBA-15 catalysts (Figure 3.21) on the other hand no major difference in the occurrence of the expected reflections are observed. An increase in the intensity is seen but powder XRD results suggest that the structural integrity of the SBA-15 support material was not dramatically affected.

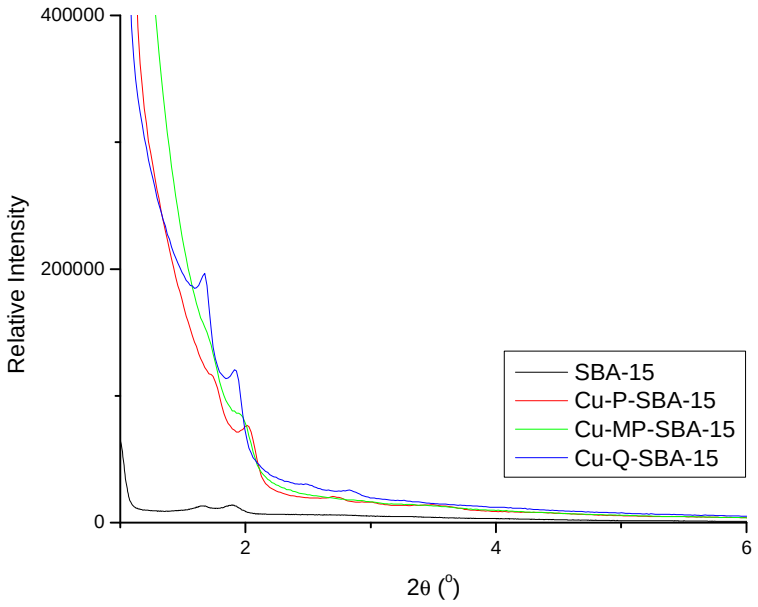

Figure 3.21 Powder XRD plots of Cu immobilized SBA-15 catalysts

For the Ti-doped catalysts very well resolved XRD patterns were obtained. An increase in the intensity of the reflections was seen for immobilized catalysts of both Ti-MCM-41 (Figure 3.22) and Ti-SBA-15 (Figure 3.23) when compared to the un-doped supports.

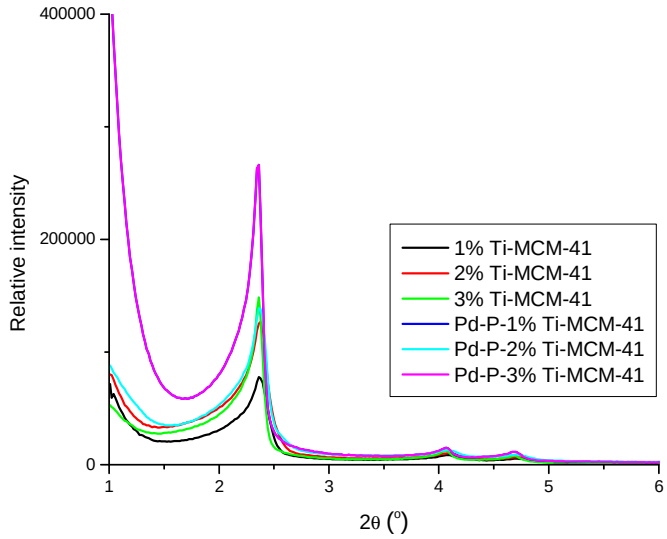

Figure 3.22 Powder XRD plots of Pd immobilized Ti-doped MCM-41 catalysts

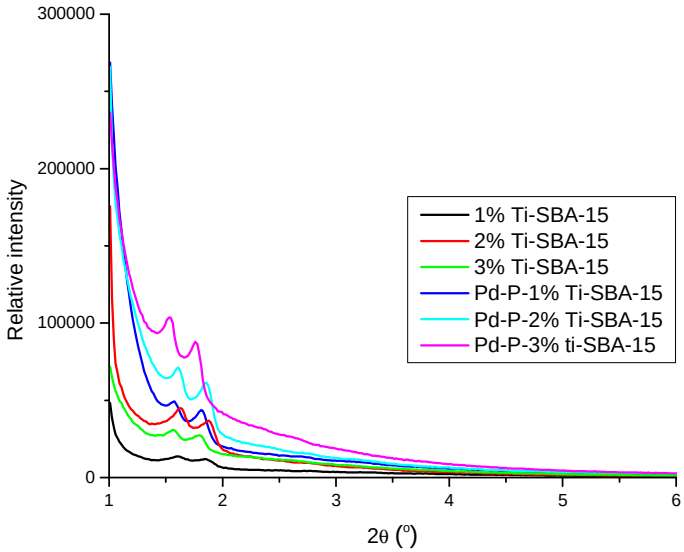

Figure 3.23 Powder XRD plots of Pd immobilized Ti-doped SBA-15 catalysts

In general for all the immobilized Pd(II) catalysts well resolved reflections are observed and it is clear that the support materials, be it normal MCM-41 and SBA-15 or Ti-doped supports, retained their structure and were not altered during immobilization. For immobilized Cu(I) catalysts however a change in the structure of the supports were observed, especially for MCM-41 catalysts. The fact that MCM-41 is more affected by Cu(I) complex immobilization shows that SBA-15 is in fact more stable and can be ascribed to its thicker pore walls.

3.3.1.4 Characterization of immobilized Pd(II) and Cu(I) catalysts by means of thermal gravimetric analysis (TGA)

All immobilized catalysts were characterized using TGA analysis. It is expected that a change in the weight will occur when the immobilized complex starts to decompose. The same general weight loss profile is observed for all of the catalysts and for this reason only a few immobilized catalysts will be compared (Figure 3.24).

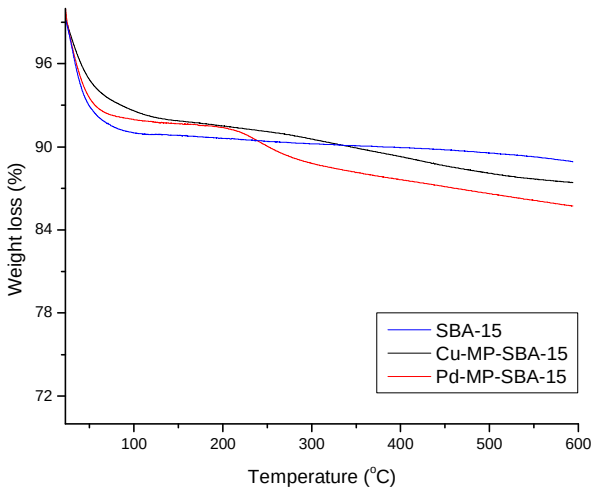

Figure 3.24 TGA analysis of SBA-15 immobilized catalysts

For the Pd-Methyl-Pyridine-SBA-15 catalyst a weight loss is seen at just over 200 ℃. This concurs with the decomposition of the supported complex and it is seen that loss of the Pd(II) complex occurs over a much smaller temperature range when compared to the Cu(I) systems. This can possibly be related to the relative stabilities of the two systems. It was previously shown that the palladium complexes are thermally more stable than their copper analogues (see chapter 2).

3.3.1.5 Characterization of Pd(II) and Cu(I) immobilized catalysts by means ICP-AES

From the obtained ICP results it is clear that successful immobilization of the complexes onto the silica supports was achieved. A summary of the results obtained for immobilized Pd(II) catalysts is shown in Table 3.6. It is seen that higher Pd loading is found for SBA-15 immobilized catalysts when compared to the MCM-41 immobilized catalysts. This concurs with the BET results showing a higher average change in surface area for SBA-15 catalysts.

The highest Pd loading for the undoped supports was found for the Pd-Q-MCM-41 and Pd-MP-SBA-15 catalysts respectively. These results compare well to work previously done by other members of our group.[27] A higher Pd loading was observed for the Ti-doped supports compared to the normal MCM-41 and SBA-15 Pd-Pyridine catalysts. For SBA-15 this is expected seeing that the surface area of the support material increased with an increase in Ti doping. MCM-41 however showed a decrease in surface area with an increase in Ti doping while the Pd loading stayed more or less constant compared to the undoped support.

Table 3.6 ICP results for immobilized Pd(II) catalysts

Material	Weight % Pd (on support)
Pd-P-MCM-41	0.971
Pd-MP-MCM-41	0.952
Pd-Q-MCM-41	1.026
Pd-P-1% Ti-MCM-41	1.002
Pd-P-2% Ti-MCM-41	1.190
Pd-P-3% Ti-MCM-41	1.097
Pd-P-SBA-15	1.051
Pd-MP-SBA-15	1.114
Pd-Q-SBA-15	1.031
Pd-P-1% Ti-SBA-15	1.098
Pd-P-2% Ti-SBA-15	1.567
Pd-P-3% Ti-SBA-15	1.833

For SBA-15 there is an increase in Pd loading with an increase in Ti doping. These results compare well with BET analysis where it was shown that there is an increase in the surface area with an increase in Ti doping. For MCM-41 there is no notable trend observed except with the Pd-P-2% Ti-MCM-41 catalyst showing a slightly higher Pd loading when compared to the other Ti-MCM-41 catalysts. This difference is however negligible.

The metal loadings of immobilized Cu(I) catalysts were also determined by ICP and are shown in Table 3.7. Relatively low copper content is observed for MCM-41 catalysts and supports results obtained with BET and XRD analysis. The weight % copper found for SBA-15 immobilized catalysts correlates well with ICP results obtained for Pd(II) catalysts. The results for immobilized SBA-15 Cu(I) catalysts are in agreement with BET results with Cu-P-SBA-15 showing the largest change in surface area with the highest metal loading and Cu-Q-SBA-15 showing the smallest change in surface area and the lowest metal loading.

Table 3.7 ICP results for immobilized Cu(I) catalysts

Material	Weight % Cu (on support)
Cu-P-MCM-41	0.357
Cu-MP-MCM-41	0.509
Cu-Q-MCM-41	0.536
Cu-P-SBA-15	1.149
Cu-MP-SBA-15	1.122
Cu-Q-SBA-15	0.949

Metal loadings obtained by ICP were fairly high and compared well to work reported by Malumbazo[27] and were calculated to be more or less 50 % of the theoretical loading. Cu immobilized MCM-41 catalysts showed the lowest metal loading and this was ascribed to the loss of integrity of the support during the immobilization process.

3.3.1.6 Characterization of immobilized Pd(II) and Cu(I) catalysts by means of scanning electron microscopy (SEM)

Immobilized catalysts were also characterized by SEM. SEM micrographs of native supports and immobilized Pd-Pyridine catalysts are shown in Figure 3.25. The top two micrographs are of MCM-41 and the bottom two of SBA-15.

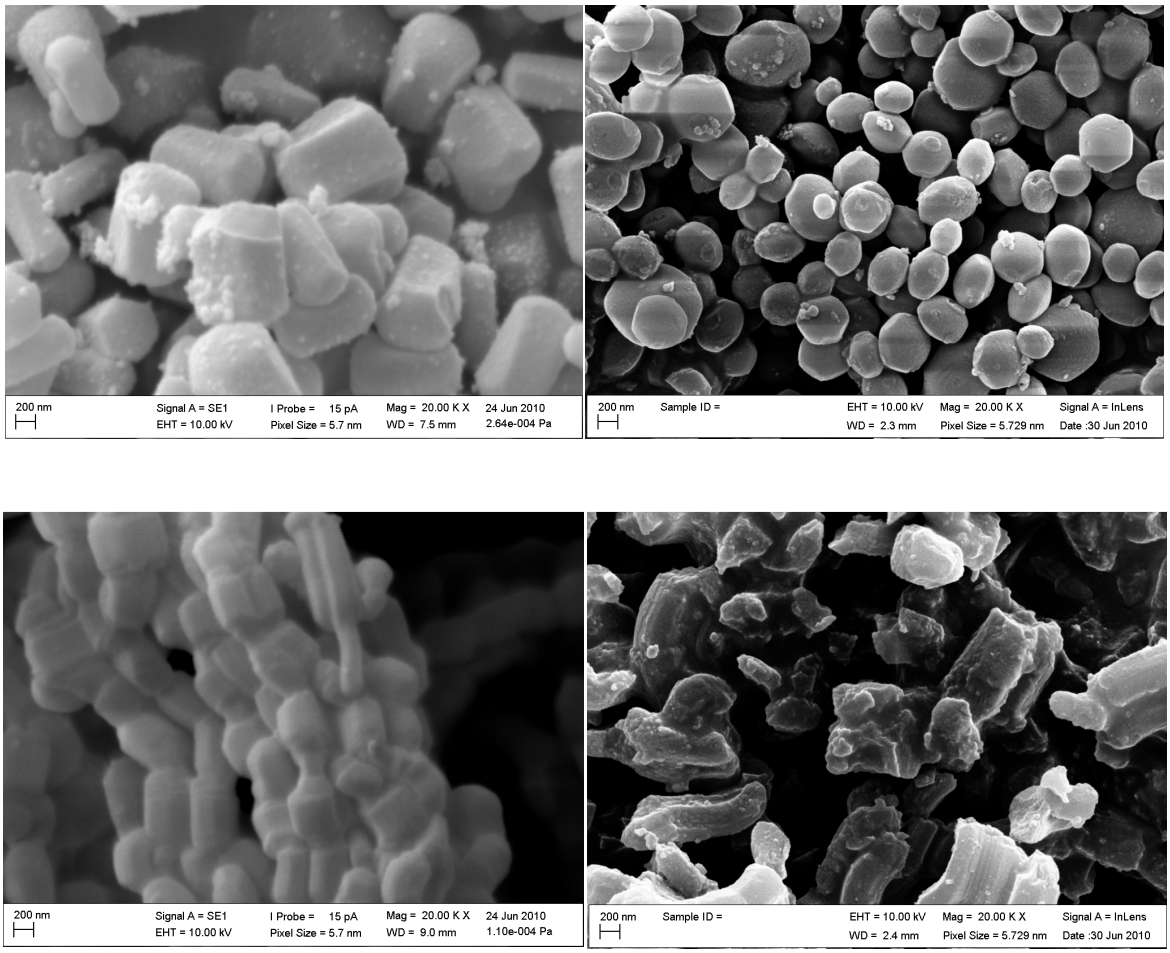

Figure 3.25 SEM micrographs of native supports MCM-41 and SBA-15 (left) and Pd-Pyridine immobilized catalysts (right)

No significant change in the microstructure of the supports was observed after the immobilization process. For MCM-41 the particles observed for the immobilized catalyst

seem to be more spherical when compared to the hexagonal MCM-41. The micrographs for SBA-15 shows the disintegration of the chain-like structures and the formation of more distinct particles are observed. Native particles seem to be larger than that of the immobilized catalysts though. This could be a result of the immobilization process whereby attrition of the particles could have occurred due to the mechanical stirring of the reaction mixture. This could possibly be confirmed by stirring some native support for the same amount of time and comparing the resulting product with the immobilized catalysts. No significant difference in SEM for the different catalysts was seen.

3.3.1.7 Characterization by means of solid state $^{13}C\{^{1}H\}$ NMR spectroscopy

Solid sate $^{13}C\{^{1}H\}$ NMR spectroscopy proved to be a very useful technique to evaluate the successful covalent immobilization of the functionalized complex to the support (Figure 3.26 and Figure 3.27). The solid state NMR spectroscopy compared well to the ^{13}C solution NMR spectra that were obtained for functionalized complex **C4**. As expected, very intense resonances are seen at 19.80 and 59.58 ppm corresponding respectively to the methyl and methylene carbons of the siloxane functionality. All the other resonances can be identified and the resonance corresponding to the imine carbon is found at around 170 ppm.

Spinning side bands are typically seen in solid state NMR. These are easy to elucidate and are found at the rotor rotation Hz value from major resonances.

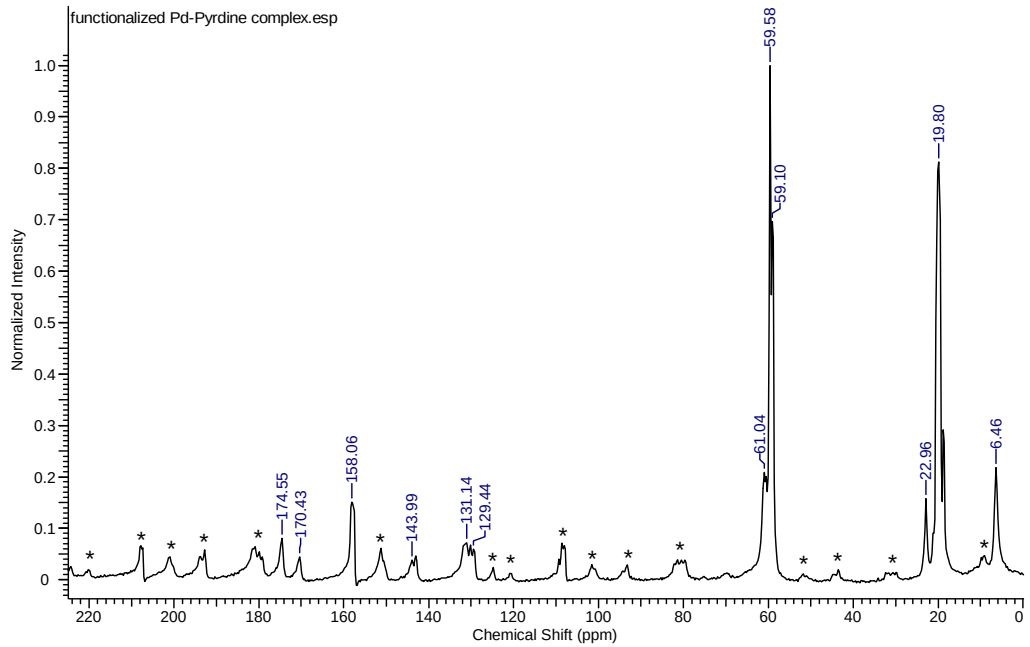

Figure 3.26 Solid state $^{13}C\{^{1}H\}$ NMR of functionalized Pd-Pyridine complex C4

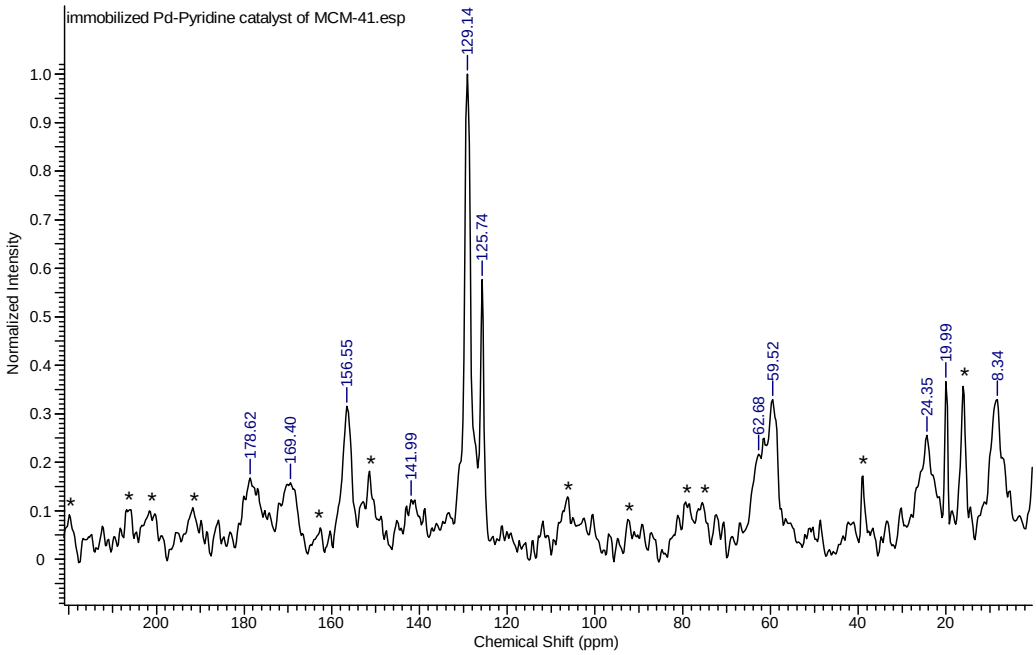

Figure 3.27 Solid state $^{13}C\{^{1}H\}$ NMR of immobilized Pd-Pyridine MCM-41 catalyst

Spinning side bands (SSB) annotated with star (*)

One would expect that when successful covalent immobilization occurs, the intensity of the siloxane resonances would decrease. This is observed for the NMR spectra of the immobilized catalyst (Figure 3.27). The methyl and methylene carbon resonances of the ethoxy functionality are almost completely absent in the spectrum of the immobilized catalyst. This is to be expected since the condensation of the siloxane tail of the functionalized complex with the surface silanols of the SiO_2 would liberate ethanol as a byproduct. The absence of EtO signals in the spectrum confirms successful immobilization of the catalyst. Only low intensity peaks compared to the other resonances are seen at 19.99 and 59.92 ppm respectively. There is a small shift in some of the resonances but all are still present. The imine carbon is observed at 169 ppm. The presence of the imine carbon after immobilization also shows that the complex did not decompose during the immobilization process.

3.4 Concluding remarks

MCM-41 and SBA-15 were successfully synthesized making use of the template synthesis method reported by Chai[18] and Zhao.[19] Ti-doped supports of MCM-41 and SBA-15 were synthesized by the introduction of a Ti source in the form of Ti-isopropoxide. These supports were characterized by a wide range of solid state techniques to obtain information on their physical and structural properties. The supports were found to have very high thermal stability (tested up to 600 ℃) and were prone to easily absorb moisture and were therefore stored in a glovebox. Immobilization of the functionalized complexes of Pd(II) and Cu(I) were observed mainly by the change

in surface areas of the supports (BET analysis) and TGA. Solid state $^{13}C\{^{1}H\}$ NMR spectra proved without a doubt that the functionalized complex was covalently bound to the silica support through the surface silanols and siloxane groups of the complex. It was not possible to see any CH vibrations or stretches when the immobilized catalysts were characterized with IR spectroscopy. This was ascribed to the relatively low amount of complex which was immobilized compared to the silica.

3.5. Experimental section

3.5.1 General remarks and instrumentation

All reactions were carried out under nitrogen making use of standard Schlenk techniques. Highly air-sensitive materials were stored in a nitrogen purged glovebox and all manipulations with these materials were carried out in the glovebox to prevent decomposition or oxidation. IR spectra were recorded using an ATR accessory on a Nicolet Avatar 330 FT-IR spectrometer. Powder XRD analysis was done on an X'Pert Pro Multi Purpose Diffractometer with a Reflection Transmission Spinner. Nitrogen adsorption/desorption analysis was done on an ASAP 2010 (Accelarated Surface Area end Porosimetry System) instrument. SEM micrographs were recorded on a Weiss Evo MA15VP SEM instrument.

ICP-AES analysis was done on the immobilized catalysts to quantify the amount of Pd(II) metal that is present in the catalyst. The samples were prepared by digesting more or less 40 mg of the immobilized catalysts in concentrated nitric acid (1 mL) while being

heated. The sample was filtered to remove any remaining solids and made up to a total volume of 50 mL.

3.5.2 Materials

Reagents were purchased from Sigma-Aldrich and used as is, these include tetra-ethylorthosilicate (TEOS), titanium-isopropoxide, cetyl trimethylammonium bromide (c-Tab) and Poly(ethylene glycol)-*block*-poly(propylene glycol)-*block*-poly(ethylene glycol) block copolymer (PEG *block*). Solvents were purchased from Sigma-Aldrich and Kimix Chemicals. Toluene was dried over sodium wire with added benzophenone while 25 % NaOH solution was used as is.

3.6. Synthesis of native supports

3.6.1 Mesoporous silica MCM-41

Ammonium hydroxide solution (205 ml, 25 weight %) was added to distilled water (270 ml) (pH 12.3). Whilst being stirred, the surfactant (cetyl trimethylammonium bromide) (1.997 g) was added. The solution was heated at 50 ℃ while being stirred. Tetraethoxysilane (TEOS) (10 mL) was added after the solution became homogeneous. A white slurry soon formed and the mixture was stirred for a further 2 hours. The mixture was left to cool to room temperature and was filtered and washed with distilled water (850 mL) and left to dry. The white solid obtained was calcined at 550 ℃

(temperature slowly increased). The calcination process was kept running for 4 hours. 1.664 g of MCM-41 was obtained.

3.6.2 Mesoporous silica SBA-15

Poly(ethylene)-*block*-poly(propylene)-*block*-poly(ethylene) (8.032 g) was dissolved in distilled water and 2 M HCl solution (360 mL) while being stirred at 35 ℃. TEOS (18.2 mL) was added to this stirred solution (after everything dissolved) and was stirred at 35 ℃ for 20 hours. The temperature of the mixt ure was then increased to 80 ℃ and the mixture "aged" for 24 hours without being stirred. A solid product formed and it was filtered off and washed with distilled water (1000 mlL) and dried at room temperature. The white product was then calcined at 550 ℃ for 8 hours.

3.7. Synthesis of Ti-doped supports of MCM-41 and SBA-15

3.7.1 Ti-MCM-41 (1-3 mol %)

Ammonium hydroxide solution (205 ml, 25 weight %) was added to distilled water (270 ml) (pH 12.3). Whilst being stirred, the surfactant (cetyl trimethylammonium bromide) (1.997 g) was added. The solution was heated at 50 ℃ while being stirred. A mixture of tetraethoxysilane (TEOS) (20 mL) and the appropriate amount of Ti-isopropoxide (1-3 mol %) was added after the solution became homogeneous. A white slurry soon formed and the mixture was stirred for a further 2 hours. The mixture was left to cool to room temperature and was filtered and washed with distilled water

(850 mL) and left to dry. The white solid obtained was calcined at 550 ℃ (temperature slowly increased). The calcination process was continued until the powder became white again.

3.7.2 Ti-SBA-15 (1-3 mol %)

Poly(ethylene)-*block*-poly(propylene)-*block*-poly(ethylene) (8.032 g) was dissolved in distilled water and 2 M HCl solution (360 mL) while being stirred at 35 ℃. A mixture of TEOS (20 mL) and Ti-isopropoxide (1-3 mol %) was added to this stirred solution (after the solution became homogeneous) and was stirred at 35 ℃ for 20 hours. The temperature of the mixture was then increased to 80 ℃ and "aged" for 24 hours without being stirred. A solid product formed and it was filtered off and washed with distilled water (1000 mL) and dried at room temperature. The white product was then calcined at 550 ℃ until it became white again.

3.8. Synthesis of immobilized catalysts

3.8.1 Pd(II) pyridyl-and quinolyl immobilized catalysts

All functionalized Pd(II) complexes were immobilized employing the same method. **C4** is taken as an example. Complex **C4** (0.103 g, 0.21 mmol) was added to a slurry of MCM-41 (1.031 g in 10 ml dry toluene) in a 50 mL round bottom flask. The slurry was refluxed at 110 ℃ for 24 hours and gave a yellow mixture. The mixture was filtered and the solid washed with toluene (3x10 mL) and dichloromethane (3x10 mL) removing any

unreacted complex. The off-white product obtained was dried under vacuum for 24 hours and then stored in a glovebox until further use.

3.8.2 Cu(I) pyridyl-and quinolyl immobilized catalysts

Complex **C12** (0.100 g, 0.13 mmol) was added to a slurry of MCM-41 (1.001 g in 10 mL dry toluene) in a 50 ml round bottom flask. The slurry was refluxed at 110 ℃ for 24 hours and gave a purple mixture. The solvent was filtered off and the precipitate washed with toluene (3x10 mL) and dichloromethane (3x10 mL) removing any unreacted complex. The obtained light purple product was dried under vacuum for 24 hours and stored in a glovebox until further use.

3.8.3 Pd(II) pyridyl immobilized catalysts (Ti-MCM-41)

Complex **C4** (0.1001g, 0.21 mmol) was added to a slurry of 1-3 % Ti-MCM-41 (1.002 g in 10 mL dry toluene) in a 50 ml round bottom flask. The slurry was refluxed at 110 ℃ for 24 hours and gave a light yellow mixture . The solvent was filtered off and the precipitate washed with toluene (3x10 mL) and dichloromethane (3x10 mL) removing any unreacted complex. The obtained off-white product was dried under vacuum for 24 hours and stored in a glovebox until further use.

3.8.4 Pd(II) pyridyl immobilized catalysts (Ti-SBA-15)

Complex **C4** (0.1003 g, 0.21 mmol) was added to a slurry of 1-3 % Ti-SBA-15 (1.003 g in 10 mL dry toluene) in a 50 ml round bottom flask. The slurry was refluxed at 110 ℃ for 24 hours and gave a light yellow mixture . The solvent was filtered off and the precipitate washed with toluene (3x10 mL) and dichloromethane (3x10 mL) removing

any unreacted complex. The obtained off-white product was dried under vacuum for 24 hours and stored in a glovebox until further use.

3.9. References

1 Dessau, R. M.; Schlenker, J. L.; Higgins, J. B. *Zeolites*, **1990**, 10, *522.*

2 Davis, M. E.; Saldarriaga, C.; Montes, C.; Garces, J.; Crowder, C. *Nature*, **1988**, 331, 698.

3 Estermann, M.; McCusker, L. B.; Baerlochcr, C.; Merrouchc, A.; Kessler, H. *Nature*, **1991**, 352, 320.

4 Beck, J. S.; VartUli, J. C.; Roth, W. J.; Leonowicz, M.; Kresge, E.; Schmitt, C. T.; Chu, K. D. C.; Olson, T-W. D.; Sheppard, H. E. McCullen, W.; Higgins, S. B.; Schlenkert, J. B. *J. Am. Chem. Soc.* **1992**, 114*,* 10834.

5 Zhao, D.; Huo, Q.; Feng, J.; Chmelka, B. F.; Stucky, G. D.; *J. Am. Chem. Soc.* **1998**, 120, 6024.

6 Bagshaw, S. A.; Prouzet, E.; Pinnavaia, T. J.; *Science*, **1995**, 269, 1242.

7 Giraldo, L. F.; López, B. L.; Pérez, L.; Urrego, S.; Sierra, L.; Mesa, M. *Macromol. Symp.* **2007**, 258, 129.

8 Li, J.; Zhang, Y.; Han, D.; Gao, Q.; Li, C.; *J. Mol. Catal. A: Chem.* **2009**, 298, 31.

9 Chmielarz, L.; Kuśtrowski, P.; Dziembaj, R.; Cool, P.; Vansant, E.F. *Appl. Catal. B*, **2006**, 62 369.

10 Ying, J. Y.; Mehnert, C. P.; Wong, M. S. *Angew. Chem. Int. Ed.* **1999**, 38, 56.

11 Sierra, L.; Guth, J.-L. *Micropor. Mesopor. Mater.* **1999**, 27, 243.

12 Sierra, L.; Lopez, B.; Ramírez, A. *Stud. Surf. Sci. Catal.* **2001**, 135.

13 Mesa, M.; Sierra, L.; Lopez, B.; Ramirez, A.; Guth, J.-L. *Solid State Sci.* **2003**, 5, 1303.

14 Ying, J. Y.; Mehnert, C. P.; Wong, Mi. S. *Angew. Chem. Int. Ed.* **1999**, 38, 56.

15 de Oliveira, E. C.; Pires, C T.; Pastore, H. O., *J. Braz. Chem. Soc.,* **2006**,17, 16.

17 Xu, L.-X.; He, C.-H.; Zhu, M.-Q.; Wu, K.-J.; Lai, Y.-L. *Catal Lett,* **2007**, 118, 248.

18 Chai, Q.; Lin, W. Y.; Xiao, F.; Pang, W.; Zhou, B. Chen, X., *Micropor. Mesopor. Mater.*, **1999**, 32.

19 Zhao, D.; Huo, Q.; Feng, J.; B Chmelka, F. G.; Stucky, D. *J. Am. Chem. Soc.*, **1998**, 120, 6024.

20 Cesarino, I.; Marino, G.; do Rosário Matos, J.; Cavalheiro, É. T. G. *J. Braz. Chem. Soc.*, **2007**, 18.

21 Galameau, A.; Cambon, H.; Martin, T.; de Ménorval, L.-C.; Brunel, D.; Di Renzo, F.; Fajula, F. *Stud. Surf. Sci. Catal.*, **2002**, 141, 395.

22 Di Renzo, F.; Desplantiér, D.; Galarneau, A; Fajula, F. *Catal. Today*, **2001**, 66 75.

23 Zhang, H.; Sun, J.; Ma, D.; Bao, X.; Klein-Hoffmann, A.; Weinberg, G.; Su, D.; Schlgl, R. *J. Am. Chem. Soc.*, **2004**, 126, 7440.

24 Huo, Q.; Margolese D.I.; Stucky, G.D. *Chem. Mater.*, **1996**, 8, 1147.

25 Zhang, A.; Li, Z.; Li, Z.; Shen, Y.; Zhu, Y. *Appl. Surf. Sci.* **2008**, 254, 6298.

26 Li, J.; Zhou, C.; Xie, H.; *Ge,* Z.; Yuan, L.; Li, X. *J. Nat. Gas Chem.* **2006**, 15, 164.

27 Malumbazo, N. *Immobilized Catalysts for Alkene Oxidation*, MSc Thesis **2007**, University of Western Cape

Chapter 4: Preliminary studies on catalytic benzyl alcohol oxidation

4. Introduction

The synthesis of aldehydes and ketones through the oxidation of alcohols is one of the most widely employed chemical transformations in organic chemistry. These oxidation products are utilized as intermediates in the synthesis of drugs, vitamins and aromatic compounds.[1,2] Although numerous methods for oxidation of alcohols are known and employed, the development and application of newer methodologies is gaining much interest. The world-wide annual production of carbonyl compounds is mostly produced by the oxidation of alcohols and therefore is an actively researched field in catalysis.[3] Two of the most widely used oxidants today are complexes of chromium (VI) and manganese. Their toxicity, corrosive properties and the harsh reaction conditions needed for the transformation have motivated researchers to develop cheaper and more environmentally friendly processes.[4] Hydrogen peroxide and molecular oxygen are nowadays preferred as oxidants given their environmental and economical benefits.

Pillai[1] and Kang[2] respectively reported the synthesis and application of vanadium phosphorus oxide and polymer-supported ruthenium complexes for the oxidation of various alcohols making use of hydrogen peroxide and iodosylbenzene as oxidants. Both these reactions were characterized by the use of mild reaction conditions and short reaction times. There are numerous reports where molecular oxygen and hydrogen peroxide are used as oxidizing agents at very low reaction temperatures.

For a general transformation of an alcohol to its appropriate aldehyde, stoichiometric amounts of the catalyst are typically used. For example when palladium is used, Pd is reduced by two oxidative units. In a catalytic cycle the oxidized palladium species can be regenerated by using co-oxidants such as oxygen, hydrogen peroxide and aromatic halides to name but a few. A general mechanism for this regeneration of Pd(II) is shown in Figure 4.1.

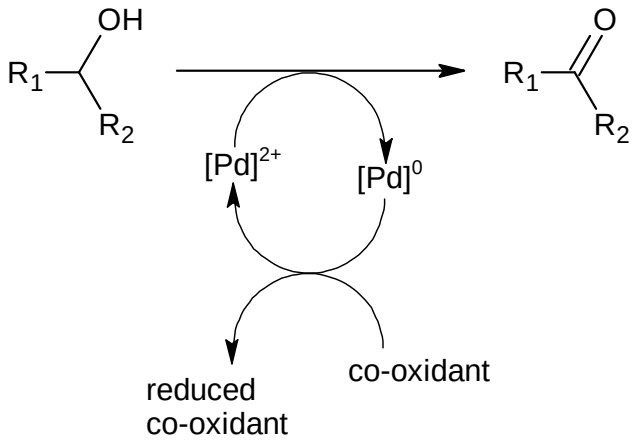

Figure 4.1 General mechanism for the oxidation of an alcohol

4.1 Application of Pd(II) and Cu(I) in oxidation

4.1.1 Pd(II) in oxidation

Stahl[5] and Muzart[6] have extensively studied the mechanism by which palladium catalyzes the oxidation of alcohols. Unfortunately these reactions were all characterized by the use of high oxygen pressures and relatively high metal loadings. However Jensen[7] and Iwasawa[8] reported catalysts capable of high turnovers using low pressures

of oxygen and much lower metal loadings. These catalysts use bulky ligands which presumably inhibit Pd-black formation.

Most of the oxidative reactions involving palladium are usually dehydrogenation reactions and form palladium hydride intermediates which are reactivated by H-acceptors. It is rather difficult though to distinguish between a co-oxidant and a H-acceptor. Most of the co-oxidants can also act as H-acceptors such as oxygen, allyl halogens, compounds containing double bonds etc. The H-acceptor can also be situated on the active catalyst, as is shown in Scheme 4.1.

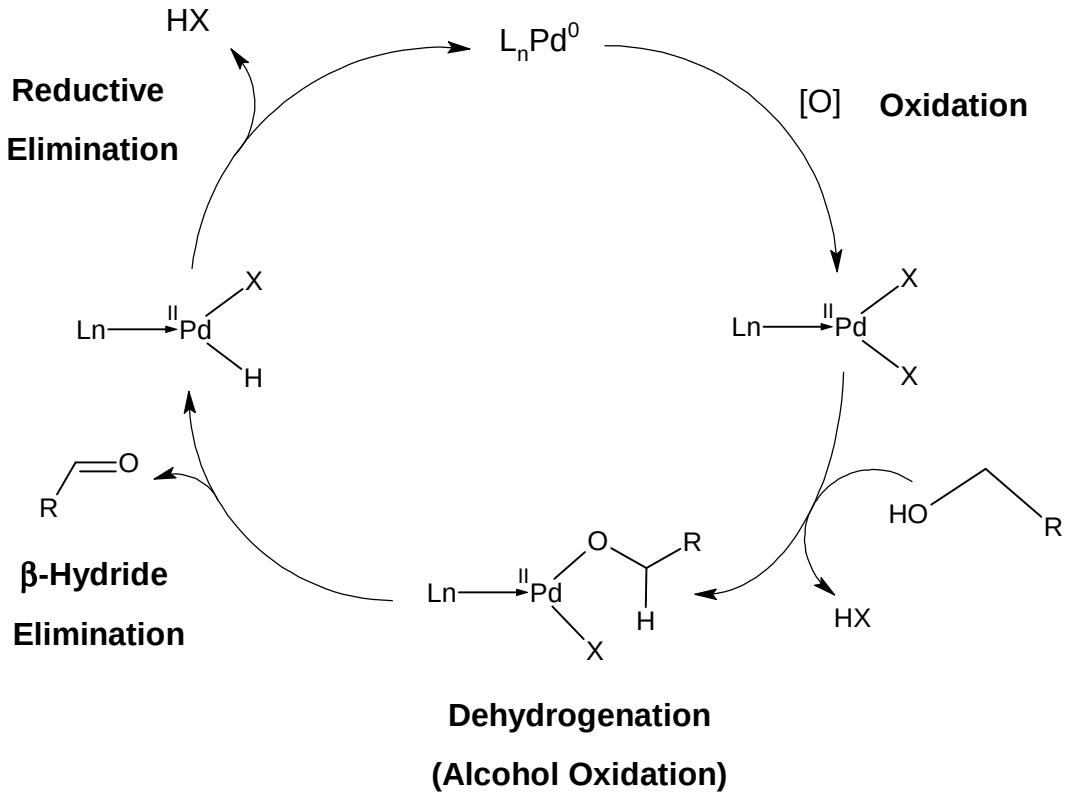

Scheme 4.1 Catalytic cycle for the oxidation of a primary alcohol to its aldehyde by Pd(II) catalyst[9]

Here HX is eliminated to afford the Pd^0 species. The Pd^0 is subsequently oxidized by the appropriate oxidant (O_2 or hydrogen peroxide) and the active catalyst is regenerated.

The growth potential in the area of alcohol oxidation by Pd is great and ultimately the use of low catalyst loadings and low levels of O_2 could create an industrially friendly oxidation system.

4.1.2 Cu(I) in oxidation

Markó *et al*. [10] reported the oxidation of a wide range of alcohols making use of a Cu(I) system in the presence of a hydrazine ligand. Their proposed catalytic cycle is shown in Scheme 4.2. The mechanistic studies carried out by this group suggested that an initial hydrogen-transfer reaction within the formed copper-alkoxide complex **4** generated the carbonyl-bound hydrazino-copper species **4**. When this Cu(I) complex was exposed to oxygen, the binuclear Cu(II) peroxide **5** was observed. The Cu(I) hydroxy species **6** is afforded after the homolytic cleavage and hydrogen atom abstraction of the complexed hydrazine have taken place. Regeneration of the alcohol coordinated catalyst **3** is achieved as a result of the rapid exchange between the OH and alcohol **1**.

Shen *et al.* [11] reported a new type of Cu(I) system utilizing ionic liquids and nitrogen containing ligands as active catalysts in alcohol transformations. Their choice of a bis-isoquinoline copper catalyst was based on the fact that CuCl can mediate the oxidation of alcohols very efficiently when used together with nitrogen containing ligands. The use of ionic liquids was found to enhance the catalytic properties of the employed catalysts.

The addition of a base in the form of K_2CO_3 was also investigated and they found that the base does not only initiate the addition of the alcohol to the copper, but also acts as a solid support onto which the active catalyst adsorbed.

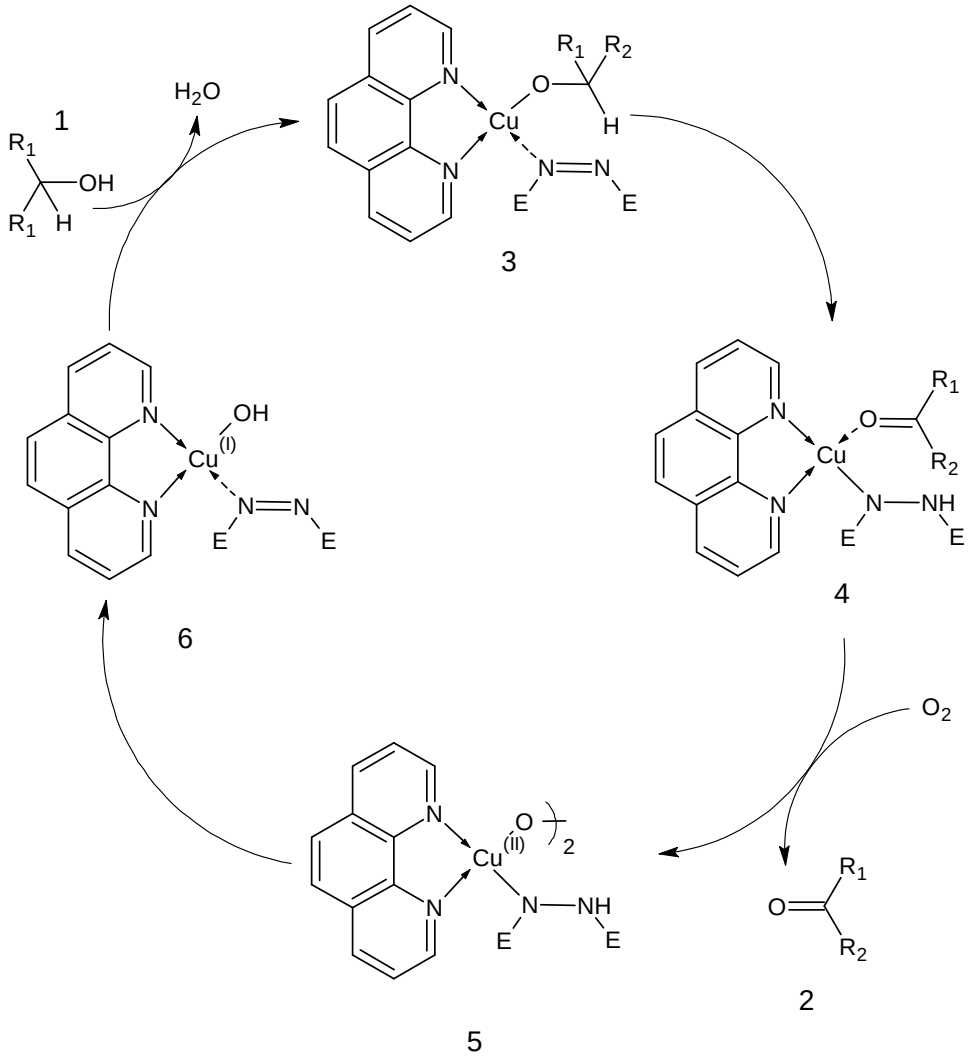

Scheme 4.2 Proposed mechanism for the oxidation of alcohol by a Cu(I) system[10]

For our study, complexes of Pd(II) and Cu(I) were employed as catalysts for the oxidation of benzyl alcohol to benzaldehyde under relatively mild conditions utilizing

molecular oxygen as co-oxidant. K_2CO_3 was added and acts as a base initiating the addition of the alcohol.

4.2 Complexes used as catalysts

The synthesis and characterization of both model complexes and immobilized catalysts were discussed in Chapter 2 and 3 respectively. In this chapter their catalytic activity in the oxidation of benzyl alcohol is evaluated.

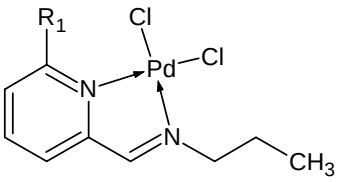

C1; $R_1 = R_2 = H$

C2; $R_1 = CH_3$

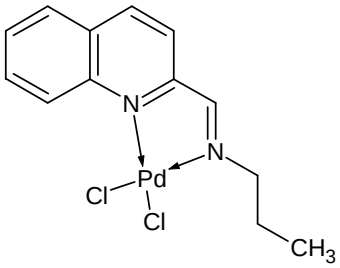

C3

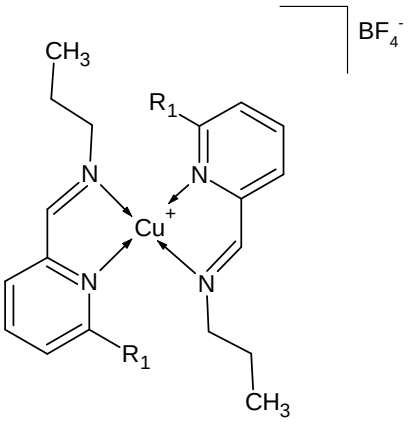

C7; $R_1 = R_2 = H$

C8; $R_1 = CH_3$

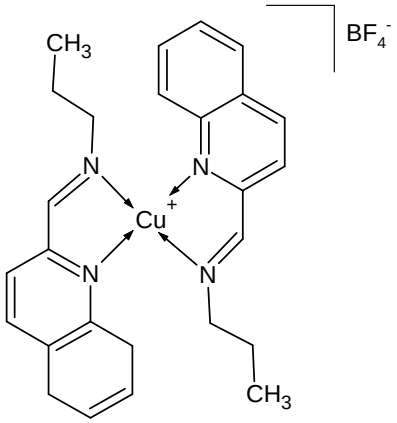

C9

Figure 4.2 Model complexes employed for catalysis

These are however only preliminary studies. This particular reaction also serves as a model reaction for the oxidation of alcohols in general, including the oxidation of polyols.

A range of model complexes were evaluated as catalysts for benzyl alcohol oxidation and are shown in Figure 4.2. Immobilized analogues of these complexes were also used as catalysts and results were compared to their model homogeneous counterparts.

4.3 Results and discussion

4.3.1 Oxidation of benzyl alcohol

Both the model (homogeneous) and immobilized catalysts were tested as catalysts. The model Pd-complex **C1** was used to determine the optimum reaction conditions for the reaction. The procedure followed was that which was reported by Zhou *et al.* [12] A generalized reaction is shown in Scheme 4.3. The effects of temperature, reaction time, metal loading, concentration and base were evaluated by testing complex **C1** under different conditions.

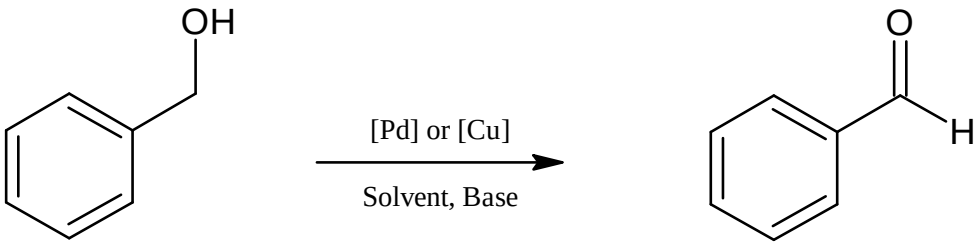

Scheme 4.3 Benzyl alcohol oxidation

4.3.2 Influence of different reaction conditions on catalyst activity

The model Pd-Pyridine complex **C1** was used to evaluate the effect of different reaction conditions on the catalyst activity. The first reaction was carried out under the optimum reported reaction conditions of Zhao and his group.[12] Typical reaction conditions were: 0.05 mmol metal, 5 mL toluene, 1 mmol alcohol, 1 mmol K_2CO_3, 100 ℃, 5 hours under 1 bar oxygen pressure.

4.3.2.1 Effect of reaction time, base addition, temperature and pressure on the reaction

Increase of the reaction time from 5 hours to 12 hours had no significant influence on the conversion of the starting material. An increase in conversion from about 10 % to 11.5 % for the model Pd-pyridine complex was observed when the reaction was done in 5 mL toluene at 1 bar pressure.

The pressure of the reaction was increased from 1 to 5 bar with no significant change in the conversion for this reaction with the rest of the reaction conditions unchanged.

A reaction was carried out to evaluate the influence that the K_2CO_3 has on the reaction. The reaction was carried out in the absence of base but under the exact same reaction conditions as employed for the other reactions (5 mL toluene, 1 mmol alcohol, 0.05 mmol Pd(II) and 1 bar oxygen pressure). The conversion was noted to decrease by half under these conditions.

The presence of the base in the reaction thus had a major impact on the conversion and although it was found that the reaction took place without the base, it was seen that the

base enhances the overall conversion of the reaction. Markó[10] and Shen[11] reported the importance of the addition of K_2CO_3 and ascribed the observed increase in activity to the increased facilitation of the alcohol addition to the metal in the presence of the base.

A reaction was performed under the same conditions (5 mL toluene, 1mmol K_2CO_3, 1 mmol alcohol, 0.05 mmol Pd(II) and 1 bar oxygen pressure) but at a lower temperature (60 ℃). A decrease in the conversion compared to reactions done at 100 ℃ was observed when the reaction is done over 5 hours. A summary of the influence of different reaction conditions on conversion is shown in Figure 4.3.

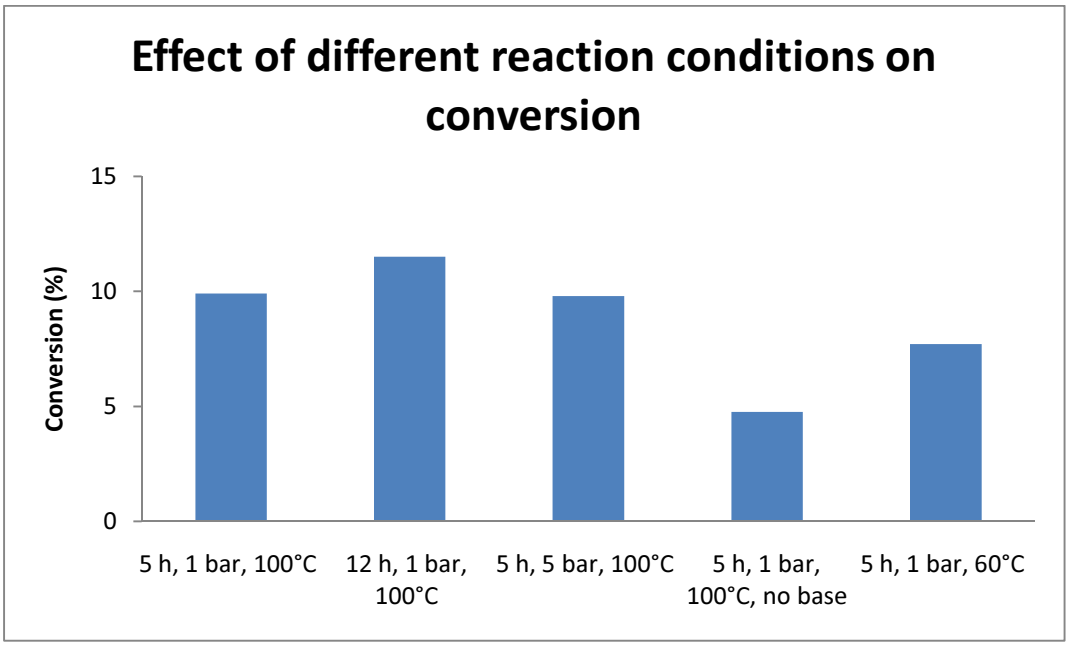

Figure 4.3 Effect of varying reaction conditions on alcohol conversion using C1 as catalyst

4.3.2.2 Effect of metal loading on conversion

Firstly the effect of metal loading on the activity of the catalyst was investigated. Three different reactions were set up containing 0.025, 0.050 and 0.100 mmol Pd(II)

respectively (5 mL toluene, 1 mmol alcohol,1 mmol K_2CO_3 and 1 bar oxygen pressure). Although very low conversions were observed for this complex under these reaction conditions, a definite increase in the conversion of the benzyl alcohol to benzaldehyde was observed with increased catalyst loading as shown in Figure 4.4.

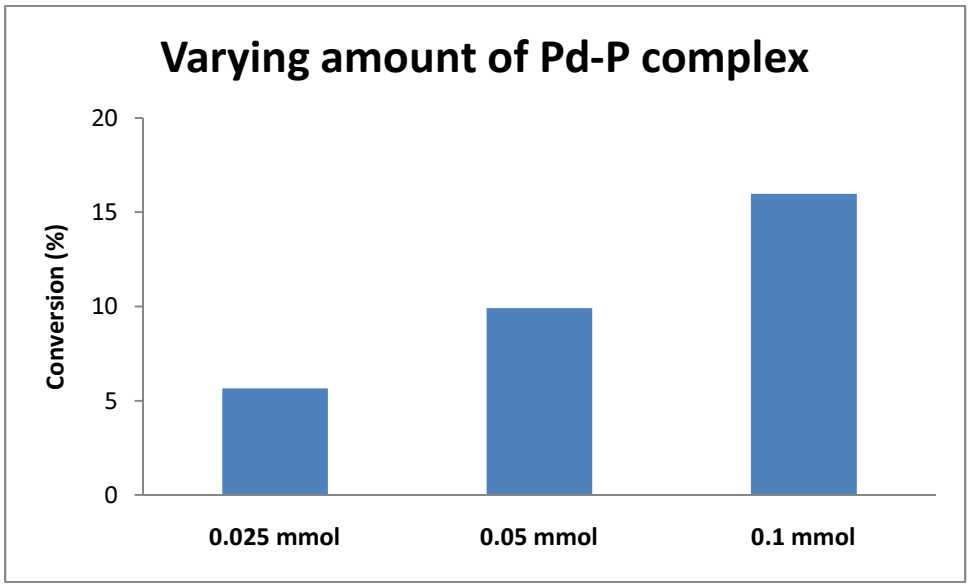

Figure 4.4 Effect of metal loading on alcohol conversion

4.3.2.3 Effect of solvent volume on conversion

Very low conversions were still obtained even at very high metal loading. It was thus decided to decrease the total reaction volume to increase the concentration of the reactants. The reaction volume was decreased from 5 mL to 2.5 and 1.25 mL and a dramatic increase in the alcohol conversion at lower reaction volume was observed (0.05 mmol Pd(II), 1 mmol alcohol, 1 mmol K_2CO_3 and 1 bar oxygen pressure). The conversion of alcohol in 1.25 mL toluene after 5 hours was double that in the other solvent volumes. All model complex reactions were subsequently carried out in 1.25 mL

toluene. The reactions using the immobilized catalysts were however performed in 5 mL of solvent. This was due to the fact that relatively large amounts of the supported material were required which posed problems with efficient stirring of the reaction mixture.

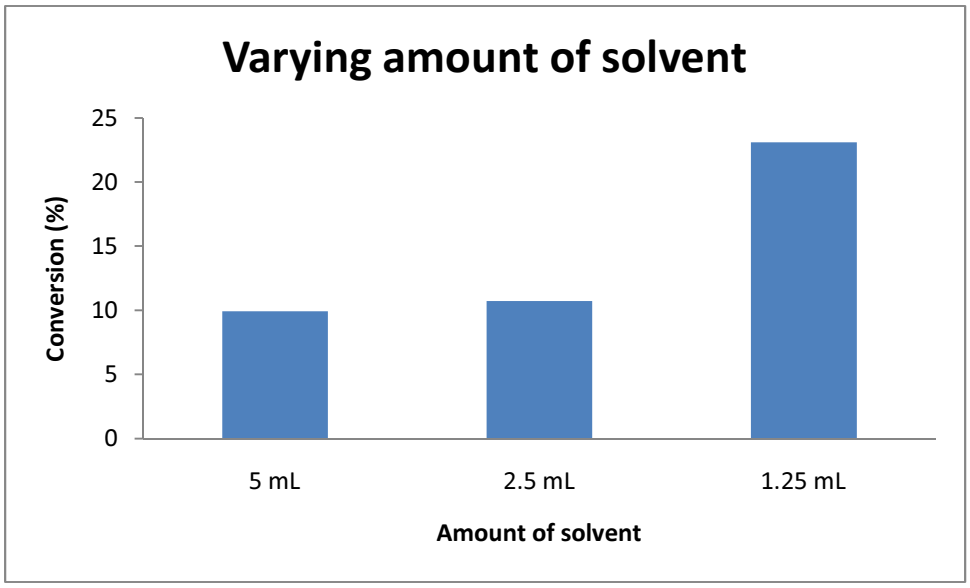

Figure 4.5 Influence of reactant concentration on alcohol conversion

The optimum conditions for the oxidation reaction using the homogeneous catalyst were previously determined to be: 5 hours, 1 bar pressure, 1.25 mL solvent, 0.1 mmol metal and 100 ℃. Unfortunately the use of 0.1 mmol meta l loading would have necessitated the use of large amounts of immobilized catalysts which would not have been practical. Therefore 0.05 mmol Pd(II) was utilized for further studies of the model complexes as catalysts. The use of 1.25 mL of solvent for the immobilized systems was also not possible and 5 mL was subsequently used.

4.4 Oxidation of benzyl alcohol by model and immobilized catalyst systems

4.4.1 Model catalyst systems

Model complexes of Pd(II) and Cu(I) were employed as catalysts using the optimum conditions established in the previous section. The results of the catalytic reactions in 1.25 and 5 mL under the obtained optimum conditions are shown in Figure 4.6.

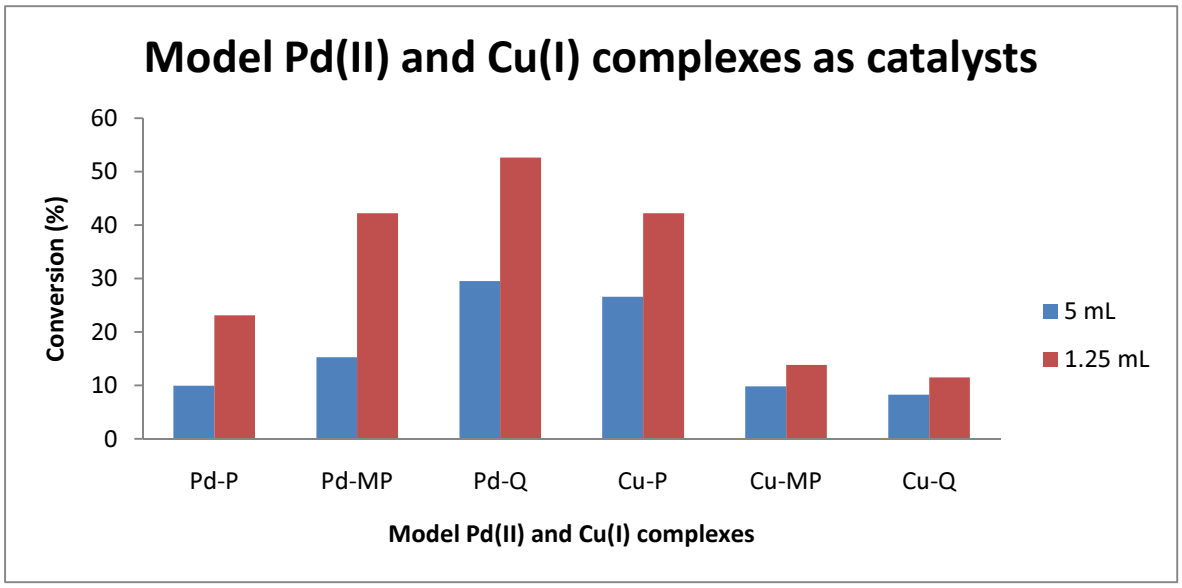

Figure 4.6 Conversion of benzyl alcohol with model Pd(II) and Cu(I) systems in different reaction volumes

A definite increase in the activity of the Pd(II) system is seen when moving in turn from pyridine to methyl-pyridine and finally to a quinoline system (in both solvent volumes). An increase in the steric bulk of the ligands follows the trend Q>MP>P. When taking a closer look at the mechanism for the Pd(II) catalyzed oxidation, we observed that one of

the steps involves the reductive elimination of HCl. It is known that reductive elimination is facilitated by sterically demanding ligands. One would therefore expect that this would enhance the rate at which the HCl is eliminated and that it would happen much easier for the bulkier quinoline ligand.

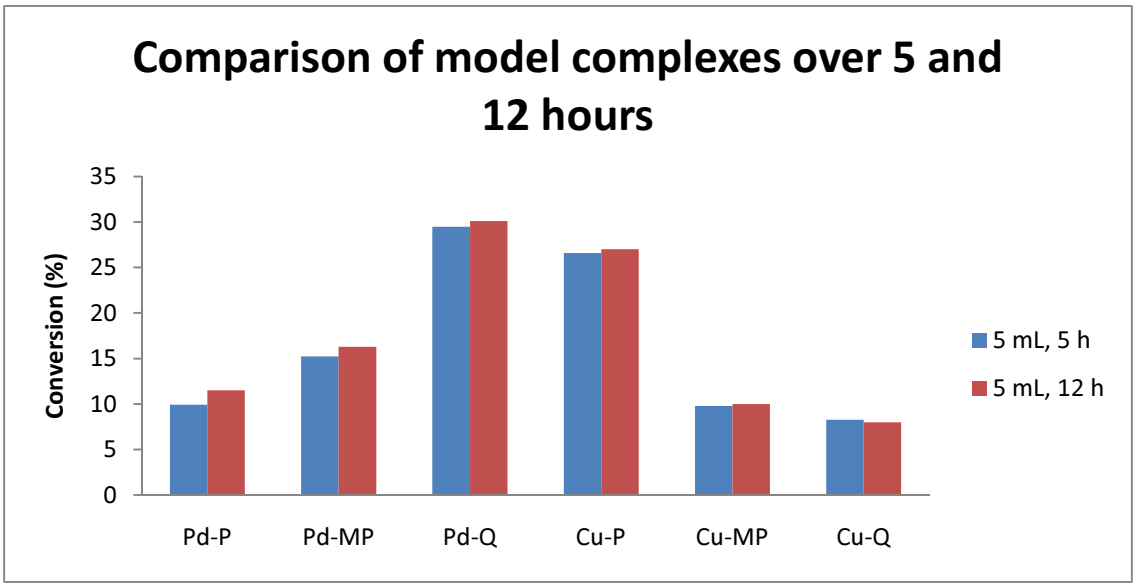

Figure 4.7 Comparison of model complexes over 5 and 12 hours

For Cu(I) systems on the other hand the exact opposite trend is observed with a decrease in the activity of the catalyst with an increase in the steric bulk of the ligands. For the two Cu(I) complexes (Cu-MP and Cu-Q) showing the lowest conversions, a change in the color of the reaction mixture from brown and purple to green was observed. This color change is believed to be caused by the oxidation of the Cu(I) to Cu(II). These two complexes were also the same complexes which showed the lowest thermal stability with melting points of 95 ℃ and 111 ℃ respectively. It is believed that the stability of these complexes at the reaction temperature of 100 ℃ was very low and could explain the low conversion when compared to the Cu-pyridine complex which

retained its brown color even after 12 hours of reaction. The Cu-MP and Cu-Q complexes presumably decomposed under the reaction conditions leading to a dramatic decrease in catalyst lifetime. This results in reduced catalyst lifetime and hence reduced overall activity.

It can be postulated that the Cu(I) is oxidized to a Cu(II) system and that the catalytical cycle proceeds via a Cu(II) mechanism. The mechanism for Cu(I) alcohol oxidation though is not widely reported and more work is needed to fully understand how exactly this Cu(I) system catalyzes the reaction.

The effect of time on the conversion of the model complexes is shown in Figure 4.7. No real change in the conversion was observed between 5 and 12 hours of reaction time. The increase in time did thus not lead to an increase in the activity of the homogeneous catalysts. A possibility is that the catalyst becomes inactive, even before 5 hours and results in no significant increase in conversion.

4.4.2 Immobilized systems

4.4.2.1 MCM-41 and SBA-15 immobilized Pd(II) and Cu(I) systems

Immobilized catalysts of the model complexes were also employed as catalysts for benzyl alcohol oxidation. For both the MCM-41 and SBA-15 systems generally higher conversion were seen for the immobilized systems in comparison to the homogeneous analogues (over 12 h period). It was observed for a test reaction that after 5 hours almost the same conversion as seen for the model systems was observed. Reaction

conditions were chosen to be: 12 h, 5 mL toluene, 1 mmol K_2CO_3, 1 mmol alcohol, 0.05 mmol metal and 1 bar oxygen pressure.

In Figure 4.8 conversions for the model homogeneous systems are compared to their immobilized counterparts under the same reaction conditions. For both the MCM-41 and SBA-15 immobilized systems a general increase in the conversion of benzyl alcohol is observed when compared to their model homogeneous analogues. However the Pd-quinoline-SBA-15 catalyst showed similar conversion when compared to its model Pd-quinoline analogue.

The same general increase in conversion is observed for the MCM-41 immobilized Pd(II) catalysts when compared to their model counterparts with the Pd-quinoline-MCM-41 immobilized system showing the highest conversion after 12 hours (46 %).

Amongst the SBA-15 systems, the Pd-methyl-pyridine-SBA-15 catalyst showed the highest activity (45 % conversion). A smaller increase in the conversion of the Pd-pyridine-SBA-15 system was observed when compared to the Pd-pyridine-MCM-41 counterpart. Both however showed higher conversions after 12 hours when they were compared to the model Pd-pyridine catalyst. A decrease in the activity of the Pd-quinoline-SBA-15 system compared to its model counterpart is observed. However only slightly lower conversion than the model system is observed.

MCM-41 immobilized catalysts showed on average a 10 % higher conversion than its homogeneous analogues. For the SBA-15 systems only the Pd-methyl-pyridine-SBA-15 catalyst showed any noticeable increase in conversion. In general immobilization of the model systems onto the MCM-41 proved to be more successful all round. The fact that

higher conversions were obtained for the immobilized Pd(II) systems suggests that the complexes were possibly stabilized by the support resulting in higher observed overall activity.

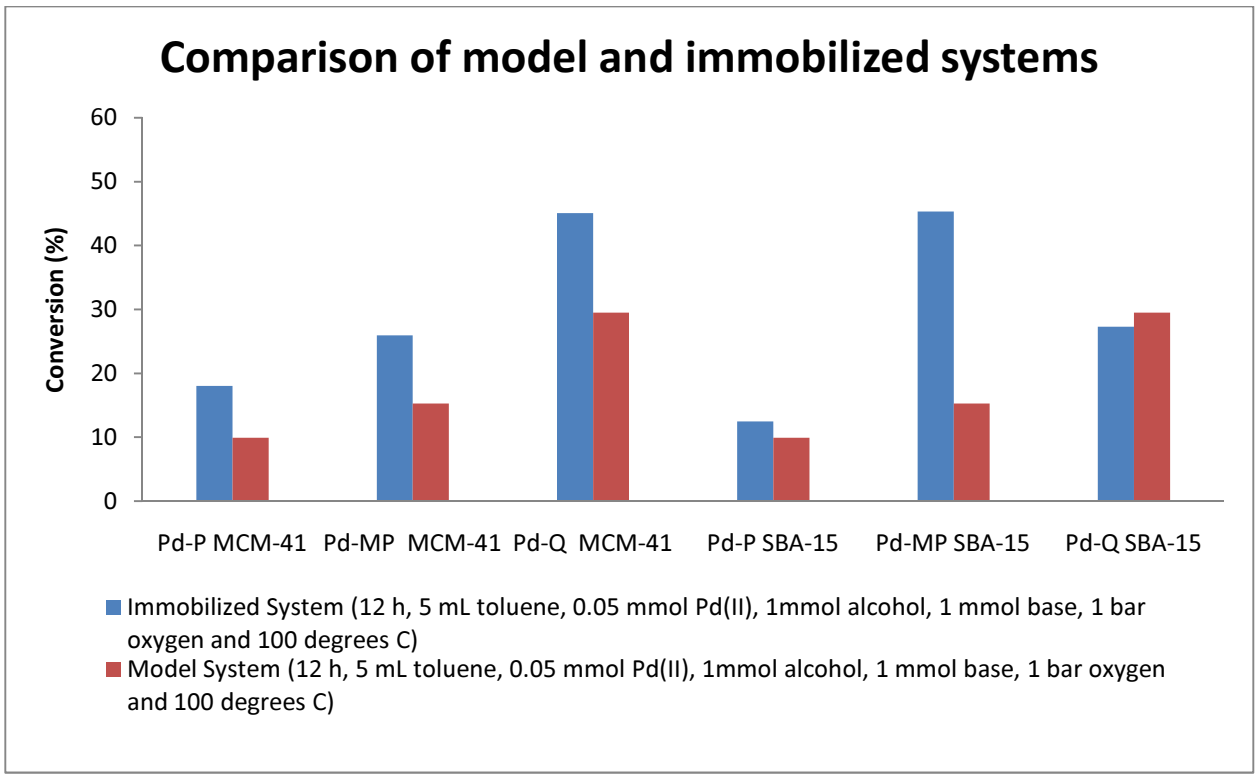

Figure 4.8 Summary of the activity of model and immobilized Pd(II) systems (MCM-41 and SBA15)

The immobilized Cu(I) systems in our hands showed no activity for alcohol oxidation whatsoever. In the previous chapter it was found that immobilization of the Cu(I) complexes onto the MCM-41 and SBA-15 supports caused the disintegration of the silica structure and possibly the complexes as well. The fact that no activity for alcohol oxidation is observed suggests that immobilization of the Cu(I) complexes onto the silica supports caused the catalysts to become inactive. The success achieved with the Pd(II) systems could unfortunately not be reproduced for the Cu(I) systems and more work

needs to be done to investigate the cause of this possible deactivation. The evaluation of other co-oxidants would have to be undertaken in this regard.

4.4.2.2 Ti-doped MCM-41 and SBA-15 immobilized Pd-Pyridine systems

A range of Pd(II) catalysts supported on Ti-doped silica was also tested in benzyl alcohol oxidation (12 h, 5 mL toluene, 1 mmol K_2CO_3, 1 mmol alcohol, 0.05 mmol metal and 1 bar oxygen pressure). Figure 4.9 summarizes the obtained conversions of the immobilized catalysts on Ti-doped supports compared to the model Pd-pyridine complex (12 h, 5 mL toluene, 1 mmol K_2CO_3, 1 mmol alcohol, 0.05 mmol metal and 1 bar oxygen pressure).

For the range of Ti-doped MCM-41 catalysts (Figure 4.9) only the Pd-P-3%-Ti-MCM-41 catalyst showed any significant improvement in conversion when compared to the model Pd-pyridine system reaching a conversion of 28 %. It seems that the increase in the Ti-doping to higher Ti/Si mol % had a more noticeable effect on the activity of the SBA-15 immobilized catalyst.

The Ti-SBA-15 range of catalysts generally showed a higher activity than their Ti-MCM-41 counterparts. With the exception of the Pd-P-3%-Ti-MCM-41 catalyst, the other Pd-P-Ti-SBA-15 catalysts show higher conversions in general. For the SBA-15 doped catalysts the Pd-P-1%-Ti-SBA-15 catalyst reaches a maximum conversion of 21 % after 12 hours.

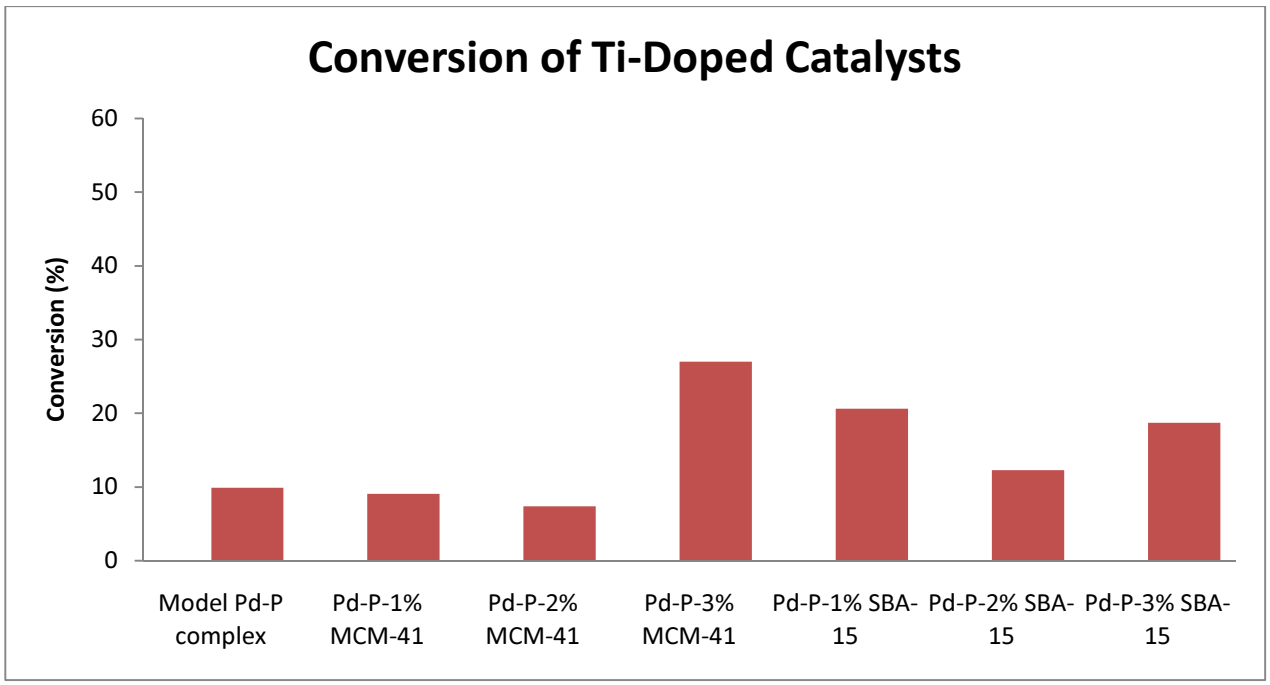

Figure 4.9 Summary of Pd-Pyridine Ti-doped systems

A comparison between the normal and Ti-doped supports containing the Pd-pyridine catalyst is shown in Figure 4.10. All of the Ti-doped SBA-15 catalysts show a higher or equal conversion compared to the normal Pd-P-SBA-15 catalyst. For the MCM-41 Ti-doped catalysts though a decrease is seen for the 1 and 2 % Ti-doped catalyst compared to the normal Pd-P-MCM-41 catalyst. The Pd-P-3%-Ti-MCM-41 catalyst however showed an increase in conversion of almost 10 % compared the normal MCM-41 system.

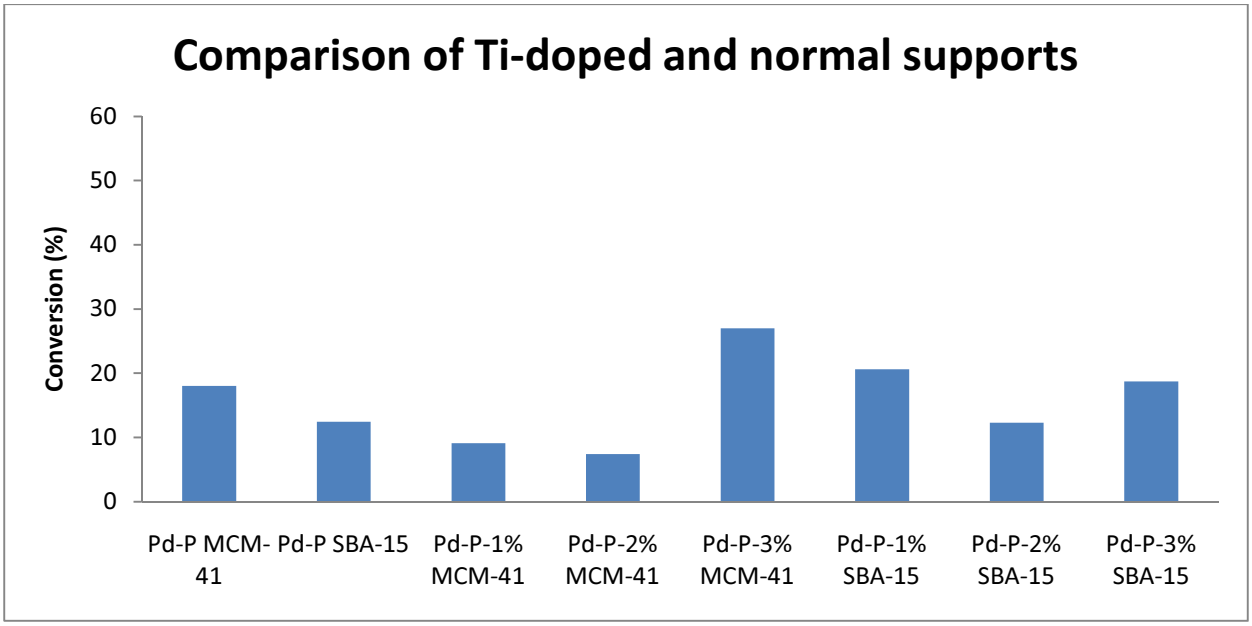

Figure 4.10 Comparison of the conversions of Pd-pyridine complex on Ti-doped and normal MCM-41 and SBA-15

4.5 Concluding remarks

Preliminary studies showed that the model Pd-quinoline catalyst was the most active catalyst for benzyl alcohol oxidation when compared to the Pd-pyridine and Pd-methyl-pyridine complexes. This higher activity shown by the quinoline derivative was attributed to the increase steric bulk introduced by the quinoline ligand possibly facilitating the reductive elimination of HCl from the Pd(II) during catalysis and hence the overall reaction rate.

For the normal MCM-41 and SBA-15 immobilized catalyst systems a general increase in the activity of the catalysts were observed when these were compared to their model counterparts with only the Pd-Q-SBA-15 catalyst showing a slight decrease in

conversion. Doping of the supports with titanium had in general a bigger influence on conversion for the SBA-15 catalysts than for the MCM-41 systems.

Overall immobilization of the complexes onto the supports seemed to have a positive effect on the stability and subsequent conversion of benzyl alcohol. Some more in-depth studies are necessary to fully understand and fine tune this oxidation reaction and would be included in future work.

4.6 Experimental section

4.6.1 Method and instrumentation

All reactions were carried out using a Radley's parallel reactor with a gas distribution system. All reactions were performed under an atmosphere of oxygen. Toluene was dried over sodium/benzophenone under nitrogen and distilled before use. K_2CO_3 was purchased from Sigma Aldrich and used as received. Samples from alcohol oxidation reactions were analyzed by ^1H NMR to calculate conversion.

4.6.2 Typical procedure for benzyl alcohol oxidation

In a typical oxidation reaction a mixture of either the model complex or immobilized catalyst (0.05 mmol Pd) and K_2CO_3 (1 mmol) was added to the reaction vessel. Half of the amount of solvent was added to this mixture while being stirred and purged with oxygen at 1 bar pressure. The other half of the solvent was added to the benzyl alcohol (1 mmol) and added to the reaction vessel. The vessel was sealed and the temperature

increased to 100 ℃ and the reaction mixture was st irred for the appropriate period of time. After the allotted time the mixture was allowed to cool to room temperature. It was then filtered and washed with dry toluene and the solvent removed under vacuum. Samples for ^{1}H NMR spectroscopy were prepared and analyzed to calculate conversion.

4.6.3 Procedure for calculating alcohol conversion

Conversion of the benzyl alcohol to benzaldehyde was determined by making use of relative integration of the methine and methylene protons of the aldehyde and alcohol respectively. An example of a typical proton NMR is shown in Figure 4.9. Benzyl alcohol and benzaldehyde were submitted for ^{1}H NMR to determine the position of the methylene and methine protons. It was found that the -C**H** of the aldehyde, as expected, had a resonance at 10 ppm and the –C$\mathbf{H_2}$ of the alcohol had a resonance at 4.70 ppm. Knowing that the signal for the alcohol represents two protons, the integration was set as 2. The aldehyde proton resonance was then integrated relative to the alcohol one. Normalization of the alcohol proton to one was necessary to be able to compare the integrations. A general formula was used to calculate the conversion of the alcohol to the aldehyde ($Conv._{alc} = interg._{ald}/(interg._{ald} + interg._{alc}) \times 100$).[13]

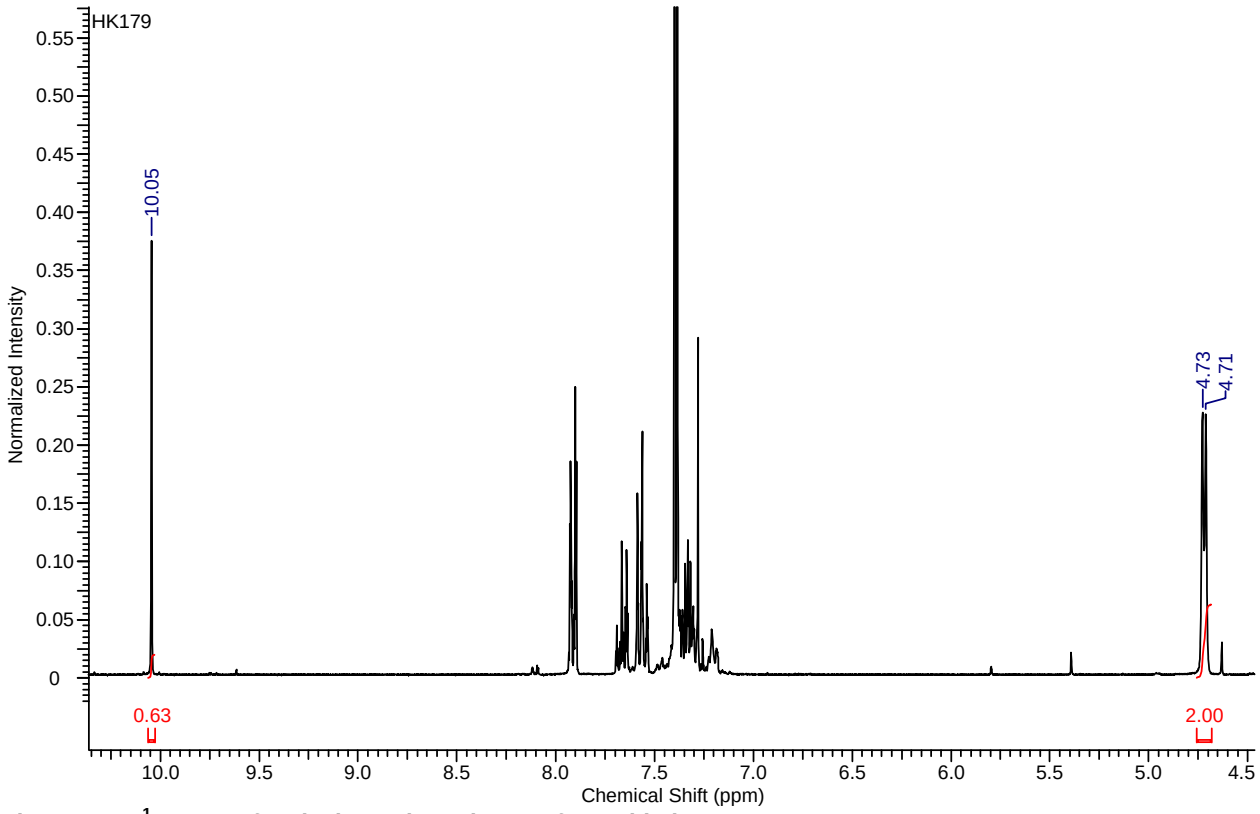

Figure 4.11 ^{1}H NMR of typical reaction mixture after oxidation

For this example it would then be: 0.63/(0.63 + 1.00) x 100 = 38.65 %

4.7 References

1 Pillai, U. R.; Sahle-Demessie, E.; *Appl. Catal., A,* **2004**, 276, 139.

2 Kang, Q.-X.; Luo, J.-J.; Bai, Y.-B.; Yang, Z.-W.; Lei, Z.-Q. *J. Organomet. Chem.* **2005**, 690, 6309.

3 Sheldon, R. A.; Arends, I. W. C. E.; Dijkman, A. *Catal. Today,* **2000**, 57, 157.

4 Griffith, W. P.; Joliffe, J. M. Dioxygen Activation and Homogeneous Catalytic Oxidation, Elsevier, Amsterdam, **1991**.

5 Stahl, S. S. *Angew. Chem., Int. Ed.* **2004**, 43, 3400.

6 Muzart, J. *Tetrahedron*, **2003**, 59, 5789.

7 Jensen, D. R.; Schultz, M. J.; Mueller, J. A.; Sigman, M. S. *Angew. Chem., Int. Ed.* **2003**, 42, 3810.

8 Iwasawa, T.; Tokunaga, M.; Obora Y.; Tsuji, Y. *J. Am. Chem. Soc.* **2004**, 126, 6554.

9 Sigman, M. S.; Schultz, M. J. *Org. Biomol. Chem*. **2004**, 2, 2551.

10 Markó, I. E.; Giles, P. R.; Tsukazaki, M.; Brown, S. M.; Urch, C. J. *Science*, **1996**, 274, 2044.

11 Shen, H.-Y.; Ying, L.-Y.; Jiang, H.-L.; Judeh, Z. M. A. *Int. J. Mol. Sci.* **2007**, *8*, 505.

12 Zhou, J.; Li, X.; Sun, H. *Can. J. Chem.* **2008**, 86, 782.

13 Tillman, E. S.; Contrella, N. D.; Leasure, J. G. *J. Chem. Educ*., **2009**, 86, 12.

Chapter 5: Concluding Remarks and Suggestions for Future Work

5.1 Concluding remarks

Chapter one of this thesis provides a thorough literature review on the synthesis of heterogenized metal catalysts. Different methods are discussed regarding the synthesis of appropriate functionalized complexes needed for successful immobilization. The focus is on MCM-41 and SBA-15 as suitable supports for complex immobilization. The salient features of the supports such as pore sizes, high thermal stability and large surface areas are also discussed.

In **Chapter two** the synthesis of both the model and functionalized ligands as well as their Pd(II) and Cu(I) complexes are described. Six model and functionalized ligands were prepared by Schiff base condensation reactions. These ligands were complexed to the metals to form the appropriate complexes. These complexes were characterized by ^{1}H NMR, FT-IR (ATR) and UV-Vis spectroscopy and the results correlated well with work previously done by our group. From the spectroscopic characterizations reported in this chapter it is clear that all of the ligands and complexes were successfully synthesized.

The synthesis and characterization of the immobilized supports are described in **Chapter three**. MCM-41 and SBA-15 were successfully synthesized making use of the template synthesis method reported by Cai and Zhao.[18,19] Ti-doped supports of MCM-41 and SBA-15 were synthesized by the introduction of a Ti source in the form of

Ti-isopropoxide. A wide range of solid state analytical techniques were employed to characterize these synthesized supports. Immobilization of the functionalized complexes of Pd(II) and Cu(I) were observed mainly by the change in surface areas of the supports (BET analysis) and TGA data. Solid state $^{13}C\{^{1}H\}$ NMR spectroscopy proved without a doubt that the functionalized complex was covalently bound to the silica support through the surface silanols and siloxane groups of the complex.

Preliminary benzyl alcohol oxidation studies are discussed in **Chapter four**. It was found that the model Pd-quinoline catalyst was the most active catalyst for benzyl alcohol oxidation when compared to the Pd-pyridine and Pd-methyl-pyridine complexes. This higher activity shown by the quinoline derivative was attributed to the increased steric bulk introduced by the quinoline ligand possibly facilitating the reductive elimination of HCl from the Pd(II) during catalysis and hence the overall reaction rate. It was observed that the immobilization of the Pd(II) functionalized complexes onto both the normal and doped supports generally had a positive effect on catalyst activity and stability. For the normal MCM-41 and SBA-15 immobilized catalyst systems a general increase in the activity of the catalysts were observed when these were compared to their model counterparts with only the Pd-Q-SBA-15 catalyst showing a slight decrease in conversion. Doping of the supports with titanium had in general a bigger influence on activity for the SBA-15 catalysts than for the MCM-41 systems.

5.2 Suggestions for future work

It would be interesting to see what the influence of the introduction of an electron withdrawing group on the pyridine-imine would have on the activity of the catalyst when complexed to Pd(II) and Cu(I). Both electron withdrawing and electron donating groups could be introduced to the quinoline-imine ligand system and subsequently complexed with Pd(II) and Cu(I).

Given that the catalytic studies were only preliminary a much more in depth examination of the reaction mechanism for both Pd(II) and Cu(I) catalyst systems are needed to fully understand the exact process taking place during the reaction. The use of a co-oxidant like TEMPO with the Cu(I) catalysts could be examined to see what influence it would have on reaction activity.